Doctoral Dissertation

Construction of Stimuli-Responsive Hydrogels Containing Hexameric Hemoprotein and β-Lactoglobulin

(ヘムタンパク質六量体およびβ-ラクトグロブリンを構成要素とする刺激応答性ゲルの開発)

January 2024

Kazuki Kageyama

Graduate School of Engineering,

Osaka University

Contents

General introduction

Hydrogels

Polymer hydrogels consist of a three-dimensional (3D) network structure which swells due to hydration of the main chains and side chains. These hydrogels have high water content and/or biocompatibility as well as exhibit characteristic viscoelasticity. These properties enable various applications as biomaterials. In particular, hydrogels are widely used for foods, cell growth media and contact lenses.[1] Figure 1 shows preparation scheme of polyacrylamide gel as a representative hydrogel. Polyacrylamide gels can be easily prepared and especially used for electrophoresis to estimate molecular weight of protein and nucleic acid. As mentioned above, hydrogels are utilized as important materials from scientific research to practical applications.

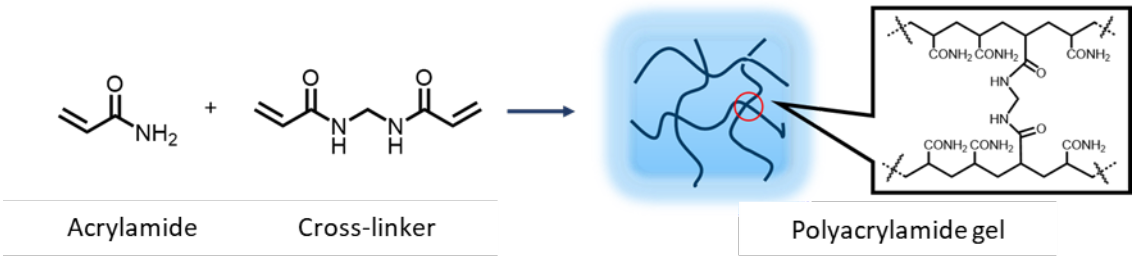

Figure 1. Schematic representation of polyacrylamide gel as a representative polymer hydrogel.

Strategies to prepare polymer networks forming hydrogels are categorized into three types: (i) copolymerization of main-chain monomers and cross-linkers(Figure 2a), (ii) conjugation of cross-linking molecules with linear polymers (Figure 2b) and (iii) condensation of branched polymer chains (Figure 2c). Methods of (i) and (ii) are versatile and applicable to various synthetic polymers with easily accessible procedures. These techniques have been adopted in a vast number of scientific studies due to their scalability, whereas low homogeneity of the obtained 3D network structures arise a problem in design.[2] In particular, precise design of hydrogels with appropriate swelling and mechanical properties is difficult. To overcome this point, Sakai and coworkers developed a tetra-PEG (polyethylene glycol) gel possessing homogeneity in its polymer structure by the preparation method (iii).[3] In the first example, two tetra-PEG components, which have amino groups and succinic imide groups, respectively, as reaction points on the four terminals of PEG moieties, were synthesized. These two tetra-PEGs were rapidly mixed to form a hydrogel with high structural homogeneity. This was revealed by small angle X-ray scattering.[4] Hydrogels with this type of homogeneity enable rational design of the swelling properties in equilibrium states by computational molecular modelling and simulation.[5,6]

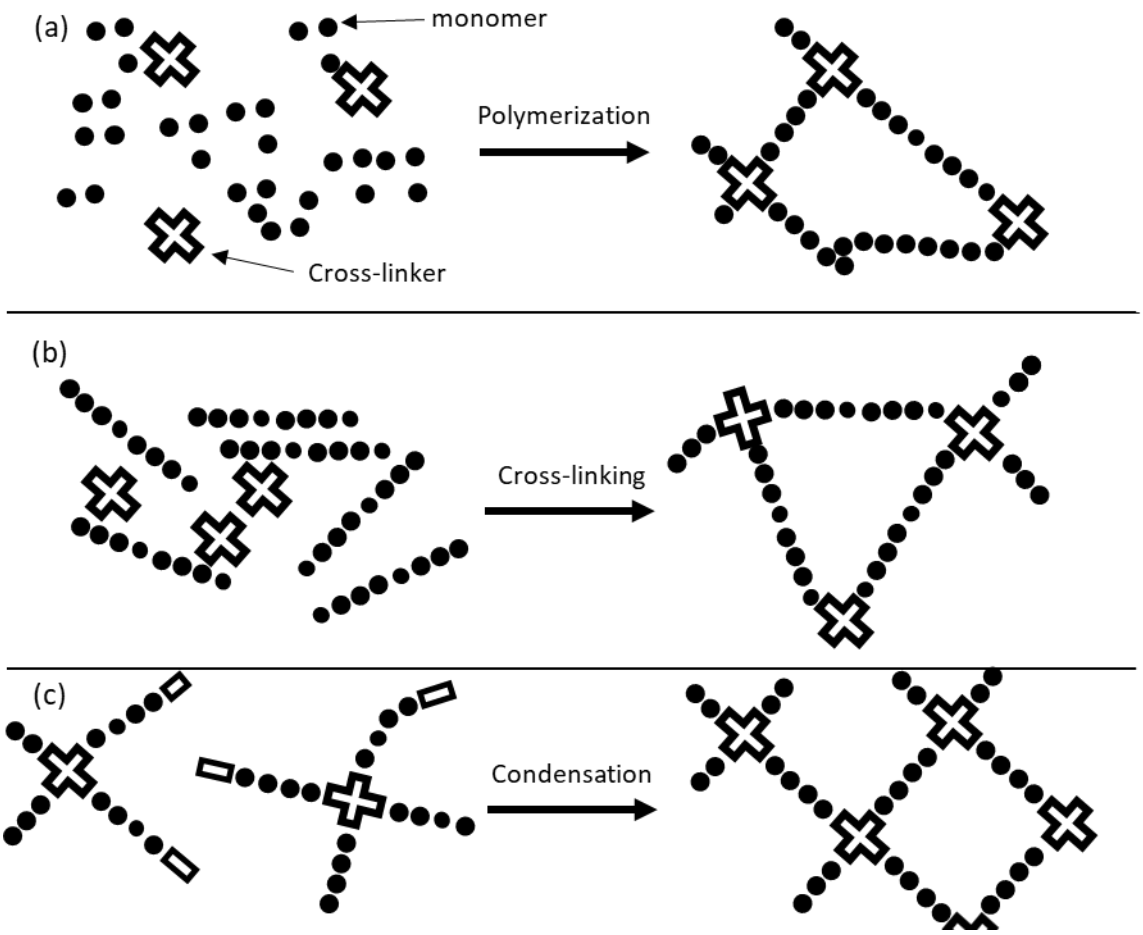

Figure 2. Schematic representation for the formation of 3D-network polymers. (a) Method (i): copolymerization of main-chain monomers with cross-linkers. (b) Method (ii): cross-linkage of polymer chains. (c) Method (iii): condensation of branched polymer chains.

Stimuli-responsive hydrogels

Stimuli-responsive hydrogels exhibit changes in shape and/or volume triggered by external stimuli such as pH and temperature changes.[7] Tuning the interactions between water molecules and polymer chains has been exploited to develop stimuli-responsive gels. For example, Tanaka's group reported dramatic volume changes of typical polyacrylamide gel via phase transition.[8,9] This phase transition behavior is caused by destabilization of hydrogen bonds with increasing temperature. Poly *N*-isopropyl acrylamide (PNIPAM) is well known as a useful component in temperature-responsive materials. This polymer has lower critical solution temperature (LCST) of approximately 32 ºC in an aqueous solution: dehydration of the polymer occurs above 32 ºC to form insoluble aggregations. LCST can be modulated by copolymerization with hydrophobic or hydrophilic monomers. New types of stimuli-responsiveness are also available by modification of functional molecules that change pH, hydrophobicity and temperature in response to external stimuli. For example, a hydrogel of PNIPAM modified with copper chlorophyllin moiety shows photoactive shrinking behavior due to photo-induced temperature increase.[10]

In recent decades, the conjugation of synthetic polymers and functional molecules has become one of the most useful strategies for constructing stimuli-responsive materials, in which the functional molecules as a component in a gel matrix are utilized to change physical properties. Three representative strategies are introduced here: (i) Utilization of structural alterations of functional molecules to induce volume changes, (ii) composition of functional molecules to control hydration and/or electric states of polymeric moieties and (iii) incorporation of supramolecular moiety (Figure 3).[11] While simple polymer hydrogels are only stimuli-responsive properties against pH, temperature, salt concentration and organic solvents, synthetic polymer hydrogels containing functional molecules, especially cross linkers, serve as stimuli-responsive materials against further stimuli such as light, redox, mechanical force, specific molecules including bioactive molecules, and so on.

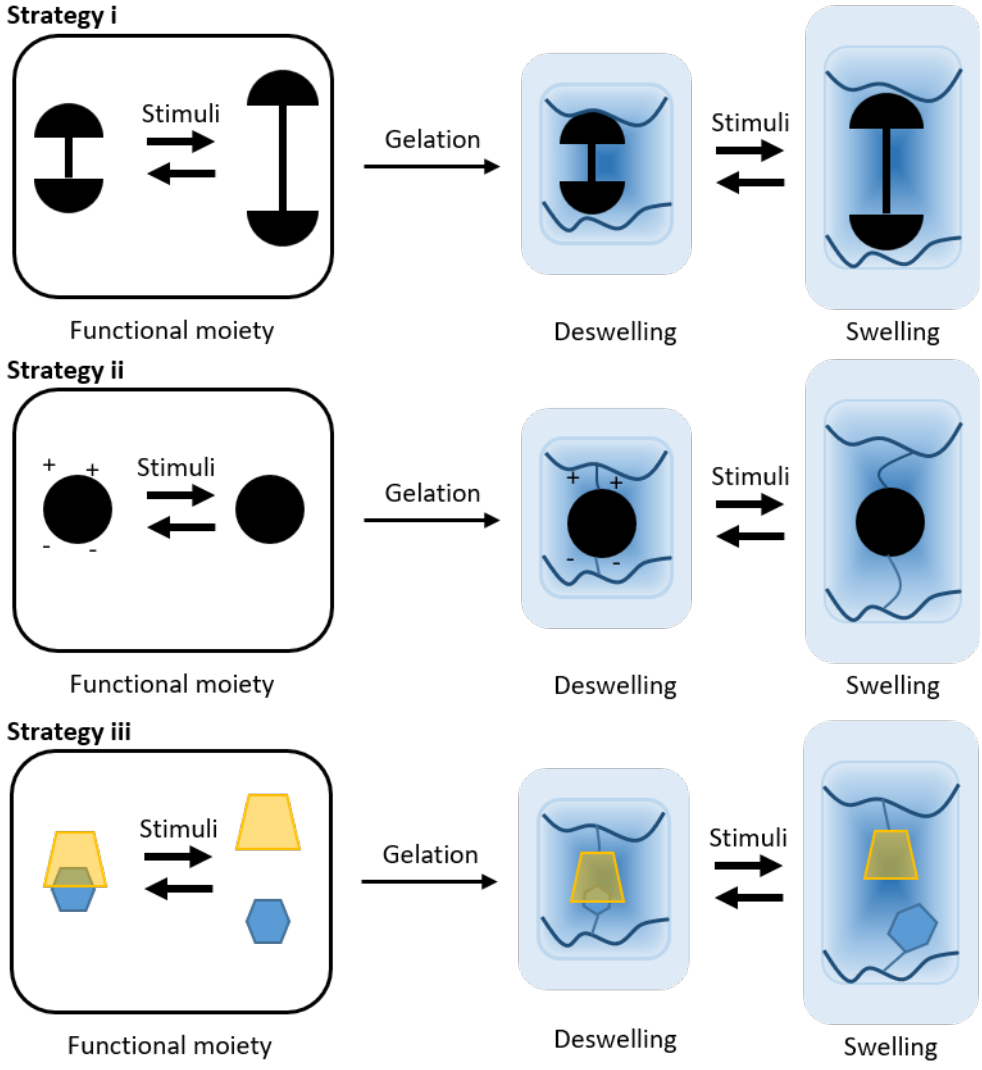

Figure 3. Schematic representation of three strategies to construct stimuli-responsive hydrogels by incorporation of functional molecules.

Hydrogels containing supramolecular moieties are emerging materials due to facile design and broad applications. Harada's group employed supramolecular recognition by cyclodextrin as a

cross-linker unit.[12] When azobenzene is selected as a guest moiety for cyclodextrin, a hydrogel shows photoactive actuator behaviors based on photo-induced *trans–cis* isomerization (Figure 4). In this hydrogel, the azobenzene moiety having the *trans*-state under ambient condition forms the host–guest complex working as a cross-linker. Irradiation of UV light converts the azobenzene moiety into the *cis*-state, inducing the dissociation of the guest molecule from the hydrophobic cavity of cyclodextrin. This behavior decreases cross-link density, resulting in swelling of the gel. Visible light irradiation or thermal relaxation reisomerizes the azobenzene moiety to the trans-state, and the hydrogel shrinks as the azobenzene moiety is incorporated into cyclodextrin. These swelling–shrinking behaviors are highly repeatable. This concept is applied to other types of host–guest interaction such as cyclodextrin–ferrocene,[13] cyclodextrin–admantane,[14] cucurbituril–viologen[15] and so on. Host–guest chemistry significantly contributes to supramolecular stimuli-responsive materials.

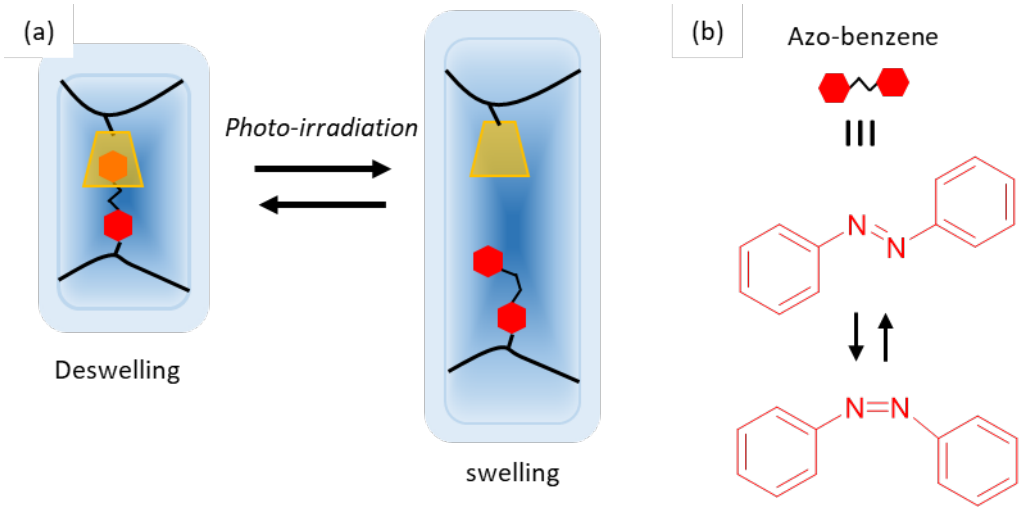

Figure 4. (a) Schematic representation of swelling behaviors of a hydrogel cross-linked by cyclodextrin–azobenzene interaction. (b) Isomerization of azobenzene upon the photoirradiation.

Mechanochromic materials are expected to have applications such as deterioration detection. These materials modulate their optical properties by mechanical stimuli and are generally prepared by incorporating stimuli-responsive chromophores into the materials. Mechanochromic behaviors are more common in organic crystals relative to other materials,[16,17] although rational design of the mechanochromic crystals is difficult. In contrast, mechanochromic elastomers or hydrogels have opportunities to be engineered by simple incorporation of stimuli-responsive chromophore units. Sottos and coworkers demonstrated mechanochromic elastomers containing spiropyran (Figure 5).[18] Isomerization reaction of spiropyran in the elastomer was triggered by mechanical stimulation, resulting in a dynamic change in its luminescent color. DNA is also utilized as an attractive component for mechanochromic materials because of its programmable duplex formation. Walther and coworkers constructed a hydrogel composed of DNA chains, which are partially modified with $Atto_{565}$ and $Atto_{488}$ fluorophores as well as a quencher of $Atto_{488}$.[19] In the initial state, the DNA gel shows green fluorescence derived from $Atto_{565}$. When tensile force is applied to the gel, $Atto_{488}$ and the quencher

were moved away from each other, enhancing the fluorescence intensity of $Atto_{488}$. These works provide inspiration for future unique mechanochromic materials.

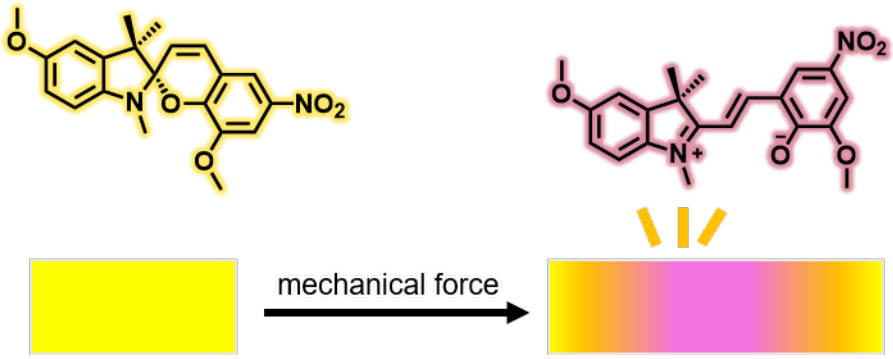

Figure 5. Chemical structure of spiropyran and schematic representation of mechanochromic materials.

Protein-based hydrogels

Protein is also an attractive building block as a component of stimuli-responsive gels. For example, Miyata and coworkers reported polyacrylamide gels containing an antigen-antibody interaction at cross-linking points (Figure 6).[20] In this report, when the corresponding antigen is added, the antigen linked to the polymer chain is displaced, the crosslink density decreases, and eventually the cross-linkage degrades. Using similar strategy, interaction between glucose and the lectin concanavalin A[21] was found to function as a cross linkage for gelation. Peptide–protein interactions are also reported as useful interactions.[22] Moreover, addition of biotin-attached tetra-PEG into an avidin solution demonstrates supramolecular hydrogel through strong biotin–avidin interaction.[23]

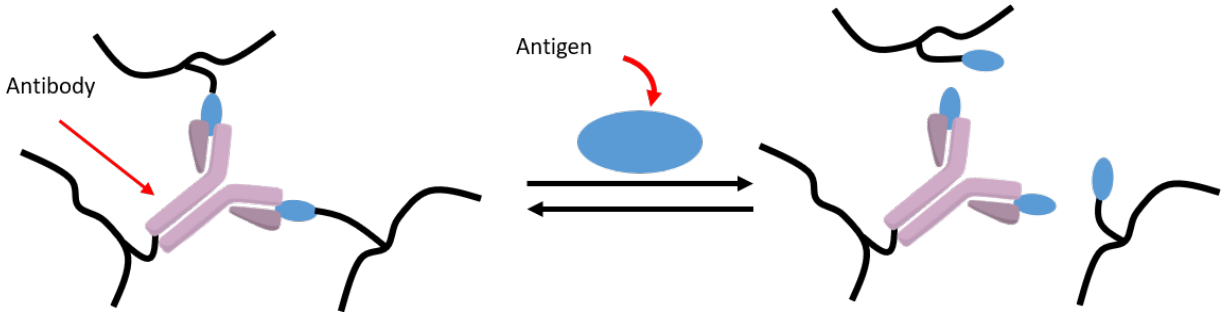

Figure 6. Schematic representation of an antigen responsive hydrogel containing antigen-antibody interaction as a cross-linkage.

Francis and co-workers constructed heavy metal ion responsive hydrogel using metal binding peptide, metallothionein.[24] Metallothionein binds various types of metal ions such as copper, zinc, cadmium, mercury and chromium selectively even in the presence of biologically abundant metal ions such as sodium, calcium, and magnesium. Engineered metallothionein with reaction points at both C and N terminals was utilized as a cross-linker connecting polymer chains to form a hydrogel. This gel shows shrinking behavior upon addition of heavy metal ions with drastic structural changes in

metallothionein moiety, and subsequent addition of chelators recovers the gel into the original size. Bruns and coworkers prepared a polymer–protein hybrid system toward mechanical nanosensor.[25] A FRET pair of fluorescent proteins, eCFP and eYFP, were incorporated into thermosome cross-linkers attached to polymer backbone of the gel. Applying mechanical force to the gel increased the distance between the two fluorescent proteins, resulting in a decrease in the fluorescence intensity derived from FRET.

In addition to the use of protein as a cross linker unit, hydrogels containing protein as a main component have also been investigated. Li and coworkers have demonstrated a series of unique protein-containing hydrogels based on genetically prepared protein oligomers as elastomeric building blocks. When leucine zipper domains, self-assembling peptides, are introduced at the N- and C-terminals, supramolecular gelation occurs under relatively low protein concentration (3.1%) conditions at room temperature.[26] The obtained gel shows phase transition to a sol state above 60 ºC by dissociation of the assembled leucine zipper domains. This temperature-dependent gel-sol transition is reversible, contributing to the development of useful protein-based gel materials. The elastic protein oligomer was also used in high modulus and toughness materials that derived their elasticity from their unique folding structure. Genetic oligomer of GB1, a subunit of antibody, as a titin mimic was prepared and further cross-linked through photochemical oxidation of tyrosine residues to form elastomer.[27] Single force curve measurement of the oligomeric building block reveals that the energy dissipation by unfolding of the folded protein contribute to the mechanical properties of the gels. Although stabilization energy in protein folding has been scientifically investigated toward protein design, a titin-inspired protein oligomerization enables the macro-level utilization of the protein folding energy for the materials. This strategy was applicable to other protein units such as ferredoxin.[28]

Protein-based hydrogels are combined with synthetic polymers to show unique functions. Popa and coworkers constructed a shape-memory hydrogel composed of bovine serum albumin (BSA), an abundant protein, with a polyelectrolyte as a synthetic polymer (Figure 7).[29] This shape-memory mechanism was regulated by the folding and unfolding transitions of BSA. In the preparation of protein gels, BSA was mixed with catalytic amounts of ammonium persulfate and tris(bipyridine) ruthenium(II) chloride in a buffer solution, and the homocoupling reaction of tyrosine residues on the surface of BSA was used to create a 3D gel by photoirradiation. The 3D network structure appears to be formed without the denaturation of BSA. Since the isoelectric point of BSA is 5.3, the protein units in the hydrogel have negative charge under neutral conditions to interact with a cationic polyelectrolyte solution, poly(L-lysine). This gel loses its original shape when soaked into a solution containing high-concentration denaturant, but the original shape is recovered after washing the denatured protein-containing gel with a buffer solution. This recovery is caused by refolding of denatured BSA in the gel. The memory-shape gel composed of protein has a potential for various applications as unique biomaterials.

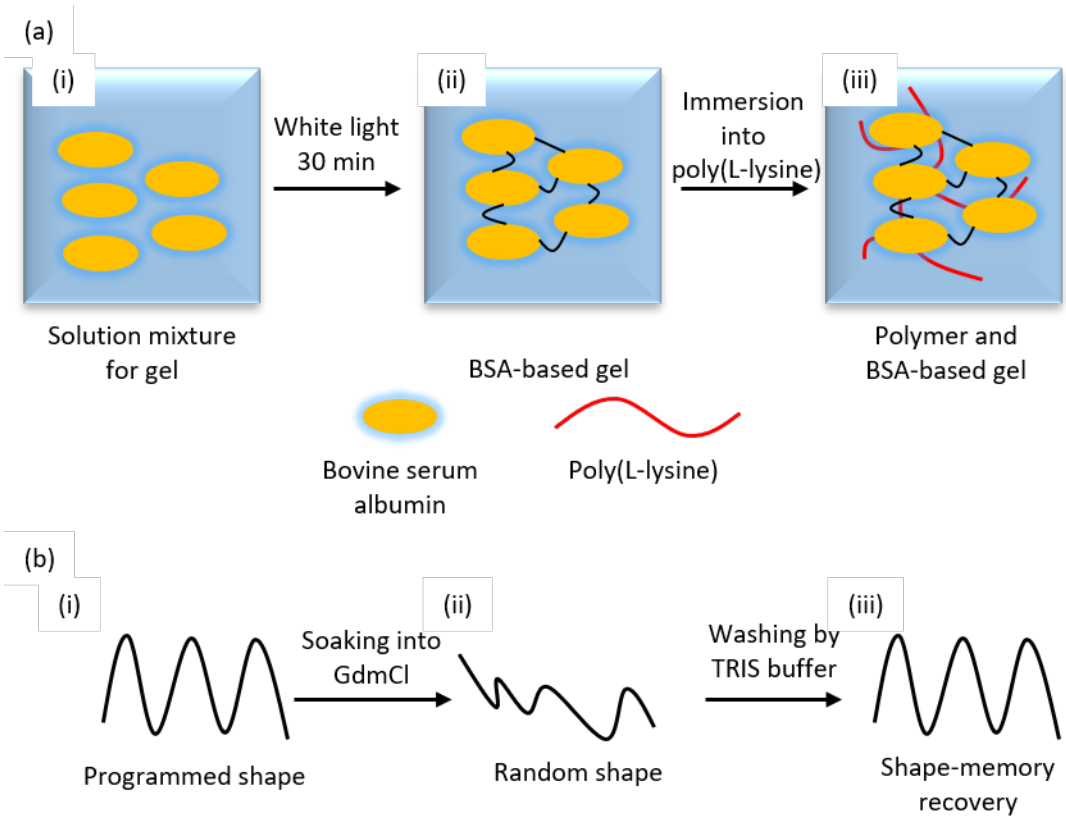

Figure 7. (a) Schematic representation of preparing hydrogel composed of BSA and polyelectrolyte: (i) BSA-based hydrogel solution mixture, (ii) BSA-based hydrogel via tyrosine–tyrosine coupling reaction, and (iii) a hydrogel composed of BSA and polyelectrolyte. (b) Shape memory of the hydrogel: (i) Program of the shape, (ii) deformation by immersion into 6 M GdmCl solution, and (iii) shape recovery by soaking in a buffer solution.

Hemoprotein assemblies toward biomaterials

Hemoprotein contains a heme cofactor which is tightly bound to a protein matrix. Especially, heme *b*, an iron complex of protoporphyrin IX, is incorporated into a protein matrix through reversible interaction (Figure 8).[30] Physiological roles of hemoprotein include oxygen transport/storage, electron transfer, gas sensing, enzymatic molecular conversion and so on. Structures, physicochemical properties and functions of various hemoproteins have been investigated. Furthermore, engineered hemoproteins have been reported for artificial metalloenzymes as well as a protein assembling systems.[31,32] In the case of hemoprotein containing heme *b*, substitution of native heme with synthetic cofactors is available toward enhancement and alteration of function in addition to mutation of amino acid residues.

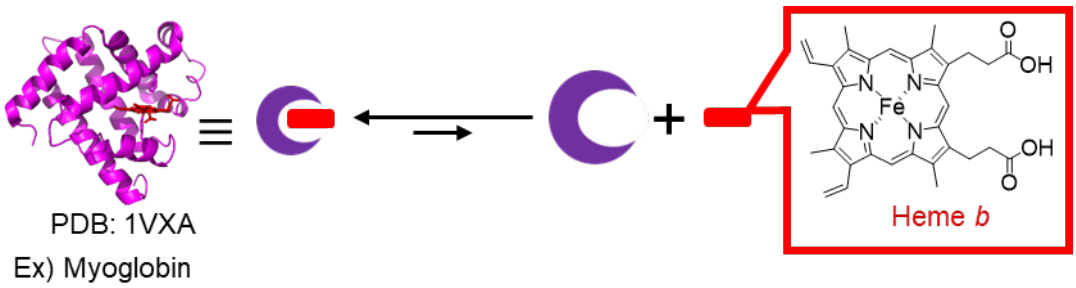

Figure 8. Schematic representation of the heme-binding in hemoprotein.

Several groups have individually reported hemoprotein assembling systems.[33] Hayashi and coworkers reported several types of artificial hemoprotein assemblies using heme–heme pocket interaction.[34] Cytochrome b_{562} (Cyt*b*), one of the simplest hemoproteins and has a 4-helix bundle structure with 106 amino acid residues and a heme *b* cofactor, is employed as a first building block. The physiological function is known to be electron transfer. To induce interprotein heme–heme pocket interaction, a cysteine residue of a Cyt*b* mutant was modified with a synthetic heme derivative tethering a maleimide moiety, resulting in a monomer having a covalently attached heme on the protein surface (Figure 9).[32] Fibrous supramolecular hemoprotein assembly spontaneously forms successive heme–heme pocket interactions after removal of native heme. AFM (atomic force microscopy) measurements indicated the formation of fibers with lengths of several hundred nanometers and heights of 5 nm, which is consistent with the total length of monomeric Cyt*b*. When this assembling strategy was applied to myoglobin, an oxygen binding hemoprotein, stability-tunable supramolecular polymer due to heme redox states or 6th ligand of the iron center was demonstrated.[35] A disulfide dimer of apomyoglobin is also a useful building block to form fibrous supramolecular assembly with synthetic heme dimer and fibrous copolymer with streptavidin via orthogonal protein–small molecule interactions as well as a hydrogel with heme-tethered polyacrylic acid.[36,37]

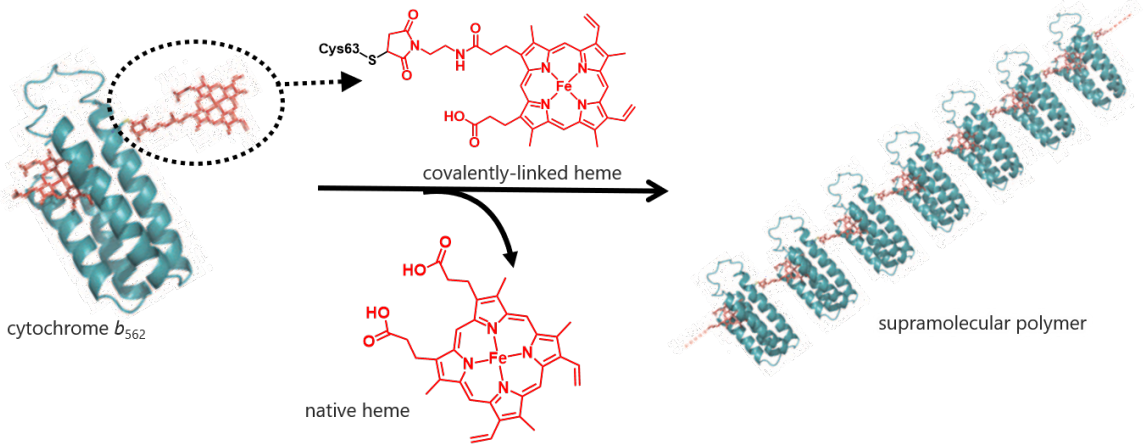

Figure 9. Schematic representation of supramolecular polymer using hemoprotein (Cyt*b*) as a building block.

Tezcan and coworkers reported hemoprotein oligomer via metal coordination.[38] They selected cytochrome *cb*$_{562}$ (Cyt*cb*), which is an engineered cytochrome *b*$_{562}$ (Cyt*b*) variant with a *c*-type heme covalently linked to the protein matrix through two thioether bonds in the heme-binding site. The artificial metal binding motifs were genetically and/or chemically introduced onto the protein surface of Cyt*cb*. Hemoprotein assemblies formed upon the addition of metal ions such as zinc, nickel and copper. Various defined structures such as tetramer[39] and trimer[40] of Cyt*cb* were revealed by X-ray crystallography (Figure 10). Giant assemblies that yield protein tubes and sheets were also produced by further protein engineering.[41]

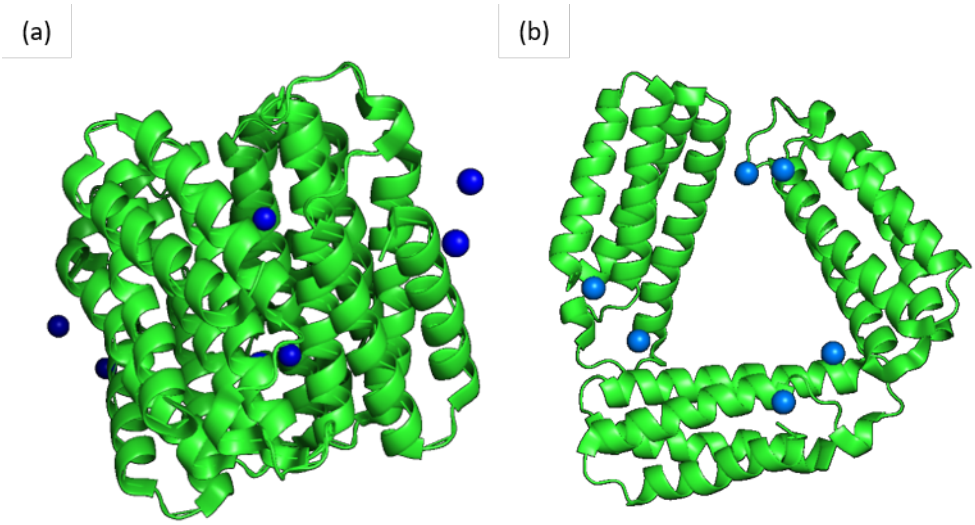

Figure 10. Crystal structures of Cyt*cb* homooligomer: (a) tetramer (PDB: 3HNJ), with zinc ions highlighted by blue and (b) trimer (PDB: 3FOO) with nickel ions highlighted by bule.

Hexameric tyrosine-coordinated heme protein

Hexameric tyrosine-coordinated heme protein, HTHP, from marine bacterium *Silicibacter pomeroyi* is a homo-hexameric hemoprotein with a ring-shaped structure first reported by Dobbek.[42] This hemoprotein has a relatively small molecular weight of 54 kDa as a hexamer (Figure 11). Positively charged residues are located around the heme-binding site, while the base of the cylindrical structure far from the heme-binding site is negatively charged. Physiological function of HTHP is unknown. Although iron centers of heme cofactors in HTHP are coordinated by tyrosine residues, similar to that in catalase, the catalytic activity of the protein for disproportionation of hydrogen peroxide is low. Peroxidase activity is low, whereas the replacement of the axial ligand by a histidine residue significantly enhances H_2O_2-dependent guaiacol oxidation activity.[43] Weidinger and coworkers determined the Fe^{II}/Fe^{III} redox potential of HTHP to be –0.54 V (vs Ag/AgCl),[44] indicating that the ferric state is energetically more favorable relative to the ferrous state. Scheller and coworkers immobilized HTHP on an electrode and evaluated its peroxidase activity.[45] According to unfavorable results for enzymatic reactions, heme storage and/or transport have been proposed because of its partial structural similarity to known heme transport proteins such as HasA and HmbR.[46]

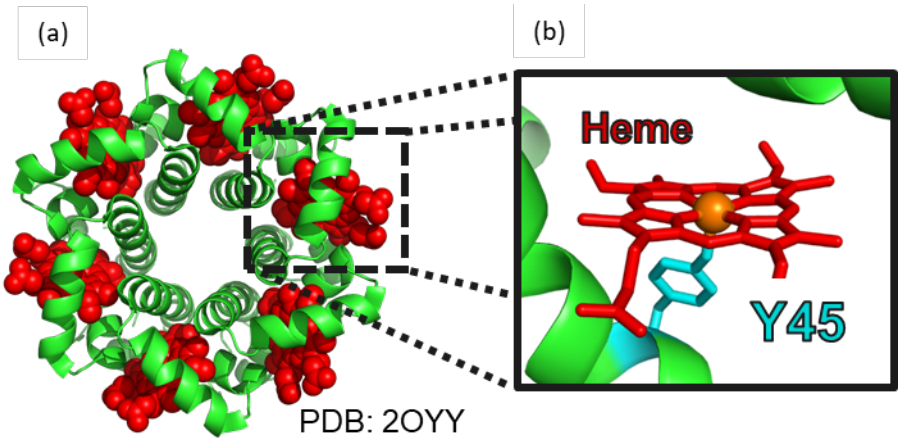

Figure 11. (a) Crystal structure of HTHP. (b) Structure of heme and the heme binding site.

The intrinsically stable oligomeric structure of HTHP is attractive to construct the artificial hemeprotein assembly. Hayashi and coworkers reported star-shaped supramolecular assembly consisting of the apo-form of HTHP and aforementioned supramolecular Cyt*b* polymer.[47] Furthermore, HTHP has been utilized as a scaffold for circular arrangement of pigments toward artificial light-harvesting systems because the natural light harvesting system of purple bacteria also has a circularly oriented chlorophyll array.[48] Each heme cofactor in an HTHP subunit was replaced with Zn porphyrin, a metal porphyrinoid photosensitizer. The fluorescence quenching titration indicated energy migration, a successive and rapid energy transfer event among the same chromophores. This finding demonstrated that HTHP is a useful scaffold to construct artificial light harvesting system. Toward huge light harvesting system similar to natural system, further assembling systems of HTHP have been investigated.[49]

β-Lactoglobulin

β-Lactoglobulin (BLG) is a whey protein with a molecular weight of approximately 18.4 kDa, that belongs to the lipocalin family. BLG is naturally abundant and easy to isolate, making it frequently used in physiological research. Several genetic variants of BLG have been discovered, particularly in bovine sources, including variants A and B. Variants A and B differ in their amino acid sequences at positions 64 (Asp/Gly) and 118 (Val/Ala). BLG is primarily composed of nine β-strands and a single α-helix at the C-terminal, where the eight β-strands form a β-barrel structure. Salmain and coworkers have constructed artificial metalloenzymes using BLG as a scaffold by introducing metal complexes with alkyl chains bound into this β-barrel.[51] Furthermore, BLG has two intramolecular disulfide bonds and one reactive cysteine residue (Cys121), where the reactive thiol group is located inside a small hydrophobic cavity surrounded by the three β-strands and an α-helix, as well as the N-terminus (Figure 12). Around the cavity, several amino acid residues have charged side chains, which become negatively charged with increasing pH, facilitating the access of positively charged reagents to the cavity. In

addition, the atomic fluctuations (*B*-factor in crystal structure) around the cavity as the pH increases, suggesting that the reactivity of Cys121 to chemical modification is kinetically enhanced. Moreover, it is also possible to enhance the reactivity of Cys121 by unfolding BLG. Hong and coworkers have successfully reacted the exposed Cys121 with tetraphenylethene carrying a maleimide group (TPE-NMI) by denaturing BLG with urea.[53] TPE-NMI does not normally show fluorescence, but it is known to exhibit fluorescence when bound to cysteine residues of proteins like BLG or enolase due to the disruption of n-π conjugation of the maleimide group and the restriction of benzene ring rotations. Thus, β-lactoglobulin is a useful building block for protein engineering.

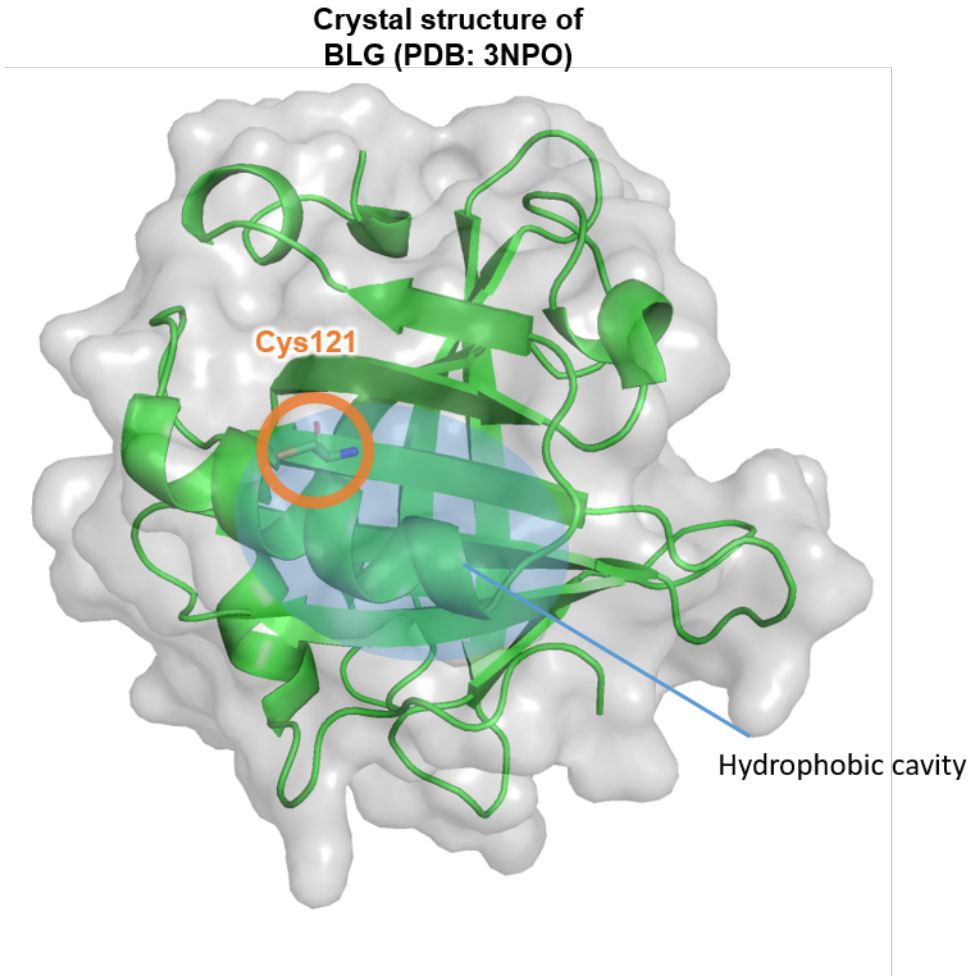

Figure 12. Crystal structure of β-lactoglobulin.

Outline of this thesis

Toward a new type of gel materials, the author focused on heme–heme pocket interaction in hemoprotein and mechanical structural changes of β-lactoglobulin (Figure 13). In this thesis, HTHP and BLG were employed as functional components of hydrogels. In chapters 1 and 2, the author describes the preparation of HTHP-based hydrogels and evaluation of their mechanical properties. Chapter 3 describes a BLG-based hydrogel toward compression-responsive materials.

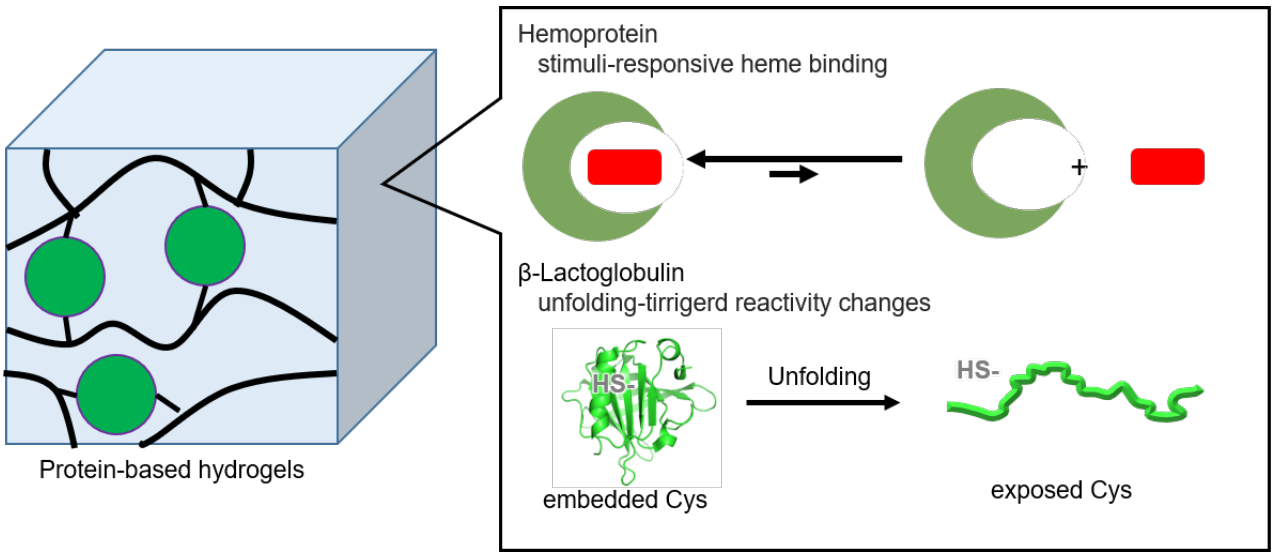

Figure 13. Concept of protein-based hydrogels in this thesis.

Chapter 1: Redox Responsive Hydrogel Containing an Engineered Hexameric Hemoprotein

A redox responsive hydrogel containing reconstituted HTHP (rHTHP) as a crosslinker unit was designed and prepared. Interaction between heme and heme pocket in Fe^{2+} and Fe^{3+} states was first evaluated to reveal the redox responsive behavior: heme–heme pocket interaction in HTHP significantly decreases upon the addition of reductant. Next, HTHP reconstituted with heme tethering an acryloyl group was prepared and utilized as a cross-linker for copolymerization with acrylamide to provide a hydrogel. The elastic properties of the gel decreased upon the addition of reductant. This is due to the weakening of the interaction between heme and heme pocket by the reduction of iron center.

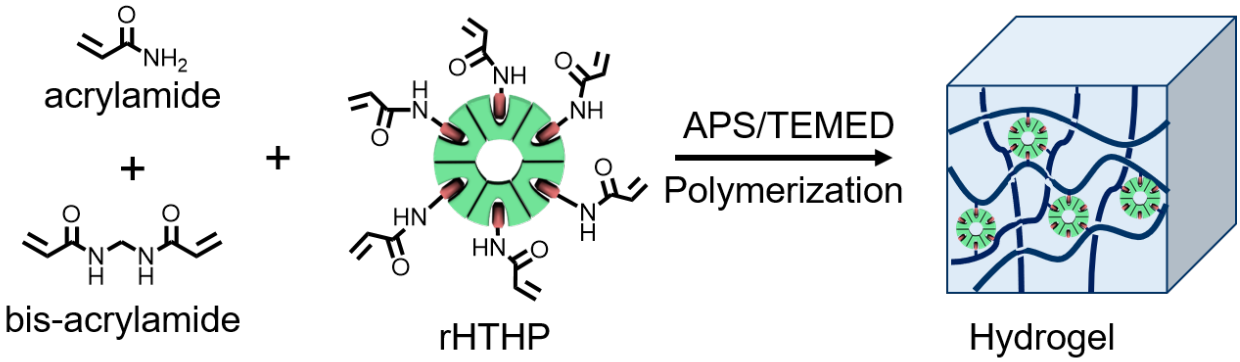

Chapter 2: Tuning Elasticity of a Hexameric Hemoprotein-based Hydrogel through Protein Building Block Mutations

The effects of mutation on heme–heme pocket interaction in HTHP was investigated toward tuning the mechanical properties of HTHP-based gels. Two arginine residues, Arg25 and Arg38, around the heme cofactor was found to be important for the heme binding in HTHP: R25A and R38A single mutants showed lower heme-binding affinities relative to the wild-type protein. Polyacrylamide gels containing the HTHP mutants were prepared, and the tensile testing of the mutant-based gels showed the decreased Young's moduli compared to the wild type-based gel. These results indicate a significant correlation between mechanical properties and the heme binding affinity for cross-linker units in HTHP-based gels.

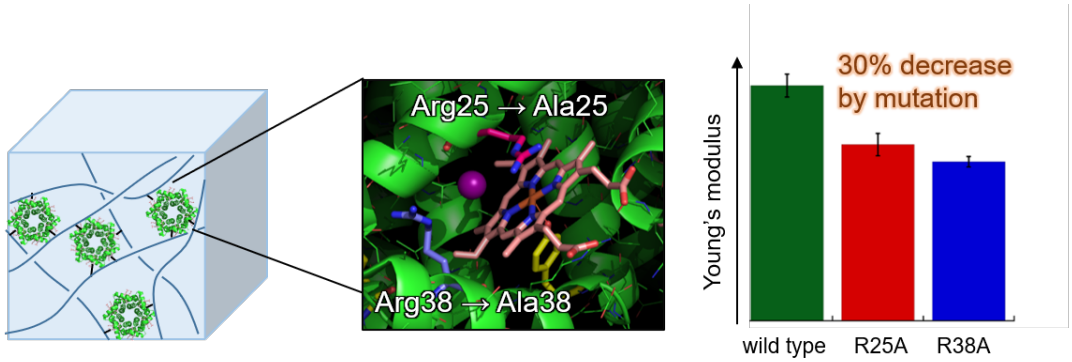

Gels containing hexameric hemoprotein cross-linkers

Chapter 3: Mechanochemical Responses of β-Lactoglobulin-based Hydrogels

BLG-based hydrogels were designed and prepared toward compression-induced chemical modification of protein. The BLG gels were prepared by the reaction of BLG with PEG tethering activated ester groups. The reactivity of an embedded cysteine residue at position 121 in BLG increased with unfolding triggered by compression of the gels, resulting in subsequent chemical modification with fluorescent molecule and protein via maleimide–cysteine coupling and disulfide bond formation, respectively.

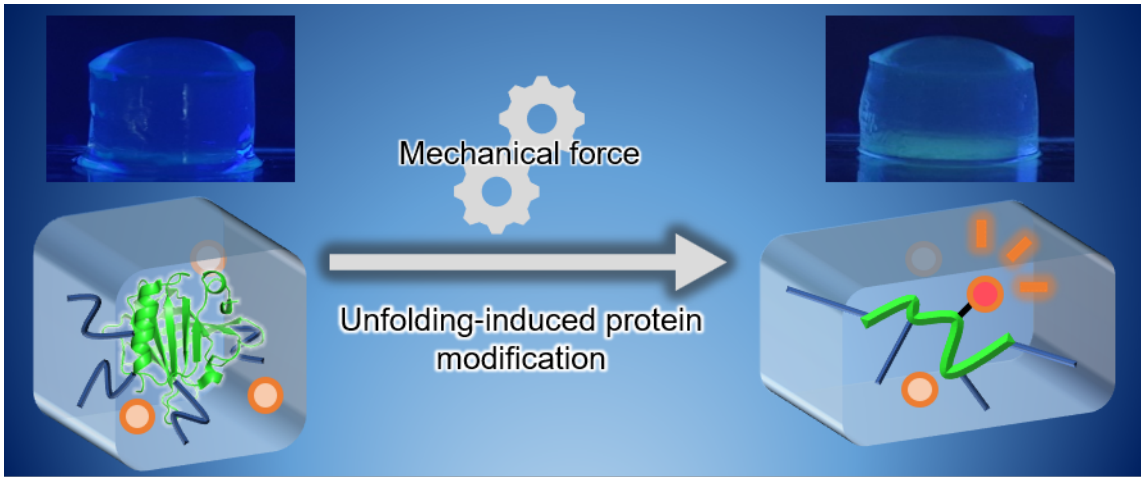

References

1 O. Wichterle, D. Lim, *Nature* **1960**, *185*, 117.

2 M. Shibayama, *Macromol. Chem*. *Phys.* **1998**, *199*, 1.

3 T. Sakai, T. Matsunaga, Y. Yamamoto, C. Ito, R. Yoshida, S. Suzuki, N. Sasaki, M. Shibayama, U. Chung, *Macromolecules* **2008**, *41*, 5379.

4 T. Matsunaga, T. Sakai, Y. Akagi, U. Chung, M. Shibayama, *Macromolecules* **2009**, *42*, 1344.

5 A. Sugimura, M. Asai, T. Matsunaga, Y. Akagi, T. Sakai, H. Noguchi, M. Shibayama, *Polym. J.* **2013**, *45*, 300.

6 X. Li, Y. Tsutsui, T. Matsunaga, M. Shibayama, U. Chung, T. Sakai, *Macromolecules* **2011**, *44*, 3567.

7 N. Roopsung, T. L. H. An, A. Sugawara, T. A. Asoh, Y. I. Hsu, H. Uyama, *Bull. Chem. Soc. Jpn.***2023**, *96*, 636.

8 T. Tanaka, *Sci. Am*. **1981**, *244*, 12.

9 T. Tanaka, *Phys. Rev. Lett.* **1978**, *40*, 820.

10 Suzuki, A.; Tanaka, T. *Nature* **1990**, *346*, 345.

11 G.Liu, Q. Yuan, G. Hollett, W. Zhao, Y. Kang, J. Wu, *Polym. Chem.* **2018**, *9*, 3436.

12 Y. Takashima, S.Hatanaka, M. Otsubo, M. Nakahata, T. Kakuta, A. Hashidzume, H. Yamaguchi, A. Harada, *Nat. Commun*. **2012**, *3*, 1270.

13 M. Nakahata, Y. Takashima, A Hashidzume, A. Harada, *Angew. Chem. Int. Ed*. **2013**, *52*, 5731.

14 T. Kakuta, Y. Takashima, M. Nakahata, M. Otsubo, H. Yamaguchi, A. Harada, *Adv. Mater.* **2013**, *25*, 2849.

15 H. D. Correia, S. Chowdhury, A. P. Ramos, L. Guy, G. J. Demets, C. Bucher, *Polym. Int.* **2019**, *68*, 572.

16 T. Abe, T. Itakura, N. Ikeda, K. Shinozaki, *Dalton Trans.* **2009**, 711.

17 Y. Sagara, T. Kato, *Nat. Chem*. **2019**, *1*, 605.

18 D. A. Davis, A. Hamilton, J. Yang, L. D. Cremar, D. V. Gough, S. L. Potisek, M. T. Ong, P. V. Braun, T. J. Martinez, S. R. White, J. S. Moore, N. R. Sottos, *Nature* **2009**, *459*, 68.

19 R. Merindol, G. Delechiave. L. Heinen, L. H. Catalani, A. Walther, *Nat. Commun*. **2019**, *10*, 528.

20 T. Miyata, N. Asami, T. Uragami, *Nature* **1999**, *399*, 766.

21 T. Miyata, A. Jikihara, K. Nakamae, A. S. Hoffman, *Macromol. Chem. Phys.* **1996**, *197*, 1135.

22 Y. Liang, K. L. Kiick, *Acta Biomater.* **2014**, *10*, 1588.

23 T. Miyata, N. Asami, T. Uragami, *J. Polym. Sci. Part B: Polym. Phys.* **2009**, *47*, 2144.

24 A. P. Esser-Kahn, A. T. Iavarone, M. B. Francis, *J. Am. Chem. Soc.* **2008**, *130*, 15820.

25 25)N. Bruns, K. Pustelny, L. M. Bergeron, T. A. Whitehead, D. S. Clark, *Angew. Chem. Int. Ed.* **2009**, *48*, 5666.

26 Y. Cao, H. Li*, Chem. Commun*. **2008**, 4144.

27 S. Lv, D. M. Dudek, Y. Cao, M. M. Balamurali, J. Gosline, H. Li, *Nature* **2010**, *465*, 69.

28 J. Fang, A. Mehlich, N. Koga, J. Huang, R. Koga, X. Gao, C. Hu, C. Jin, M. Rief, J. Kast, D. Baker,

H. Li, *Nat. Commun.* **2013**, *4*, 2974.
29 L. R. Khoury, L. Popa, *Nat. Commun*. **2019**, *10*, 5439.
30 C. J. Reedy, B. R. Gibney, *Chem. Rev.* **2004**, *104*, 617.
31 K. Oohora, A. Onoda, T. Hayashi, *Acc. Chem. Res.* **2019**, *52*, 945.
32 H. Kitagishi, Y. Kakikura, H. Yamaguchi, K. Oohora, A. Harada, T. Hayashi, *Angew. Chem. Int. Ed.* **2009**, *48*,1271.
33 K. Oohora, T. Hayashi, *Curr. Opin. Chem. Biol.* **2014**, *19*, 154.
34 K. Oohora, A. Onoda, T. Hayashi, *Chem. Commun.* **2012**, *48*, 11714.
35 K. Oohora, A. Onoda, H. Kitagishi, H. Yamaguchi, A. Harada, T. Hayashi, *Chem. Sci.* **2011**, *2*, 1033.
36 A. Onoda, A. Takahashi, K. Oohora, Y. Onuma, T. Hayashi, *Chem. Biodivers.* **2012**, *9*, 1684.
37 K. Oohora, S. Burazerovic, A. Onoda, Y. M. Wilson, T. R. Ward, T. Hayashi. *Angew. Chem. Int. Ed.* **2012**, *51*, 3818.
38 E. N. Salgado, R. J. Radford, F. A. Tezcan, *Acc. Chem. Res.* **2010**, *43*, 661.
39 E. N. Salgado, X. I. Ambroggio, J. D. Brodin, R. A. Lewis, B. Kuhlman, F. A. Tezcan, *Proc. Natl. Acad. Sci. USA*, **2010,** *107*, 1827.
40 R. J. Radford, F. A. Tezcan, *J. Am. Chem. Soc*. **2009**, *131*, 9136.
41 J. D. Brodin, X. I. Ambroggio, C. Tang, K. N. Parent, T. S. Baker, F. A. Tezcan, *Nat. Chem.* **2012**, *4*, 375.
42 J. H. Jeoung, D. A. Pippig, B. M. Martins, N. Wagener, H. Dobbek, *J. Mol. Biol.* **2007**, *368*, 1122.
43 T. Mashima, K. Oohora, T. Hayashi, *J. Porphyrins Phthalocyanines* **2017**, *21*, 824.
44 P. Kielb, T. Utesch, J. Kozuch, J.-H. Jeoung, H. Dobbek, M. A. Mroginski, P. Hildebrandt, I. Weidinger, *J. Phys. Chem. B* **2017**, *121*, 3955.
45 L. Peng, T. Utesch, A. Yarman, J. Jeoung, S. Steinborn, H. Dobbek, M. A. Mroginski, J. Tanne, U. Wollenberger, F. W. Scheller, *Chem. Eur. J.* **2015**, *21*, 7596.
46 M. Kanadani, T. Sato, T. Hino, S. Nagano, S. Ozaki, *J. Inorg. Biochem*. **2015**, *151*, 26.
47 J. W. Soon, K. Oohora, S. Hirayama, T. Hayashi, *Int. J. Mol. Sci*. **2021**, *22*, 1012.
48 K. Oohora, T. Mashima, K. Ohkubo, S. Fukuzumi, T. Hayashi, *Chem. Commun.* **2015**, *51*, 11138.
49 S. Hirayama, K. Oohora, T. Uchihashi, T. Hayashi, *J. Am. Chem. Soc.* **2020**, *142*, 1822.
50 S. Brownlow, J. H. M. Cabral, R. Cooper, D. R. Flower, S. J. Yewdall, I. Polikarpov, A. C. North, L. Sawyer, *Structure* **1997**, *5*, 481.
51 A. Chevalley, M. V. Cherrier, J. C. Fontecilla-Camps, M. Ghasemi, M. Salmain, *Dalton Trans.* **2014**, *43*, 5482.
52 B. Y. Qin, M. C. Bewley, L. K. Creamer, H. M. Baker, E. N. Baker, G. B. Jameson, *Biochemistry* **1998**, *37*, 14014–14023.
53 S. Zhang, M. Liu, L. Y. F. Tan, Q. Hong, Z. L. Pow, T. C. Owyong, S. Ding, W. W. H. Wong, Y. Hong, *Chem. Asian J.* **2019**, *14*, 904.

Chapter 1
Redox Responsive Hydrogel Containing an Engineered Hexameric Hemoprotein

Reproduced in part with permission from [*RSC. Adv.* **2023**, *13*, 34610–34617.]
DOI: 10.1039/D3RA05897B

1-1. Introduction

Stimuli-responsive hydrogels demonstrate changes in the physicochemical properties, volumes, and/or shapes triggered by external stimuli such as temperature, chemicals, pH, ionic strength, electric field/voltage/current, and light intensity.[1–3] These properties have been widely expected to be harnessed in fabrication of smart biomaterials for use in chemical sensors, actuators, and other applications.[4] Efforts to develop stimuli-responsive materials have focused on rational design of composites of functional molecules and polymeric matrices.[5–7] In the polymer network, several functional molecules provide non-covalent connections including hydrophobic,[8] hydrogen bonding,[9,10] π–π,[11,12] electrostatic,[13] coordination,[14–17] and host-guest interactions.[18–21] In particular, a series of stimuli-responsive hydrogels containing cyclodextrin-based host-guest systems have been demonstrated by Harada and co-workers. Various combinations with guest molecules such as azobenzene[22] and ferrocene[23] have produced photo- and redox-responsive hydrogels. Furthermore, other host molecules, crown ethers,[24,25] cucurbit[n]urils,[26–28] calix[n]arenes,[29–31] and pillar[n]arenes,[32–34] have been employed to provide stimuli responsive interactions, leading to the development of various stimuli-responsive gels.[35]

Proteins are also potent building blocks due to their attractive properties. Protein-based hydrogels and elastomers have been prepared by taking advantage of covalent connections as well as supramolecular linkages.[36–40] Folding and denaturation properties in protein units provide unique mechanical properties and responsiveness to stimuli. Miyata and co-workers utilized the supramolecular interaction between a protein and small molecules to generate a cross-linking unit of a gel.[41–47] A polyacrylamide gel formed by strong and specific interaction between antibody and antigen has been demonstrated to display swelling behavior upon the addition of free-antigen.[41] In another example, a biotin-attached four-armed poly(ethylene glycol) was reacted with avidin to demonstrate supramolecular gelation via the biotin-avidin interaction.[45] Further addition of free biotin induces its dissociation to a sol state. Similarly, the glucose–lectin concanavalin A interaction[46,47] was found to serve as a cross linkage for gelation as well as providing peptide–protein interactions.[48–50] The specific molecular binding behavior of proteins provides gel systems with useful properties for applications in chemical sensors and drug delivery systems.[51,52]

The heme–heme pocket interaction in hemoproteins is known as one of the most stable supramolecular interactions in biological systems.[53–55] Unique stimuli-responsive properties are expected to be provided by materials that have a heme–heme pocket interaction because the affinity

depends on the properties of the sixth ligand and the redox states of the iron center.[53,54,56,57] Hayashi and co-workers have reported a series of supramolecular hemoprotein assembling systems driven by successive heme–heme pocket interactions.[58–62] In particular, the supramolecular assembly of myoglobin (Mb), a dioxygen binding hemoprotein, demonstrates stimuli-responsive stability.[62] The interaction was also utilized to provide a connection between a gel containing the apo-form of heme-dependent peroxidase and a gel containing heme moieties, indicating that an enzymatic reaction can occur at the gel interface.[63] The heme–heme pocket interaction has been recognized as an attractive cross linkage of the polymer network in hydrogels. In his previous work, supramolecular hydrogels were prepared by heme-tethering of polyacrylic acid and the apo-form of the Mb dimer.[64] However, the low solubility of the heme-tethering polymer and the intrinsically monomeric structure of Mb have imposed limits on further investigations. In the present work, the author focuses on development of hexameric tyrosine coordinated heme protein (HTHP),[65] an intrinsically oligomeric hemoprotein, as a cross-linking unit for a redox-responsive polyacrylamide hydrogel (Figure 1-1). The axial ligand of the heme cofactor in each monomer of HTHP is a tyrosine residue located at position 45 of the protein. The Fe(III) state is highly stabilized in tyrosine-coordinated hemoproteins,[66] inspiring significantly redox-dependent heme-binding behavior. Furthermore, the remarkably high thermal stability (T_m > 130 °C) and the ability to replace heme with synthetic cofactors are useful features for development of a cross-linking unit.[65,67,68] In this study, the author demonstrates the preparation of a gel by copolymerization of acrylamide with an engineered HTHP as a cross-linking unit and evaluate its redox-responsive behavior.

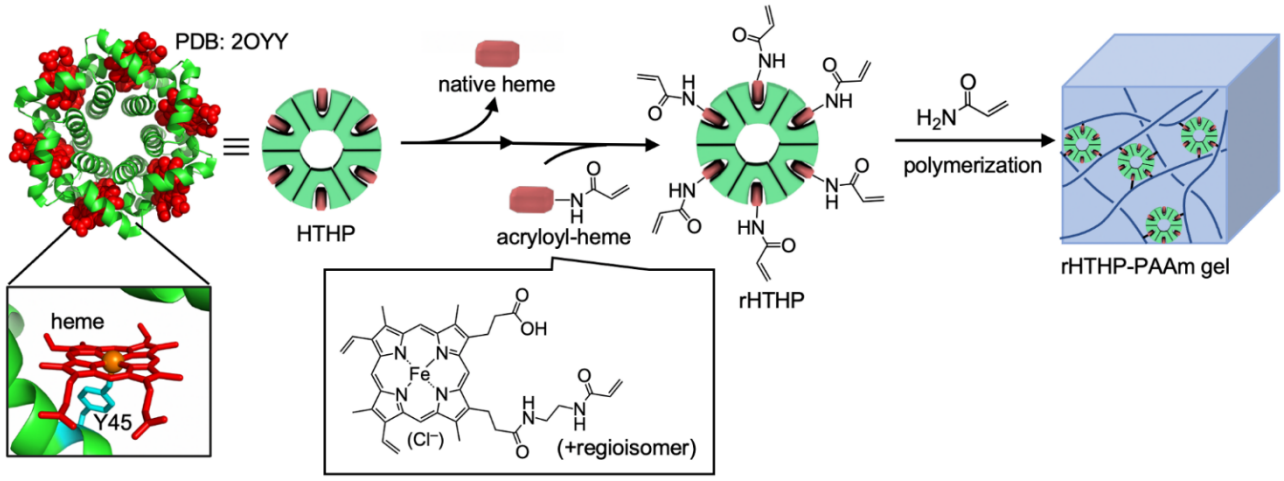

Figure 1-1 Schematic representation for preparation of HTHP reconstituted with acryloyl-heme (rHTHP) and a polyacrylamide gel containing rHTHP (rHTHP-PAAm gel).

1-2. Results and discussion

1-2-1. Evaluation of heme–heme pocket interaction in Fe(II) and Fe(III) states of HTHP

Redox-dependent heme-binding behavior of HTHP was first investigated. The iron center of HTHP is in the Fe(III) state under ambient conditions, whereas the Fe(II) state is obtained upon the addition of dithionite as a reductant. The UV-vis spectrum of the Fe(III) state of HTHP displays a strong absorption Soret band at 402 nm and several Q band peaks near 550 and 620 nm. Upon conversion to the Fe(II) state of HTHP, the Soret band shifts to 420 nm and the Q bands shift to 559 and 590 nm.[34] Circular dichroism (CD) spectra of the Fe(III) and Fe(II) states of HTHP were also measured. In the Fe(III) state, an obvious CD signal at 418 nm is observed due to the chiral heme-binding sites of HTHP (Figure 1-2a).[66] Upon addition of dithionite, this CD signal shifts to 438 nm, indicating that the Fe(II) states of heme molecules are also bound in the protein matrix of HTHP (Figure1-3b). Next, ΔG^{o}, the energy gap in heme dissociation from the HTHP matrix, was evaluated to assess the stability of the heme–heme pocket interaction in HTHP (Figure 1-3a), because the ΔG^{o} values are known to represent a thermodynamic parameter indicating the stability of folding in proteins as well as heme-binding in hemoproteins.[57,69–71] The ΔG^{o} values were determined by titration of guanidium chloride (GdmCl), a chemical denaturant, into a solution of wild-type HTHP in potassium phosphate buffer at pH 7.0.[72]

Due to HTHP's high thermodynamic stability, the author used severe denaturing conditions at a high temperature of 90 ºC. Figure 1-3b shows plots of normalized CD signal changes of the Fe(III) state of HTHP in the presence of various concentrations of GdmCl. The two-state equilibrium transition is considered as below:

$$\text{heme-bound state} \rightleftharpoons \text{unbound state} \qquad (1)$$

In Figure 1-3b, a clear decrease of the CD intensity in the Fe(III) state was observed in the concentration range of 4.0 M to 5.8 M GdmCl. This indicates that the heme-bound state at 4.0 M GdmCl converts to the unbound state at 5.8 M GdmCl. The equilibrium constants at each GdmCl concentration were calculated using the following equation:

$$F_B(C) = 1 - F_U(C) = (y_x(C) - y_U(C)) / (y_B(C) - y_U(C)) \qquad (2)$$

where $F_B(C)$ and $F_U(C)$ represent fractions of the heme-bound and unbound states, respectively, at a given GdmCl concentration (C). $y_x(C)$ is an observed CD signal intensity at a GdmCl concentration (C). $y_B(C)$ and $y_U(C)$ are the dependencies of the assumed CD signal intensities on denaturant concentrations for the fully heme-bound and unbound states, respectively. Subsequently, the equilibrium constants, K_{eq}, were determined as:

$$K_{eq}(C) = F_B(C) / F_U(C) = (y_x(C) - y_U(C)) / (y_B(C) - y_x(C)) \qquad (3)$$

The $K_{eq}(C)$ values were converted into $\Delta G^{o}(C)$ values using equation (4), as follows:

$$\Delta G^{o}(C) = -RT \ln K_{eq}(C) \qquad (4)$$

The ΔG^{o} value in the absence of chemical denaturant was determined as the y-intercept of the linear extrapolation model,[72] as shown in Figure 1-3c. The ΔG^{o} value for heme binding in the Fe(III) state of HTHP was determined to be –57 kJ/mol. In the presence of an excess amount of dithionite at 25 ºC, ΔG^{o} for the Fe(II) state of HTHP was also determined to be –25 kJ/mol. For reference, the ΔG^{o} values for the Fe(II) and Fe(III) states of Mb were evaluated using UV-vis spectral changes which occur upon addition of GdmCl. The ΔG^{o} values are summarized in Table 1-1. The ΔG^{o} value of HTHP in the Fe(III) state is notably lower than that of other hemoproteins such as Mb (–45.7 kJ/mol)[70] or cytochrome b_{562} (–46 kJ/mol).[71] In the case of Mb, which has a histidine residue as an axial ligand of heme, the Fe(II) state is more stable than the Fe(III) state. In contrast, the Fe(II) state of HTHP exhibits weakened heme binding, possibly because the heme cofactors are coordinated by phenolate moieties derived from tyrosine residues in HTHP. The high energy difference of heme binding between the Fe(II) and Fe(III) states corresponds to the Fe(II)/Fe(III) redox potential of HTHP at –0.54 V (vs. Ag/AgCl).[73]

Table 1-1. ΔG^{o} values of HTHP and Mb in different redox states

Hemoprotein	Redox state	ΔG^{o} (kJ/mol)
HTHP	Fe(III)	–57 ± 6[a]
HTHP	Fe(II)	–25 ± 2[b]
Mb	Fe(III)	–46 ± 4[c]
Mb	Fe(II)	–49 ± 2[d]

[a] The ΔG^{o} values were determined by the CD signal changes at 90 ºC. [b] The ΔG^{o} values were determined the CD signal changes at 25 ºC in the presence of excess dithionite. [c] The ΔG^{o} values were determined by UV-vis absorbance changes at 25 ºC. [d] The ΔG^{o} values were determined by UV-vis absorbance changes in the presence of 100 mM dithionite at 25 ºC

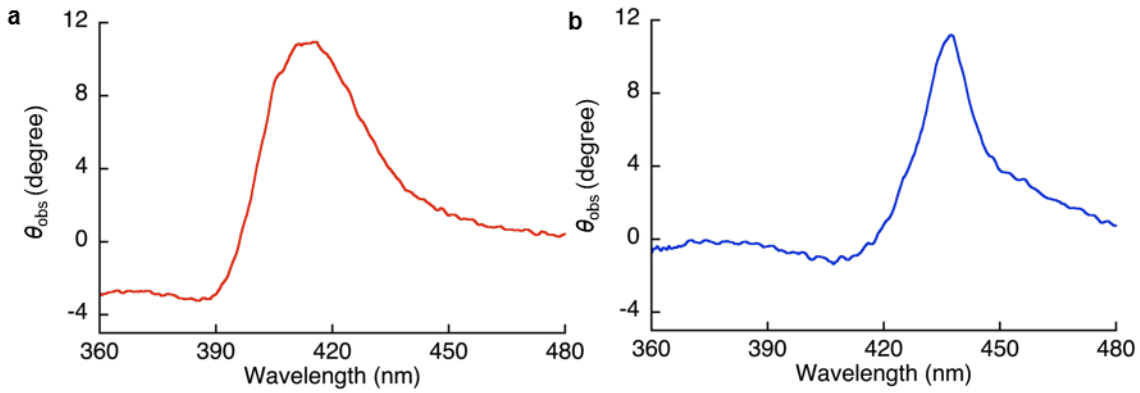

Figure 1-2. CD spectra of HTHP in (a) Fe(III) state and (b) Fe(II) state in 100 mM potassium phosphate buffer.

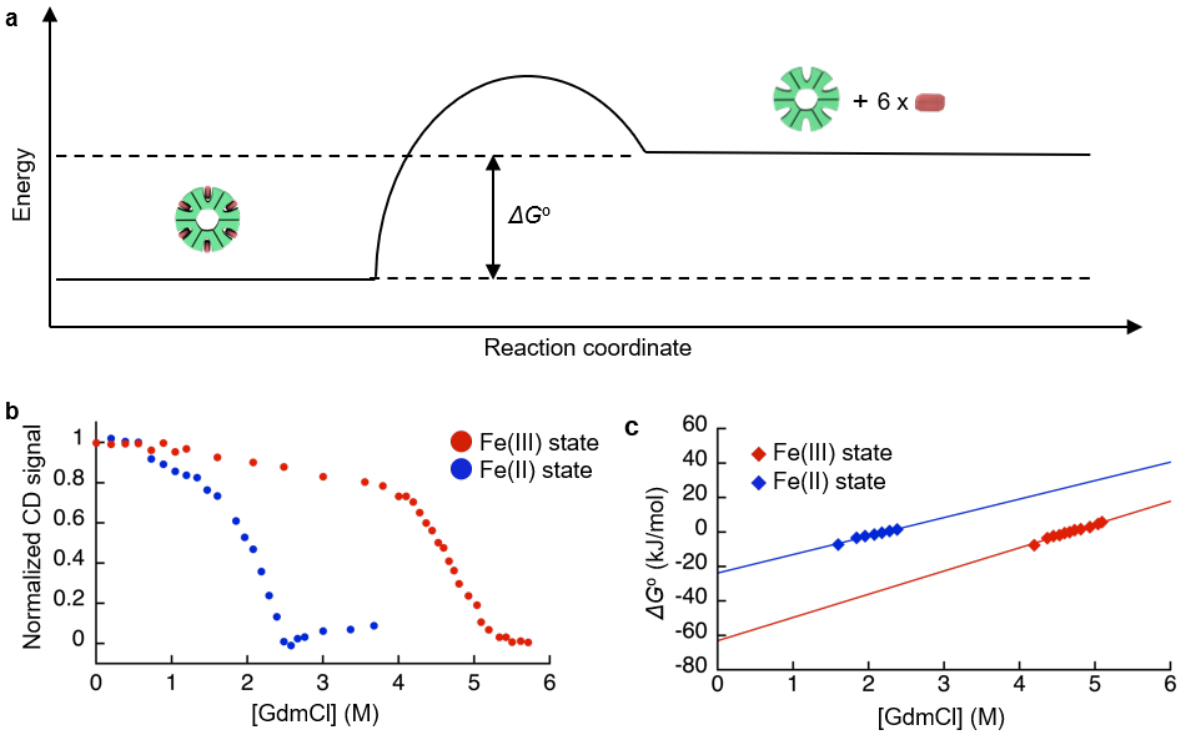

Figure 1-3. (a) Schematic energy diagram of heme binding in HTHP. (b) CD signal changes of the Fe(III) and Fe(II) states of HTHP upon addition of various concentration of GdmCl. (c) Plots of ΔG^{o} values of the Fe(III) and Fe(II) states of HTHP against concentration of GdmCl. Conditions: 100 mM potassium phosphate buffer, pH 7.0, at 90 °C (Fe(III) state) or 25 °C (Fe(II) state).

1-2-2. Preparation of a polyacrylamide gel containing an engineered HTHP as a cross-linking unit

Reactive moieties were introduced into HTHP to convert it to a cross-linking unit for a polyacrylamide gel and HTHP was reconstituted with an artificial cofactor. In this context, acryloyl-heme was designed and synthesized, in which heme b has an acryloyl group attached to to one of the heme-propionate side chains via an ethylene diamine linker unit. This freebase precursor was characterized by ^{1}H NMR and ESI MS, and the acryloyl-heme unit was confirmed by ESI-MS and UV-vis spectroscopy. Preparation of apoHTHP and its reconstitution were conducted using conventional methods (Figure 1-1).[67] Acryloyl-heme, dissolved in DMSO was added to the apo-form of HTHP (apo-HTHP) in a 100 mM potassium phosphate buffer, pH 7.0, containing 1 M NaCl, potentially enhancing hydrophobic interaction between acryloyl-heme and the heme pocket of HTHP. The obtained protein, reconstituted HTHP (rHTHP), was characterized using UV-vis spectroscopy. The R_z value (ratio of absorbances at 402 nm and 280 nm) is similar to that of the holo-form of HTHP (Figure 1-4a). The CD spectrum in the far-UV region indicates the typical α-helical structure of HTHP (Figure 1-4b). Analytical size exclusion chromatography of rHTHP shows a similar elution volume as wild type HTHP (Figure 1-5), indicating that the hexameric structure is maintained.

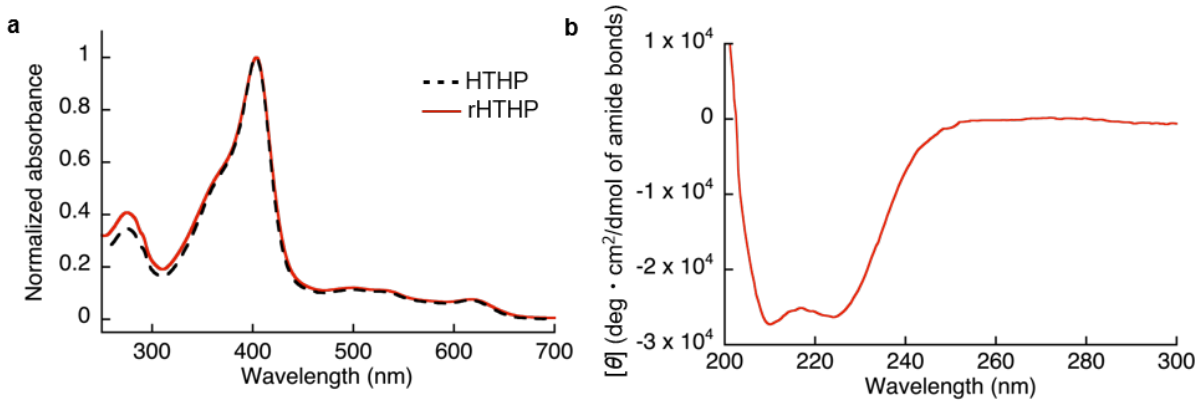

Figure 1-4. (a) UV-vis absorption spectra of the Fe(III) states of wild type and rHTHP in 100 mM potassium phosphate buffer, pH 7.0, containing 1 M NaCl, (b) Far-UV CD spectrum of rHTHP in 100 mM potassium buffer, pH7.0.

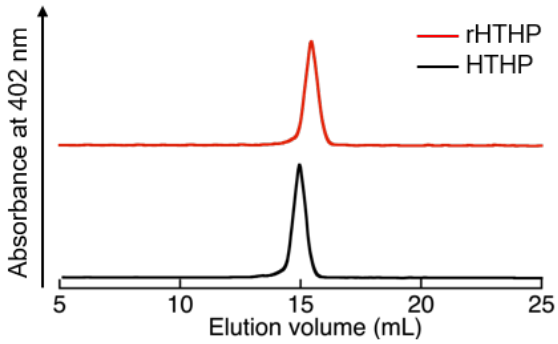

Figure 1-5. Size exclusion chromatography traces of HTHP and rHTHP. Eluent: 100 mM potassium buffer, pH 7.0, temperature: 4 ºC, column: Superdex^{TM} 200 increase 10/300 GL (GE healthcare).

Copolymerization of acrylamide with rHTHP as a cross-linking unit was performed using conventional radical polymerization in the presence of ammonium persulfate and *N,N,N',N'*-tetramethylethylenediamine. Interestingly, gelation occurred within a few hours without the support of other covalent cross-linkers such as methylene bis-acrylamide. Figure 1-6a displays a representative image of the polyacrylamide gel containing rHTHP (rHTHP-PAAm gel). A control experiment using HTHP instead of rHTHP did not produce a gel. This observation confirms that rHTHP acts as a cross-linking unit. The UV-vis spectrum of the gel has a Soret band near 400 nm and Q-bands near 500 nm (Figure 1-6b), which are typical bands for the heme cofactors bound into each HTHP matrix. This suggests that the radical polymerization reaction does not significantly affect the environment of the heme cofactor in rHTHP.

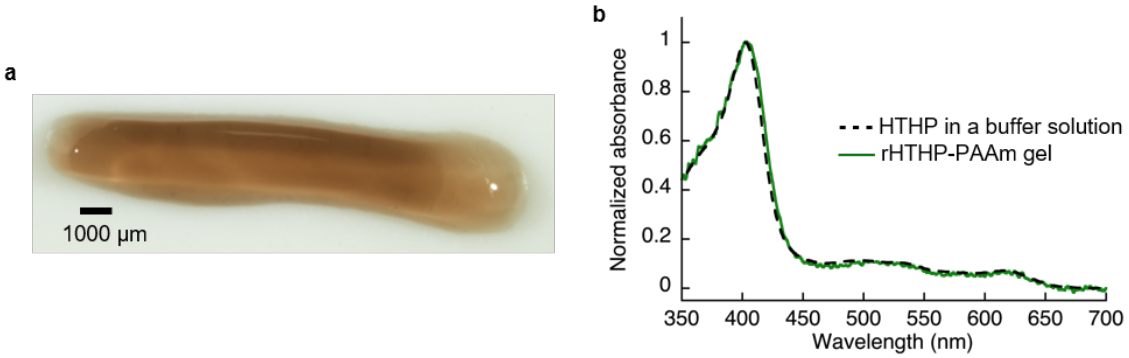

Figure 1-6. (a) Photograph of rHTHP-PAAm gel, (b) UV-vis absorption spectra of the Fe(III) states of rHTHP-PAAm gel and HTHP in solution.

1-2-3. Gel-sol transition in rHTHP-PAAm gel induced by a heme-transfer event using the apo-form of Mb

As shown in Table 1-1, the author characterized the cross linkage provided by the heme–heme pocket interaction in the gel, noting the high energy gap of the heme binding between Mb and HTHP in the Fe(II) states. This observation encouraged us to reconstitute the apo-form of Mb (apoMb) with heme in the Fe(II) state, as depicted in Figure 1-7a. This type of heme-transfer event was previously utilized for removal of heme in cytochrome P450-BM3 upon the addition of apoMb in the Fe(II) state.[74] First, the heme transfer reaction from HTHP to apoMb was attempted in solution. The UV-vis spectral changes of the Fe(II) state of HTHP were monitored upon the addition of excess apo-Mb at room temperature.

The characteristic spectrum of the Q-band of the Fe(II) state of HTHP was converted within one hour, revealing a spectrum consistent with that of the Fe(II) state of Mb (Figure 1-7b). This finding clearly indicates that the Fe(II) state of the heme cofactor was transferred from HTHP to apoMb, following the determined energy difference in the heme-binding process. Next, this experiment was applied to the rHTHP-PAAm gel (Figure 1-7c). The gel with a height of 3 mm and a diameter of 6 mm was prepared in a small vial, as shown in Figure 1-7d. When the vial was inverted, the rHTHP-PAAm

gel was located at the bottom of the vial. A 0.1 mM apoMb solution was then added to the vial. After 3 hours, apoMb diffused into the gel and the gel state was maintained and located at the bottom of the inverted vial. Into this mixture, an equal volume of a 200 mM dithionite solution was added. Interestingly, the gel was observed to change to the sol state upon gentle shaking. These behaviors were caused by reduction-triggered heme transfer from HTHP to apo-Mb, leading to the decomposition of the cross linkage in the polymer network. Furthermore, the UV-vis spectrum of the resulting solution is consistent with that of Fe(II) state of Mb (Figure 1-8). This type of gel-sol transition is typical for hydrogels containing supramolecular interactions as cross linkages, demonstrating that the heme–heme pocket interaction in rHTHP is the principal cross linkage formed in the gelation process.

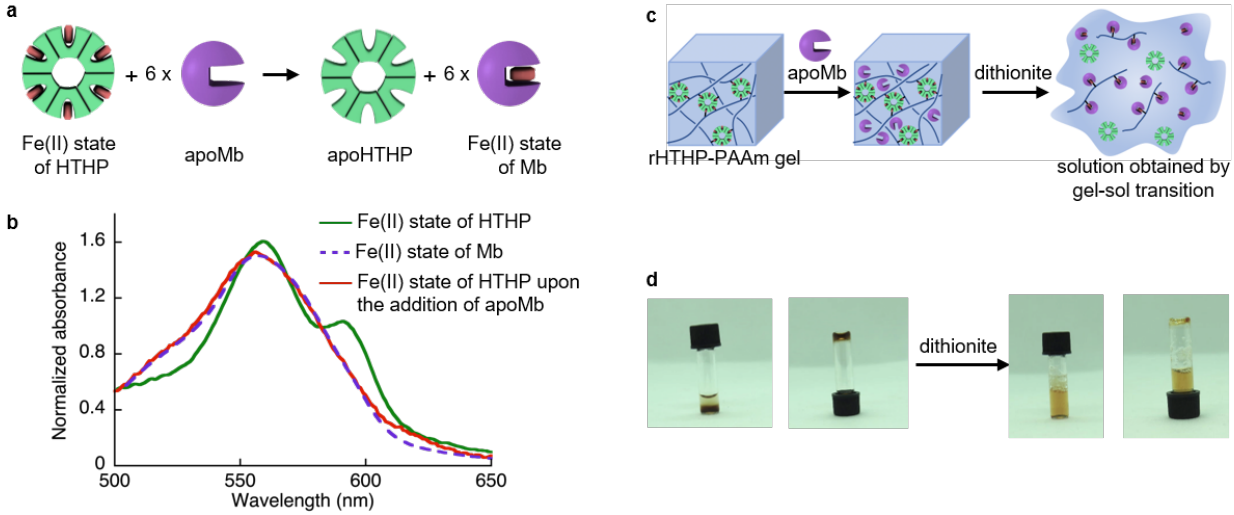

Figure 1-7. (a) Scheme of a heme-transfer event from Fe(II) state of HTHP to apoMb. (b) Absorption spectra of the Fe(II) state of HTHP (green solid line), the Fe(II) state of Mb (purple broken line) and the Fe(II) state of HTHP upon the addition of apoMb (red solid line) in 100 mM potassium phosphate buffer, pH 7.0. (c) Scheme of gel-sol transition by the reduction-triggered heme transfer in the presence of apoMb. (d) Photographs of the gel-sol transition experiment. The left-side photographs show the Fe(III) state of rHTHP-PAAm gel immersed in apoMb solution. The right-side photographs show the solution obtained by liquefaction of rHTHP-PAAm gel containing apo Mb upon addition of 200 mM dithionite solution.

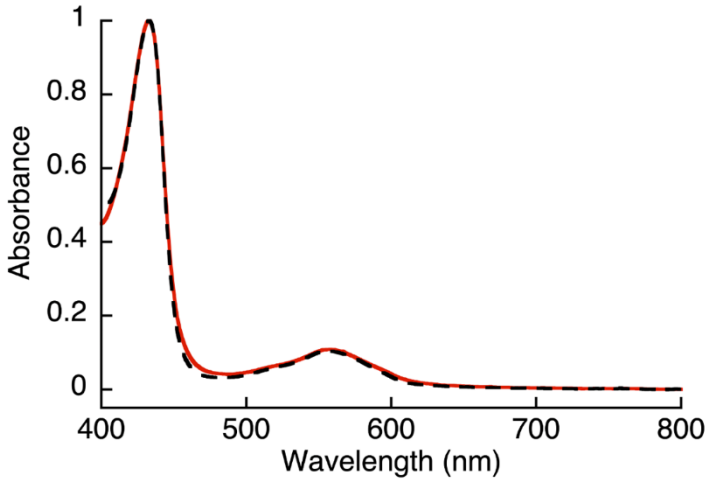

Figure 1-8. UV-vis absorption spectra of a solution obtained upon the addition of dithionite into the rHTHP-PAAm gel containing apoMb (red solid line) and the Fe(II) state of Mb in a buffer solution (black broken line).

1-2-4. Mechanical properties of the gel containing rHTHP and its redox responsiveness

The mechanical properties of the gels were investigated. Initially, an evaluation of the polyacrylamide gel containing rHTHP as a cross-linking unit was attempted, but the gel was too fragile to quantify the properties. Therefore, a dual cross-linked gel was prepared by radical polymerization of 1.0 M acrylamide with 1.5 mM rHTHP and 5.0 mM *N,N′*-methylene bis-acrylamide as cross-linking units (Figure 1-9). The obtained gel, which the author designates "rHTHP-MBA-PAAm gel," exhibits sufficient toughness to conduct a mechanical evaluation. As a control sample, the gel prepared without rHTHP, MBA-PAAm gel, was also investigated. The tensile tests of the gels were carried out at a strain speed of 10 mm/min. The gels were swollen in a buffer solution overnight at room temperature to reach the equilibrium state before obtaining measurements. Figure 1-10a shows the stress-strain curves of the gels. The Young's modulus value was determined as a slope of the curve from 0% to 10% of the rupture points. The rupture energy was calculated as the area under the curve representing the gel deformation until rupture. The Young's modulus and rupture energy values are summarized in Figure 1-10b and c, respectively. The Young's modulus values of MBA-PAAm gel and rHTHP-MBA-PAAm gel were determined to be 8.5 kPa and 14 kPa, respectively. The elastic property of the rHTHP-MBA-PAAm gel is obviously higher than that of the MBA-PAAm gel. The rupture energies of MBA-PAAm gel and rHTHP-MBA-PAAm gel were determined to be 8.8 kJ/m^3 and 11 kJ/m^3, respectively. The heme–heme pocket interaction of rHTHP which provides the cross linkage in the gel contributes to enhancement of the mechanical property of the gel due to increased cross-linking density.[75,76]

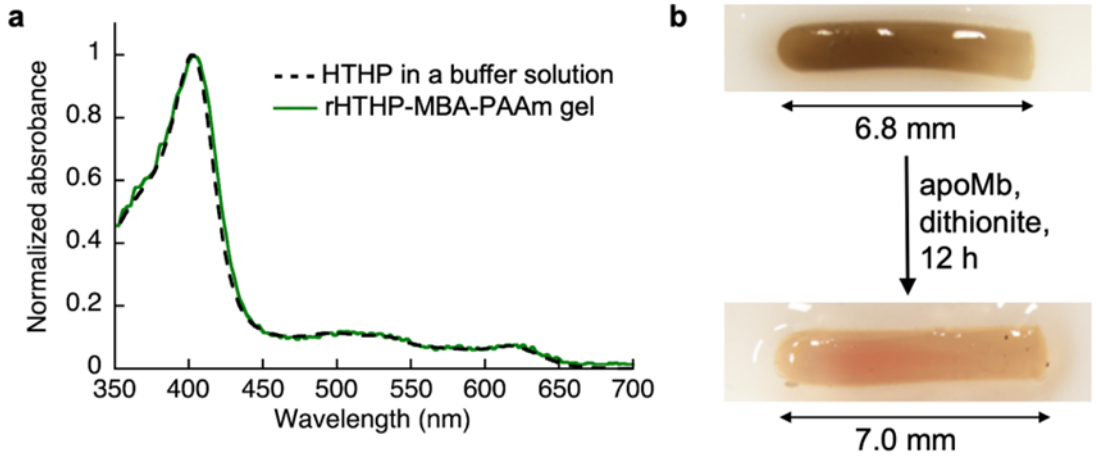

Figure 1-9. (a) UV-vis absorption spectra of the Fe(III) states of rHTHP-MBA-PAAm gel and HTHP in a buffer solution. (b) Photographs of the Fe(III) state of rHTHP-MBA-PAAm gel (top) and the gel after soaking into a solution containing apoMb and dithionite for 12 h (bottom). In contrast to the gel-sol transition of the rHTHP-PAAm gel, the gel state was maintained by the reduction in the presence of apoMb due to a covalent cross linkage but the gel was slightly swollen.

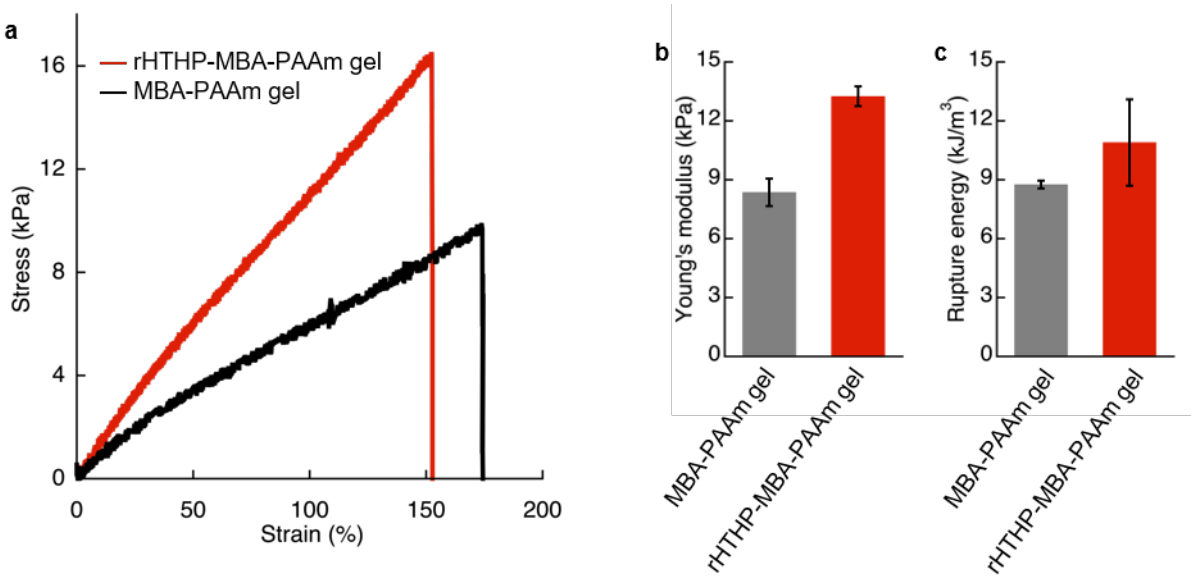

Figure 1-10. (a) Stress-strain curves obtained by tensile tests of the Fe(III) state of rHTHP-MBA-PAAm gel (red) and MBA-PAAm gel (black). (b) Young's modulus of rHTHP-MBA-PAAm gel and MBA-PAAm gel. (c) Rupture energy of rHTHP-MBA-PAAm gel and MBA-PAAm gel.

Since the heme binding in HTHP strongly depends on the redox states of the iron center, the mechanical properties of the gel containing rHTHP were evaluated in the Fe(II) and Fe(III) states. Due to the easily oxidized feature of the Fe(II) states of HTHP in air, the gel sample must be rapidly evaluated. Thus, a compression test was employed. First, reduction of the iron center in the rHTHP-MBA-PAAm gel was carried out by soaking a cylindrical gel into a buffer solution, pH 7.0, containing excess dithionite as shown in Figures 1-11a,b. No significant differences in size were observed with or without dithionite. The reduction of the iron center was confirmed by UV-vis spectra of the gel: the peaks near 500 nm are consistent with the peaks of the characteristic Q bands of the Fe(II) state HTHP in a solution (Figure 1-11c). Compression tests of the gels with or without dithionite were conducted at a 0.05 mm/s loading rate up to 60% height changes (Figure 1-12). The compressive modulus values were determined by slopes during the decrease in height ranging from 0% to 40%. Figure 1-11d summarizes the compressive modulus values. The compressive modulus values of the rHTHP-MBA-PAAm gels containing the Fe(III) and Fe(II) states of heme are 11 kPa and 8.5 kPa, respectively. The reduction of the iron center significantly decreases the compressive modulus without changes in size. This finding ruled out changes in modulus due to differences in water content. The decrease of compressive modulus due to reduction appears to correspond to the redox-dependent heme binding in HTHP. Although mechanical properties of the gel are typically regulated by swelling of the gels and/or interactions between main-chain polymers, the present result is mainly caused by a cross-linking unit of the gel. This indicates that the heme–heme pocket interaction in HTHP provides a sufficiently stable cross linkage to affect the mechanical property. To the best of this knowledge, this is the first demonstration of a stimuli-responsive hydrogel triggered by a redox-dependent heme–heme pocket interaction.

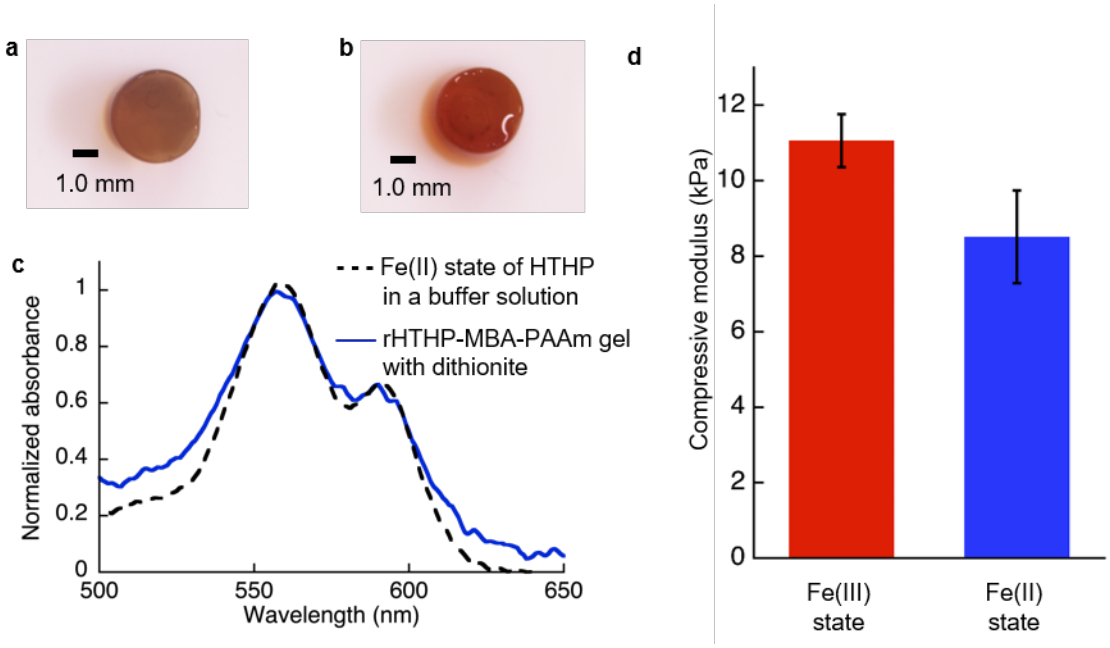

Figure 1-11. (a) Photograph of the Fe(III) state of the rHTHP-MBA-PAAm gel. (b) Photograph of the rHTHP-MBA-PAAm gel soaked in 50 mM dithionite solution for 2 h. (c) UV-vis spectra of the Fe(II) state of HTHP in a solution (black broken line) and rHTHP-MBA-PAAm gel with dithionite (blue solid line). (d) Compressive modulus of the Fe(III) and Fe(II) states of rHTHP-MBA-PAAm gels.

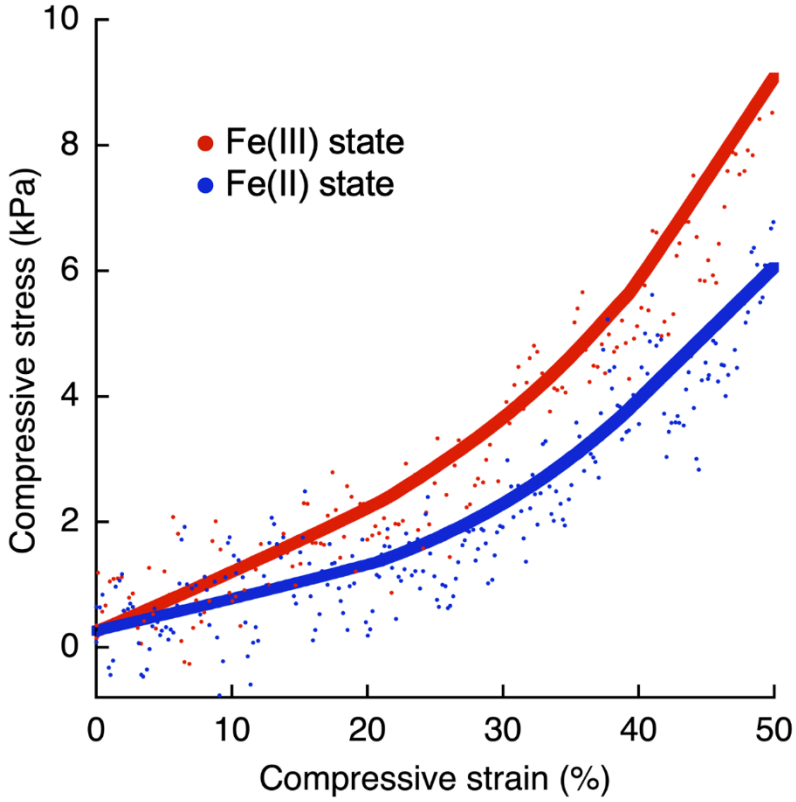

Figure 1-12. Stress-strain curves obtained by compression tests of Fe(III) state (red) and Fe(II) state (blue) of rHTHP-MBA-PAAm gel, respectively. The solid lines show weighted averages of raw values shown as dots.

1-3. Summary

The hexameric hemoprotein reconstituted with acryloyl group-tethered heme derivatives functions as a cross-linking unit to provide a functional polyacrylamide hydrogel. The obtained hydrogels clearly exhibit redox-responsive mechanical properties without significant changes in volume, and the responsiveness arises from a large decrease of the heme–protein affinities generated by reduction of the iron center. The elastic modulus of the hydrogel depends on the supramolecular heme-binding behavior in the cross-linking unit. This finding suggests that the process of heme binding of hemoproteins in cross-linking units is useful for generating redox-responsive mechanical properties. Further details will be investigated to clarify the relationship between heme binding and mechanical properties of gels. Compared to previous redox-responsive hydrogels containing simple host–guest systems such as ferrocene–cyclodextrin interaction,[23] the present hemoprotein-based hydrogels have two potential advantages: (i) redox potentials and/or binding constants for the heme moieties can be fine-tuned by protein mutation as well as metal substitution of the heme derivative, and (ii) specific heme-binding to the protein can create unique hydrogels in combination with various other

supramolecular systems. Processes to control the gel properties by modulation of heme-binding behavior such as small molecule ligation and protein matrix mutation will be investigated.

1-4. Materials and methods

Instruments

UV-vis spectral measurements of aqueous solution samples were carried out with a Shimadzu UV-2700 or a Shimadzu UV-3600 plus spectrophotometer. UV-vis spectra of the gels were recorded using a Shimadzu UV-3600 plus spectrophotometer equipped with an integrating sphere attachment. CD spectra were recorded on a JASCO (Model J-820). ^{1}H NMR spectra were recorded on a Bruker BioSpin AVANCE III HD NMR spectrometer (400 MHz). The chemical shifts were calibrated by residual solvent signals. ESI-TOF MS analyses were performed with a Bruker Daltonics micrOTOF-II mass spectrometer. The pH values were monitored with a Horiba F-52 pH meter. Tensile tests were conducted using an EZ Graph with a 10 N EZ Graph load cell. Compression analysis was carried out on an HAAKE RheoStress 6000 rheometer equipped with a P20 TiL plate.

Materials

Ultrapure water (Milli-Q) was prepared by a Millipore Integral 3 apparatus. All reagents were of the highest commercially available guaranteed grade and were used as received unless otherwise indicated. HTHP and apoHTHP were prepared according to the previous report.[67] Mb was purchased from Sigma Aldrich and purified by a CM-Sepharose column.

Scheme 1-1 Synthesis of acryloyl-heme

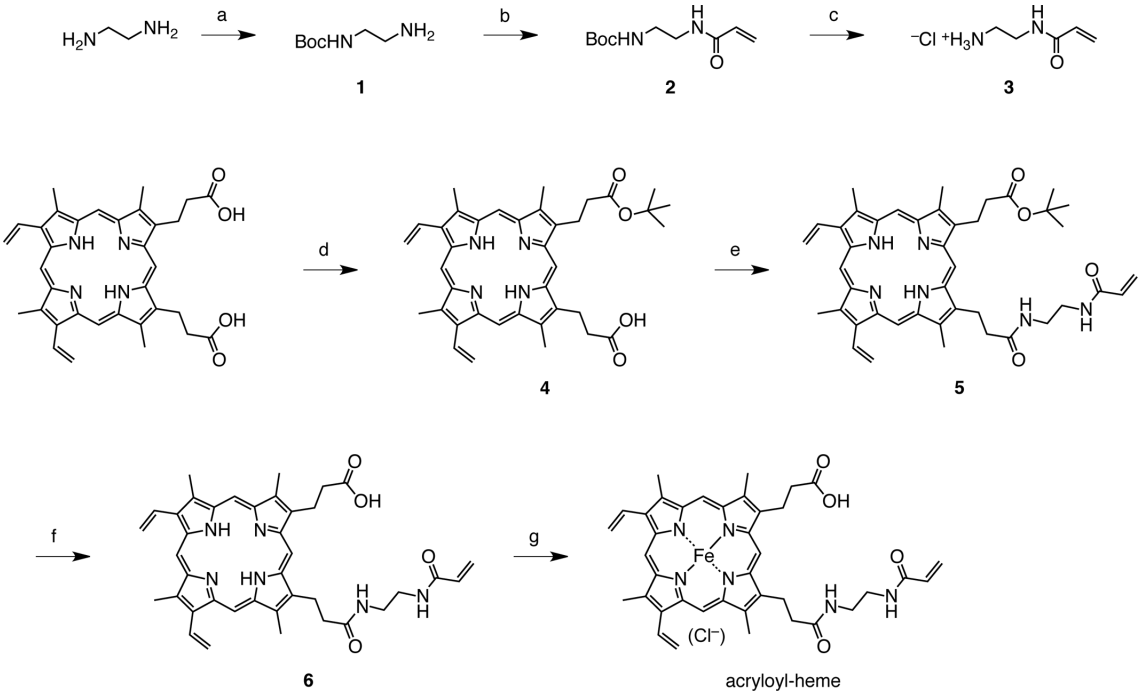

Compound **4** consists of two regioisomers due to the substitution position of the *tert*-butoxy group at the two heme-propionate side chains of protoporphyrin IX. Each compound, **5**, **6** and acryloyl-heme, also forms a similar mixture of two regioisomers. a) $(Boc)_2O$, b) acryloyl chloride, c) HCl, d) $(Boc)_2O$, *tert*-BuOH, e) **3**, 1-ethyl-3-(3-dimethylaminopropyl)carbodiimide, 1-hydroxybenzotriazole, f) trifluoroacetic acid, formic acid, g) $FeCl_2$

Acryloyl heme was synthesized according to Scheme 1-1. Compounds **1** and **4** were synthesized according to the previous report.[77]
Detailed synthetic procedures for compounds **3**, and **4**-**6** and acryloyl-heme are described below.

Synthesis of compound 2

Compound **1** (1.00 g, 6.24 mmol), triethylamine (2.08 g, 20.6 mmol, 3.3 eq.), and chloroform (200 mL) were added to a two-necked flask. Acryloyl chloride (677 mg, 7.49 mmol, 1.2 eq.) dissolved in 70 mL of chloroform was added dropwise over 3 h under ice bath conditions followed by stirring for 2 h. The solvent was then removed, redissolved in 100 mL of chloroform, and washed three times with 50 mL brine. After drying over sodium sulfate and filtration, the solvent was evaporated. Recrystallization from hexane/chloroform yielded compound **2** as a white solid (773 mg, 3.58 mmol, 57%).
^{1}H NMR (400 MHz, $CDCl_3$) δ (ppm) = 1.47 (s, 9H), 3.35 (m, 2H), 3.47 (m, 2H), 4.91 (brs, 1H), 5.67 (d, 1H, J = 10.4 Hz), 6.11 (dd, 1H, J = 10.4, 17.2 Hz), 6.29 (d, 1H, J = 17.2 Hz), 6.39 (brs, 1H).

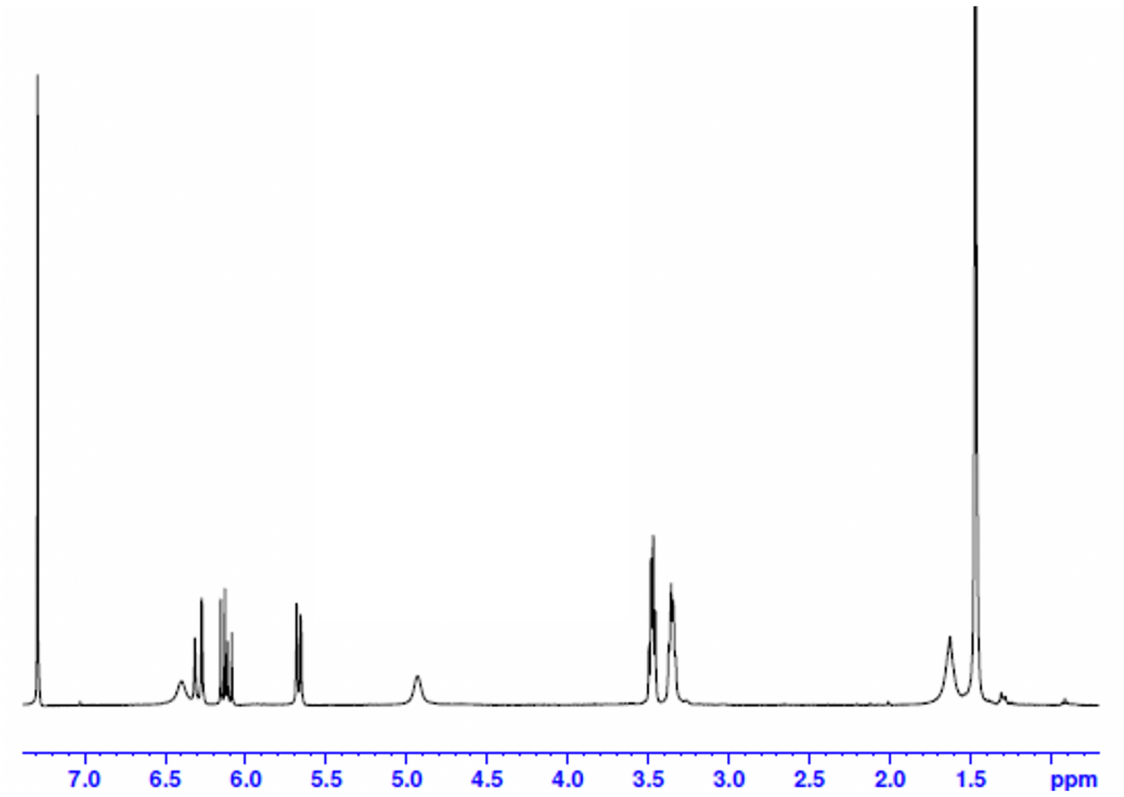

Figure 1-13. ^{1}H NMR(400 MHz, $CDCl_3$) spectrum of compound **2.**

Synthesis of compound 3

Compound **2** (50.0 mg, 233 μmol) was dissolved in 10 mL of chloroform. Approximately 4 M HCl/dioxane solution (4.2 mL) was added and stirred at room temperature for 2 h, then the solvent was evaporated. Methanol (20 mL) was added and evaporated twice. After overnight vacuum drying, compound **3** was obtained quantitatively (35.5 mg, 233 μmol).

^{1}H NMR(400 MHz, DMSO-d_6) δ (ppm) = 2.89 (m, 2H), 3.38 (m, 2H), 6.39 (brs, 1H), 5.63 (dd, 1H, J = 2.4, 10.0 Hz), 6.12 (dd, 1H, J = 10.0, 17.2 Hz), 6.23 (dd, 1H, J = 2.4, 17.2Hz).

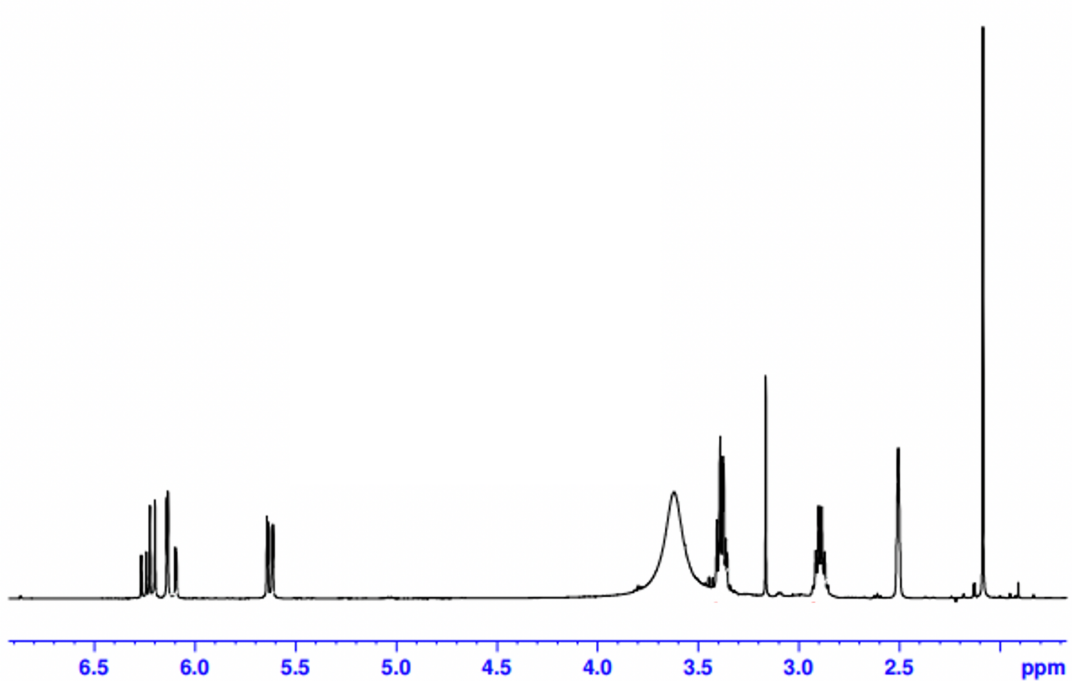

Figure 1-14. ^{1}H NMR(400 MHz, DMSO-d_6) spectrum of compound **3.**

Synthesis of compound 5

Compound **4** (50 mg, 83 μmol), EDC (62 mg, 332 μmol, 4eq.), HOBt (43 mg, 334 μmol, 4 eq.), and chloroform (30 mL) were added to a two-necked flask and stirred at room temperature for 1 h. In another flask, compound **3** (59 eq., 757 μmol) was added to methanol (15 mL) and triethylamine (100 mg) and stirred at room temperature for 2 h. The reaction mixtures were combined and stirred overnight at room temperature. After the completion of the reaction, the solvent was evaporated, and the residue was taken up in 50 mL of chloroform and washed three times with 5% citric acid. After evaporation, the residue was purified by silica gel chromatography using chloroform/methanol = 0% to 10% (v/v) as an eluent. Recrystallization from hexane/THF yielded compound **5** as a red solid (35.5 mg, 59 μmol, 71%).

ESI-TOF-MS (positive mode, MeOH) *m/z* 715.40 $(M + H)^+$, calcd for $C_{43}H_{50}N_6O_4$ 715.40

^{1}H NMR(400 MHz, DMSO-d_6) δ (ppm) = –3.92 (s, 2H) 1.25 (s, 9H), 3.03 (m, 4H), 3.22 (m, 4H), 3.68 (m, 12H), 4,34 (m, 4H), 5.37 (m, 1H), 5.91 (m, 2H), 6.22, (m, 2H) 6.45, (m, 2H), 7.85 (brs, 1H), 7.97 (brs, 1H), 8.457-8.55 (m, 2H), 10.213-10.241 (m, 4H).

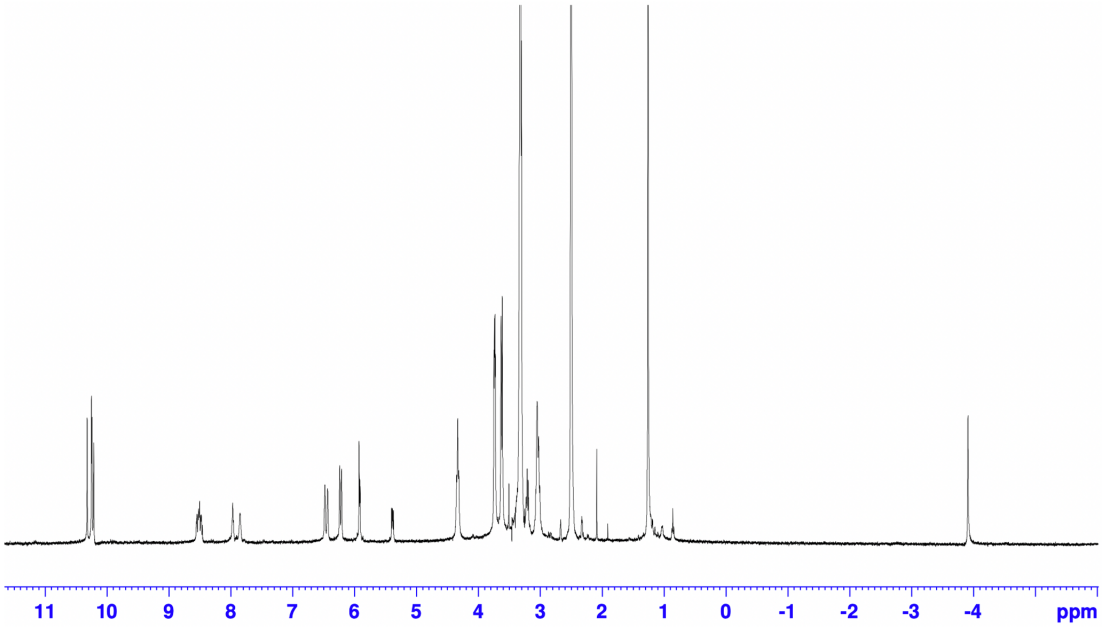

Figure 1-15. ^{1}H NMR(400 MHz, DMSO-d_6) spectrum of compound **5**.

Synthesis of compound 6

Compound **5** (10.7 mg, 14.0 μmol) was added to a two-necked flask and purged with nitrogen. Anhydrous dichloromethane (5 mL), formic acid (0.3 mL), and TFA (0.7 mL) were added and stirred at room temperature. After stirring for 2.5 h, the solvent was removed. Precipitation from hexane/THF yielded compound **6** as a red solid (6.4 mg, 60%, 9.71 μmol).

ESI-TOF-MS (positive mode, MeOH) *m/z* 681.32 $(M + Na)^+$, calcd for $C_{39}H_{42}N_6O_4$ 681.31

^{1}H NMR(400 MHz, DMSO-d_6) δ (ppm) = –3.79 (s, 2H), 3.03 (m, 4H), 3.19 (m, 4H), 3,64 (dd, J = 8.8, 4.4 Hz, 6H), 3.78 (m, 6H), 4.36 (brs, 4H), 5.40 (brs, 1H), 5.93 (m, 2H), 6.24 (m, 2H), 6.48 (m, 2H), 7.91 (m, 2H), 8.56 (m, 2H), 10.31 (m, 4H).

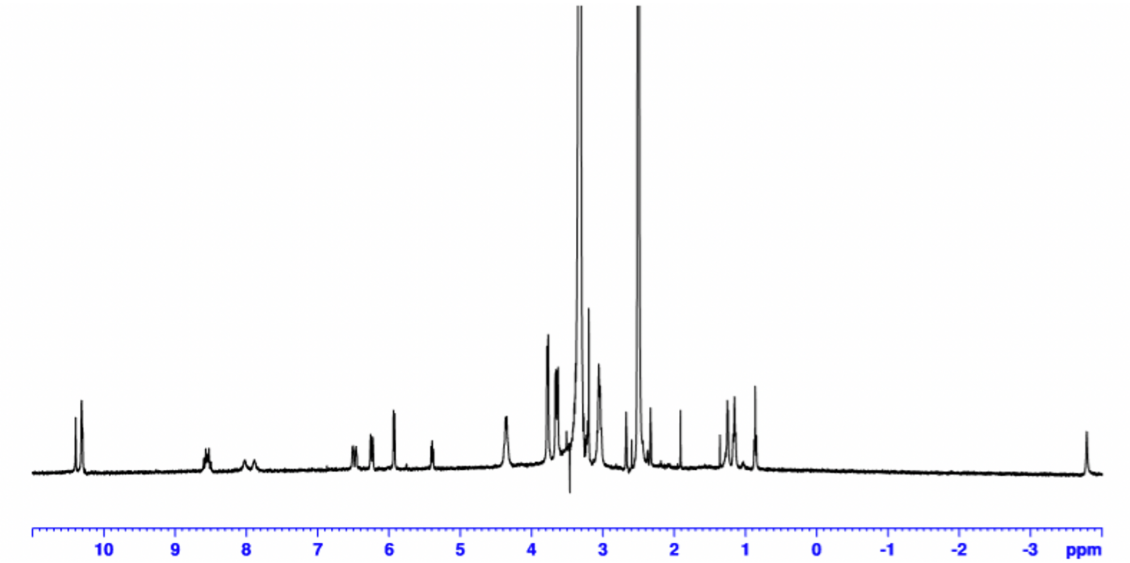

Figure 1-16. ^{1}H NMR(400 MHz, DMSO-d_6) spectrum of compound **6.**

Synthesis of acryloyl-heme

Compound **6** (5.5 mg, 8.4 μmol) and ferric chloride tetrahydrate (27.2 mg, 168 μmol, 20 eq.), and sodium bicarbonate (23.2 mg) were added to a two-necked flask under a nitrogen atmosphere. Chloroform/methanol = 10:1 (v/v) (15 mL), which was bubbled with nitrogen, was added, and the mixture was refluxed at 60 °C for 5.5 h. After evaporation of the solvent, a mixture of chloroform/methanol (50 mL) was added, and the organic layer was washed five times with 0.05 M HCl. After drying over sodium sulfate and evaporation, the residue was recrystallized from hexane/THF, and acryloyl-heme was obtained as a red solid (3.0 mg, 48%, 4.2 μmol).

ESI-TOF -MS (positive mode, MeOH) *m/z* 712.25 $(M - Cl)^+$, calcd. for $C_{39}H_{40}FeN_6O_4$ 712.25

CD spectra for ΔG^0 evaluation

CD spectra were measured in a solution containing wild-type HTHP in 100 mM potassium phosphate buffer at pH 7.0, with or without 100 mM dithionite. In the case of the Fe(III) state, the temperature was maintained at 90 °C by an equipped thermal controller. In the case of the Fe(II) state, CD signals were recorded at 25 °C. The optical path length was 1 cm, and the bandwidth was 2 μm.

Preparation of rHTHP

Five equivalents of acryloyl-heme in DMSO (stock solution: 5 mM) were added into a solution of apoHTHP (10 μM in 100 mM potassium phosphate buffer containing 1 M NaCl) at room temperature, and the reaction mixture was gently shaken overnight. Dialysis was carried out to remove the DMSO against 100 mM potassium phosphate buffer, pH 7.0, at 4 °C. The excess acryloyl-heme was removed by a HiTrap Desalting column. The obtained rHTHP was characterized by UV-vis spectrum. Purity was confirmed by an R_Z value >2.3.

Preparation of polyacrylamide gel containing rHTHP

Reconstituted HTHP was concentrated to 5 mM by ultrafiltration using a 30-kDa cut-off Amicon Ultra tube via centrifugation at 6000 rpm. Polymerization of 1.0 mM rHTHP and 1 M acrylamide in 100 mM potassium phosphate buffer, pH 7.0, containing 1 M NaCl was carried out with 0.25% ammonium sulfate and 0.38% *N,N,N',N'*-etramethylethylenediamine as radical initiators. Then, a dual cross-linked hydrogel was prepared in the presence of 5 mM *N,N'*-methylene bis-acrylamide and 1.5 mM rHTHP under the same radical polymerization conditions.

Mechanical properties evaluation

Samples were prepared in cuboid shapes with ca. 14 mm x ca. 1.0 mm x ca. 1.0 mm in equilibrium swelling states. During tensile tests, samples were attached to a metal sheet using the adhesive reagent Aron Alpha®, within 8 mm. The Young's modulus was determined by the slope in the strain ranging from 0% to 10% of the rupture point. The rupture energy was determined by the area sum in the strain-stress curve. Compression analysis was performed using a HAAKE RheoStress 6000 instrument in compression mode using P20 TiL as a plate. The compression test was carried out with a 0.05 mm/s stroke at 20 °C.

1-5. References

1 M. Annaka, T. Tanaka, *Nature* **1992**, *355*, 430.

2 H. Katono, A. Maruyama, K. Sanui, N. Ogata, T. Okano, Y. Sakurai, *J. Controlled Release* **1991**, *16*, 215.

3 T. Tanaka, *Sci. Am.* **1981**, *244*, 124.

4 L. Lonov, *Mater. Today* **2014**, *17*, 494.

5 J.-Y. Sun, X. Zhao, W. R. K. Illeperuma, O. Chaudhuri, K. H. Oh, D. J. Mooney, J. J. Vlassak, Z. Suo, *Nature* **2012**, *489*, 133.

6 A. Suzuki, T. Tanaka, *Nature* **1990**, *346*, 345.

7 H. Yang, H. Liu, H. Kang, W. Tan, *J. Am. Chem. Soc.* **2008**, *130*, 6320.

8 D. C. Tuncaboylu, M. Sari, W. Oppermann, O. Okay, *Macromolecules* **2011**, *44*, 4997.

9 P. Cordier, F. Tournilhac, C. Soulié-Ziakovic, L. Leibler, *Nature* **2008**, *451*, 977.

10 Y. Chen, A. M. Kushner, G. A. Williams, Z. Guan, *Nat. Chem.* **2012**, *4*, 467.

11 S. Burattini, H. M. Colquhoun, J. D. Fox, D. Friedmann, B. W. Greenland, P. J. F. Harris, W. Hayes, M. E. Mackay, S. J. Rowan, *Chem. Commun.* **2009**, 6717.

12 J. Fox, J. J. Wie, B. W. Greenland, S. Burattini, W. Hayes, H. M. Colquhoun, M. E. Mackay, S. J. Rowan, *J. Am. Chem. Soc.* **2012**, *134*, 5362.

13 Q. Wang, J. L. Mynar, M. Yoshida, E. Lee, M. Lee, K. Okuro, K. Kinbara, T. Aida, *Nature* **2010**, *463*, 339.

14 M. Burnworth, L. Tang, J. R. Kumpfer, A. J. Duncan, F. L. Beyer, G. L. Fiore, S. J. Rowan, C. Weder, *Nature* **2011**, *472*, 334.

15 R. J. Wojtecki, M. A. Meador, S. J. Rowan, *Nat. Mater.* **2010**, *10*, 14.

16 P. Wei, X. Yan, F. Huang, *Chem. Soc. Rev.* **2015**, *44,* 815.

17 C. Li, J. Tan, Z. Guan, Q. Zhang, *Macromol. Rapid Commun.* **2019**, *40*, 1800909

18 G. Liu, Q. Yuan, G. Hollett, W. Zhao, Y. Kang, J. Wu, *Polym. Chem.* **2018**, *9*, 3436.

19 T. Kakuta, Y. Takashima, M. Nakahata, M. Otsubo, H. Yamaguchi, A. Harada, *Adv. Mater.* **2013**, *25*, 2849.

20 Y. Yang, E. M. Terentjev, Y. Wei, Y. Ji, *Nat. Commun.* **2018**, *9*, 1906.

21 X. Yan, F. Wang, B. Zheng, F. Huang, *Chem. Soc. Rev.* **2012**, *41*, 6042.

22 K. Iwaso, Y. Takashima, A. Harada, *Nat. Chem.* **2016**, *8,* 625.

23 M. Nakahata, Y. Takashima, A. Hashidzume, A. Harada, *Angew. Chem. Int. Ed.* **2013**, *52,* 5731.

24 M. Zhang, D. Xu, X. Yan, J. Chen, S. Dong, B. Zheng, F. Huang, *Angew. Chem. Int. Ed.* **2012**, *51,* 7011.

25 D. Liu, D. Wang, M. Wang, Y. Zheng, K. Koynov, G. K. Auernhammer, H.-J. Butt, T. Ikeda, *Macromolecules* **2013**, *46,* 4617.

26 E. A. Appel, F. Biedermann, U. Rauwald, S. T. Jones, J. M. Zayed, O. A. Scherman, *J. Am. Chem. Soc.* **2010**, *132*, 14251.

27 J. Liu, C. S. Y. Tan, Z. Yu, N. Li, C. Abell, O. A. Scherman, *Adv. Mater.* **2017**, *29,* 1605325.
28 C. S. Y. Tan, J. Liu, A. S. Groombridge, S. J. Barrow, C. A. Dreiss, O. A. Scherman, *Adv. Funct. Mater.* **2018**, *28,* 1702994.
29 K.-P. Wang, Y. Chen, Y. Liu, *Chem. Commun.* **2015,** *51,* 1647.
30 Q. Zhao, Y. Chen, S. H. Li, Y. Liu, *Chem. Commun.* **2018**, *54*, 200.
31 H. Yang, J. Tang, C. Shang, R. Miao, S. Zhang, K. Liu, Y. Fang, *Macromol. Rapid Commun.* **2018**, *39,* 1700679.
32 S. Wang, Z. Xu, T. Wang, T. Xiao, X.-Y. Hu, Y.-Z. Shen, L. Wang, *Nat. Commun.* **2018**, *9,* 1737.
33 H. Ju, F. Zhu, H. Xing, Z. L. Wu, F. Huang, *Macromol. Rapid Commun.* **2017**, *38,* 1700232.
34 S. Wang, Z. Xu, T. Wang, X. Liu, Y. Lin, Y.-Z. Shen, C. Lin, L. Wang, *J. Photochem. Photobiol. A* **2018,** *355,* 60.
35 T. Xiao, L. Xu, L. Zhou, X.-Q. Sun, C. Lin, L. Wang, *J. Mater. Chem. B* **2019**, *7,* 1526.
36 J. Fang, A. Mehlich, N. Koga, J. Huang, R. Koga, X. Gao, C. Hu, C. Jin, M. Rief, J. Kast, D. Baker, H. Li, *Nat. Commun.* **2013**, ***4,*** 2974.
37 Y. Cao, H. Li, *Chem. Commun.* **2008**, 4144.
38 S. Lv, D. M. Dudek, Y. Cao, M. M. Balamurali, J. Gosline, H. Li, *Nature* **2010,** *465,* 69.
39 H. Li, N. Kong, B. Laver, J. Liu, *Small* **2016,** *12,* 973.
40 S. Lyu, J. Fang, T. Duan, L. Fu, J. Liu, H. Li, *Chem. Commun.* **2017,** *53,* 13375–13378.
41 T. Miyata, N. Asami, T. Uragami, *Nature* **1999,** *399,* 766.
42 T. Miyata, M. Jige, T. Nakaminami, T. Uragami, *Proc. Natl. Acad. Sci. U.S.A.* **2006,** *103,* 1190.
43 T. Miyata, N. Asami, T. Uragami, *Macromolecules* **1999,** *32,* 2082.
44 C. Norioka, K. Okita, M. Mukada, A. Kawamura, T. Miyata, *Polym. Chem.* **2017,** *8,* 6378.
45 T. Miyata, N. Asami, T. Uragami, *J. Polym. Sci. Part B: Polym. Phys.* **2009,** *47,* 2144.
46 T. Miyata, A. Jikihara, K. Nakamae, A. S. Hoffman, *Macromol. Chem. Phys.* **1996,** *197,* 1135.
47 T. Miyata, A. Jikihara, K. Nakamae, A. S. Hoffman, *J. Biomater. Sci. Polym. Ed.* **2004,** *15,* 1085.
48 Y. Liang, K. L. Kiick, *Acta Biomater.* ***2014,*** *10,* 1588.
49 N. Yamaguchi, L. Zhang, B. Chae, C. S. Palla, E. M. Furst, K. L. Kiick, *J. Am. Chem. Soc.* **2007,** *129,* 3040.
50 K. L. Kiick, *Soft Matter* **2008,** *4,* 29.
51 L. Chen, X. Wang, W. Lu, X. Wu, J. Li, *Chem. Soc. Rev.* **2016,** *45,* 2137.
52 T. Miyata, T. Uragami, K. Nakamae, *Adv. Drug Deliv. Rev.* **2002,** *54,* 79.
53 C. J. Reedy, B. R. Gibney, *Chem. Rev.* **2004,** *104,* 617.
54 S. Schneider, J. Marles-Wright, K. H. Sharp, M. Paoli, *Nat. Prod. Rep.* **2007,** *24,* 621.
55 K. Oohora, T. Hayashi, *Dalton Trans.* **2021,** *50,* 1940.

56 B. A. Springer, S. G. Sligar, J. S. Olson, G. N. Jr. Phillips, *Chem. Rev.* **1994,** *94,* 699.
57 M. S. Hargrove, J. S. Olson, *Biochemistry* **1996,** *35,* 11310.
58 K. Oohora, A. Onoda, T. Hayashi, *Chem. Commun.* **2012,** *48,* 11714.
59 K. Oohora, N. Fujimaki, R. Kajihara, H. Watanabe, T. Uchihashi, T. Hayashi, *J. Am. Chem. Soc.* **2018,** *140,* 10145.
60 K. Oohora, R. Kajihara, M. Jiromaru, H. Kitagishi, T. Hayashi, *Chem. Lett.* **2019,** *48,* 295.
61 K. Oohora, Y. Onuma, Y. Tanaka, A. Onoda, T. Hayashi, *Chem. Commun.* **2017,** *53,* 6879.
62 K. Oohora, A. Onoda, H. Kitagishi, H. Yamaguchi, A. Harada, T. Hayashi, *Chem. Sci.* **2011,** *2,* 1033.
63 Y. Kobayashi, Y. Takashima, A. Hashidzume, H. Yamaguchi, A. Harada, *Sci. Rep*. **2015,** *5,* 16254.
64 T. Ono, Y. Hisaoka, A. Onoda, K. Oohora, T. Hayashi, *Chem. Asian J.* **2016,** *11,* 1036.
65 J.-H. Jeoung, D. A. Pippig, B. M. Martins, N. Wagener, H. Dobbek, *J. Mol. Biol.* **2007,** *368,* 1122.
66 T. Mashima, K. Oohora, T. Hayashi, *J. Porphyrins Phthalocyanines* **2017,** *21,* 824.
67 K. Oohora, T. Mashima, K. Ohkubo, S. Fukuzumi, T. Hayashi, *Chem. Commun.* **2015,** *51,* 11138.
68 S. Hirayama, K. Oohora, T. Uchihashi, T. Hayashi, *J. Am. Chem. Soc.* **2020,** *142,* 1822.
69 M. S. Hargrove, A. J. Wilkinson, J. S. Olson, *Biochemistry* **1996,** *35,* 11300.
70 P. A. Sykes, H.-C. Shiue, J. R. Walker, R. C. Bateman Jr. *J. Chem. Educ.* **1999,** *76,* 1283.
71 C. R. Robinson, Y. Liu, J. A. Thomson, J. M. Sturtevant, S. G. Sligar, *Biochemistry* **1997,** *36,* 16141.
72 G. I. Makhatadze, *J. Phys. Chem. B* **1999,** *103,* 4781.
73 P. Kielb, T. Utesch, J. Kozuch, J.-H. Jeoung, H. Dobbek, M. A. Mroginski, P. Hildebrandt, I. Weidinger, *J. Phys. Chem. B* **2017,** *121,* 3955.
74 S.-C. Chien, O. Shoji, Y. Morimoto, Y. Watanabe, *New J. Chem.* **2017,** *41,* 302.
75 T. Sun, T. Kurokawa, S. Kuroda, A. B. Ihsan, T. Akasaki, K. Sato, Md. A. Haque, T. Nakajima, J. P. Gong, *Nat. Mater*. **2013,** *12,* 932.
76 J. P. Gong, *Soft Matter* **2010,** *6,* 2583.
77 H. Kitagishi, K. Oohora, H. Yamaguchi, H. Sato, T. Matsuo, A. Harada, T. Hayashi, *J. Am. Chem. Soc.* **2007, 129,** 10326.

Chapter 2
Tuning Elasticity of a Hexameric Hemoprotein-based Hydrogel through Protein Building Block Mutations

2-1. Introduction

Hydrogels containing protein components can provide useful materials with unique functional and mechanical properties.[1–3] These hydrogels are mainly categorized into two types formed by covalent bonding and supramolecular network structures. In the case of protein-based covalent bonding networks, the folding/unfolding process contributes to the elasticity and/or stretchability of the hydrogels.[4–9] Genetically engineered oligomeric proteins have been prepared to mimic titin, a natural elastic protein. These proteins are often employed as building blocks for this type of protein-based hydrogels. A metal binding protein–polymer covalent conjugate provides another route for developing functional hydrogels.[10,11] The swelling and shrinking behaviors of these gels are triggered upon addition of specific protein ligands and metal ions. In contrast, supramolecular protein¬–protein interactions are harnessed in development of stimuli-responsive materials such as temperature- and pH-responsive hydrogels.[12–14] Unique stimuli-responsive hydrogels have been constructed using supramolecular interactions between a small molecule and a protein.[15–19] Binding of an antibody to a synthetic polymer modified by an antigen has been used to form supramolecular hydrogels where the gel converts to a solution state upon the addition of excess antigen.[15] In another representative example, the interaction between streptavidin and biotin provides an injectable gel.[16] These results indicate that protein-based hydrogels have the potential to function as unique biomaterials in addition to a variety of unique stimuli-responsive gel materials[20] that do not contain biomolecules.

Hemoproteins provide useful building blocks for supramolecular materials because heme–heme pocket interactions are very stable under physiological conditions.[21,22] Moreover, the affinity depends on pH and temperature as well as redox states and external ligands of the heme cofactor, inspiring the fabrication of stimuli-responsive materials. Hayashi and co-workers have previously reported a polyacrylamide gel containing an engineered hemoprotein as a cross-linking unit.[23] Hexameric tyrosine-coordinated hemoprotein, HTHP,[24] was employed as a hemoprotein unit and reconstituted with a synthetic heme cofactor with a tethered acryloyl group attached to one of the propionate side chains at the position where the polymerization reaction with acrylamide occurs. The mechanical properties are changed by redox states of the heme cofactor. The Fe(III) state has a higher elastic modulus than the Fe(II) state. Mutation of amino acid residues in hemoproteins is known to alter the binding affinity of heme for a protein matrix.[21,245,26] Although there have been no reports of any HTHP mutations affecting the heme binding, the mutation of key residues is expected to change the heme affinity and this may provide the capacity to tune the elasticity of HTHP-based gels. This study investigates the relationship between heme binding and Young's modulus in the HTHP mutation (Figure 2-1).

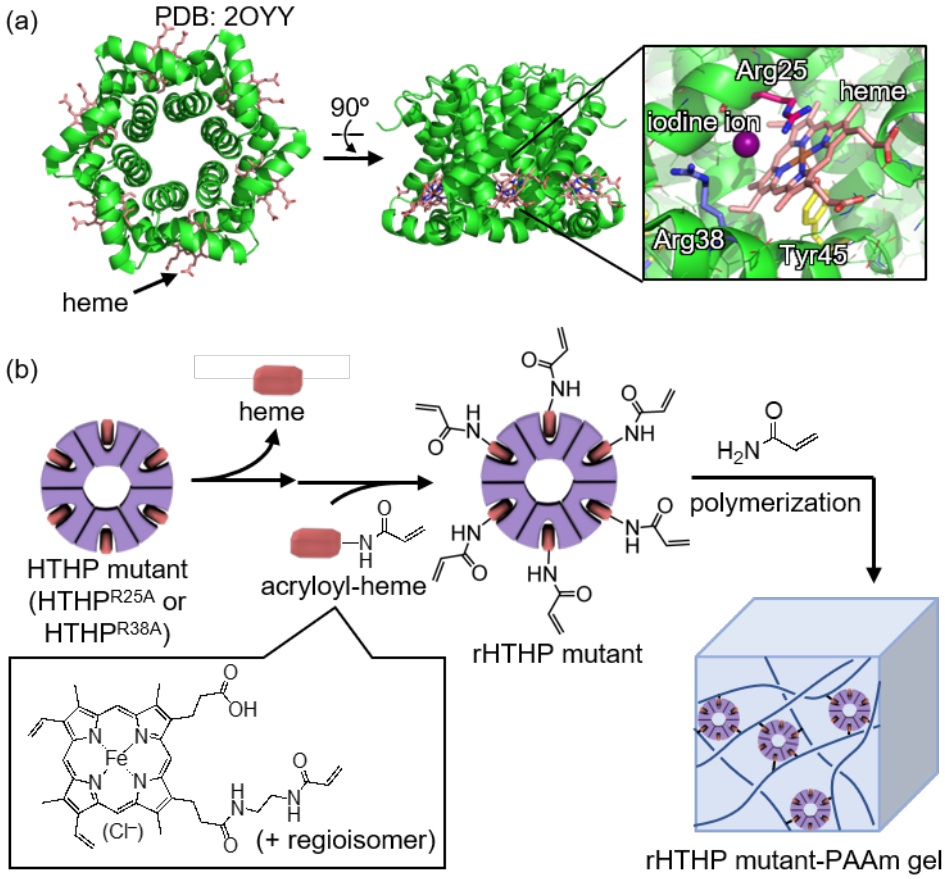

Figure 2-1. (a) Crystal structure of HTHP and mutation sites in this work. (b) Schematic representation for preparation of reconstituted HTHP mutants and rHTHP mutant-based gels.

2-2. Results and discussion

2-2-1. Design, preparation and characterization of HTHP mutants

First, the author designed HTHP mutants which affect the binding of heme to the protein matrix. $HasA_{ypt}$, a heme-acquisition protein from Yersinia pseudotuberculosis, has a similar heme binding site as HTHP, with axial tyrosine coordination to heme (Figure 2-2).[27] In the previous report for $HasA_{ypt}$, two arginine residues, Arg40 and Arg144, at the distal side in the heme binding site were individually mutated to alanine residues.[28] The R40A and R144A mutants of $HasA_{ypt}$ show lower heme affinity than the wild-type protein. Two arginine residues, Arg25 and Arg38, are also located close to the heme binding site of each subunit of HTHP (Figure 2-1a). Arg25 is clearly stacked with the porphyrin macrocycle, potentially involving a cation–π interaction, whereas Arg38 does not appear to interact directly with the heme molecule. However, an iodine ion, used as an additive reagent for crystallization (Figure 2-1a), may cause displacement of the Arg38 residue from the heme distal site in the crystal structure. The structural insights into HasAypt suggest the presence of an interaction of the Arg38 residue of HTHP with the porphyrin macrocycle and/or the propionate side chain in a solution state (Figure 2-2). Thus, the author selected Arg25 and Arg38, as mutation points and prepared

the alanine mutants, R25A and R38A by site-directed mutagenesis. The mutants were successfully expressed in E. coli, and purified by anion exchange and size exclusion chromatography columns. MALDI MS shows the expected m/z values for the monomers of R25A mutant (calcd. as $[M + H]^+$: 8146, found, 8146) and R38A mutant (calcd. as $[M + H]^+$: 8146, found, 8147). Dynamic light scattering measurements indicate that the hexameric structure is maintained in the mutants (Figure 2-3). UV-vis spectra of the ferric state of the mutants are consistent with those of wild-type HTHP ($HTHP^{WT}$) and the phenolate axial ligand in Tyr45 remains in place (Figure 2-4). Negative Cotton effects with two peaks at 222 nm and 208 nm were observed in circular dichroism (CD) spectra of the mutants in the far-UV region and the molar ellipticities of the mutants are consistent with those of $HTHP^{WT}$ (Figure 2-5). CD spectra in the Soret band region also show positive Cotton effects as typical signals of HTHP, indicating that heme b is bound to the intrinsic heme-binding site in each unit (Figure 2-6). Thus, the HTHP mutants were successfully prepared without any significant alterations of spectroscopic characteristics.

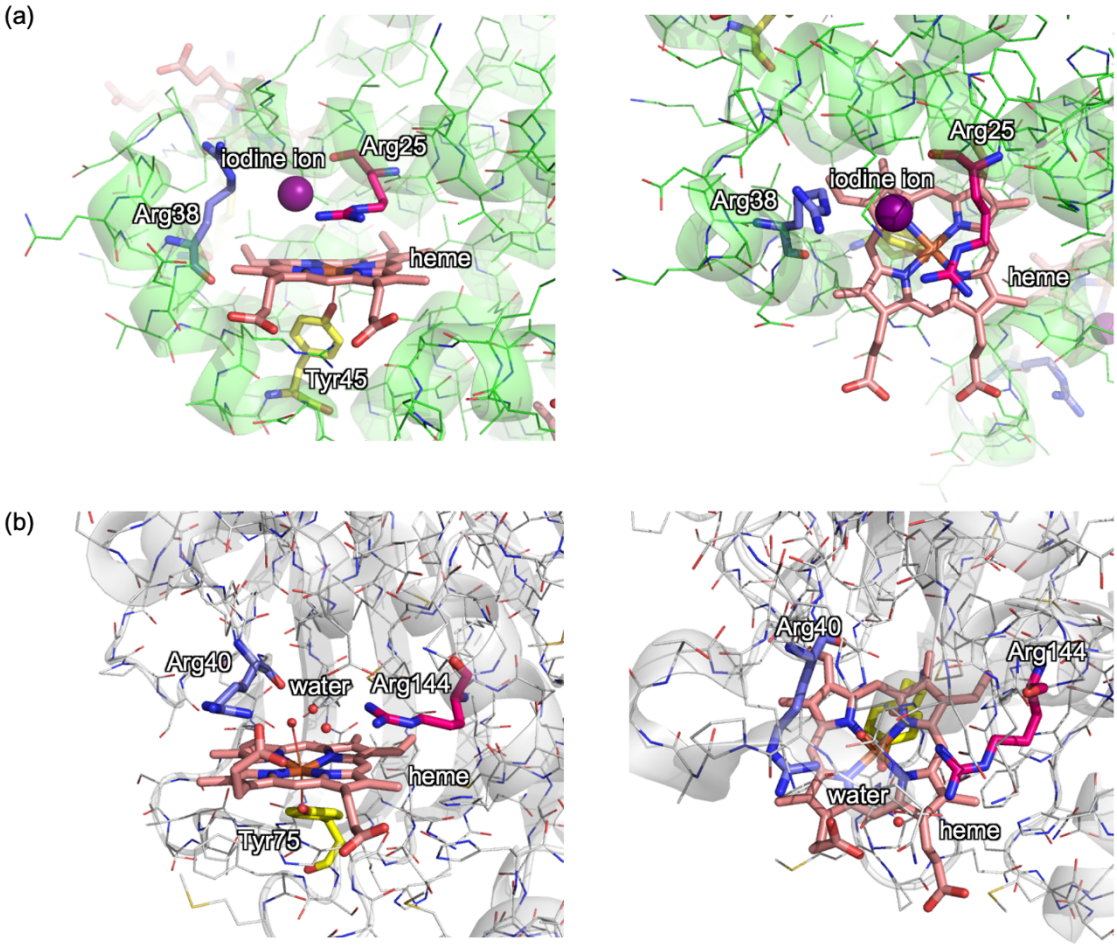

Figure 2-2. Crystal structures of the heme binding sites of (a) HTHP (PDB ID: 2OYY) and (b) $HasA_{ypt}$ (PDB ID: 4XZD). Left and right images show side and top views, respectively.

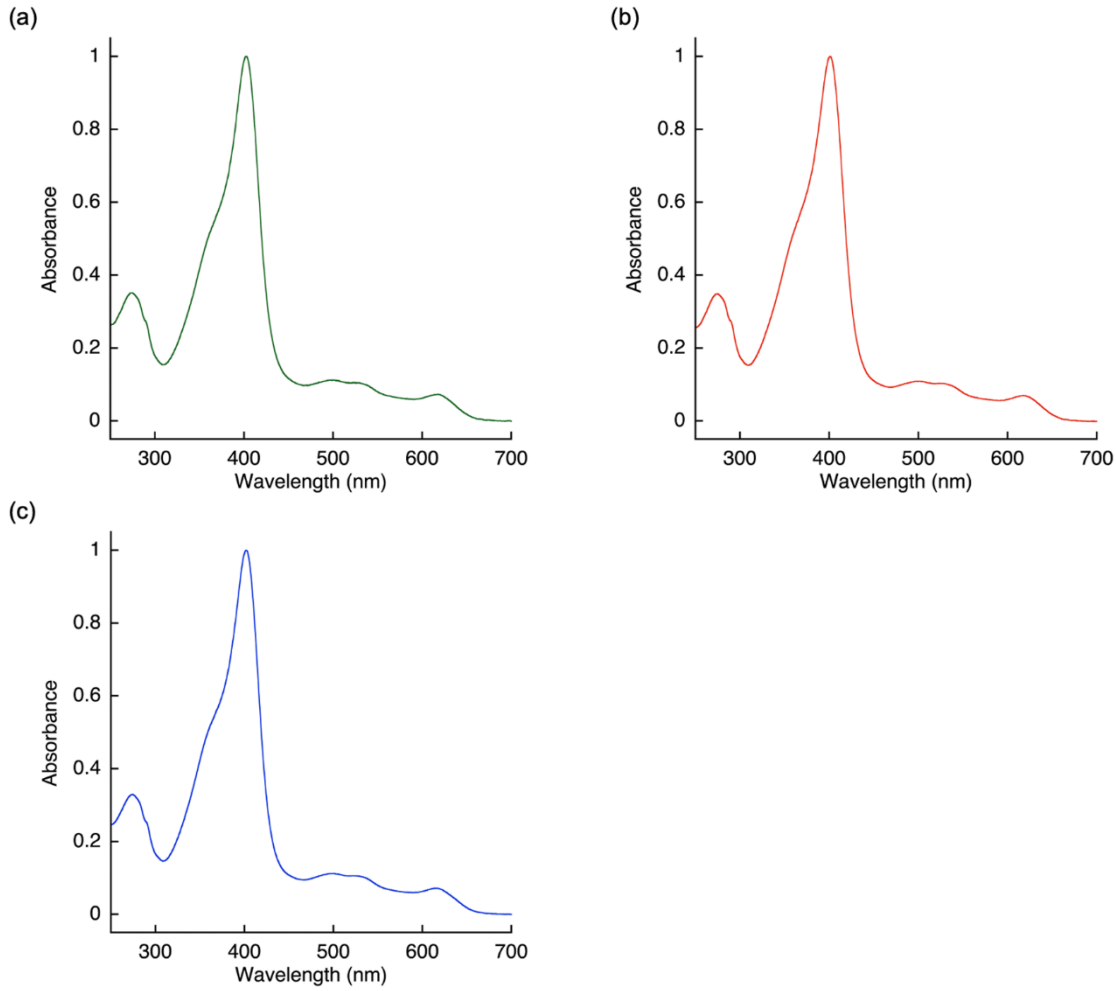

Figure 2-3. UV-vis spectra of (a) $HTHP^{WT}$, (b) $HTHP^{R25A}$ and (c) $HTHP^{R38A}$ in 100 mM potassium phosphate buffer at pH 7.0.

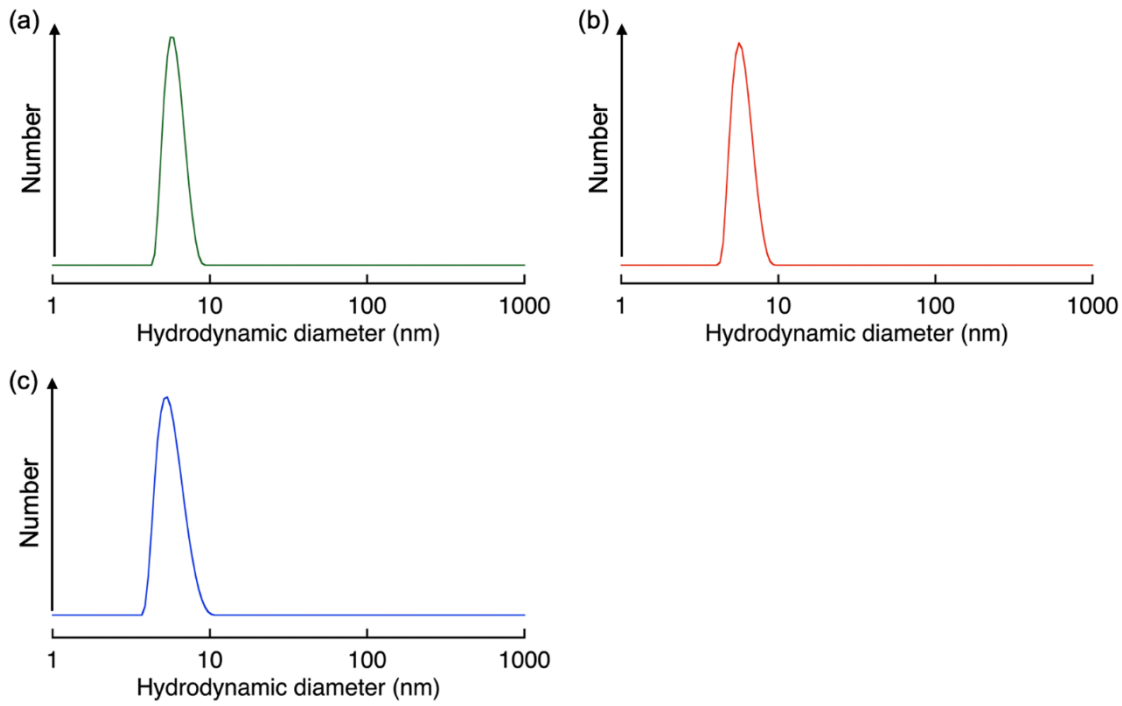

Figure 2-4. Size distribution of (a) $HTHP^{WT}$, (b) $HTHP^{R25A}$ and (c) $HTHP^{R38A}$ by dynamic light scattering in 100 mM potassium phosphate buffer at pH 7.0.

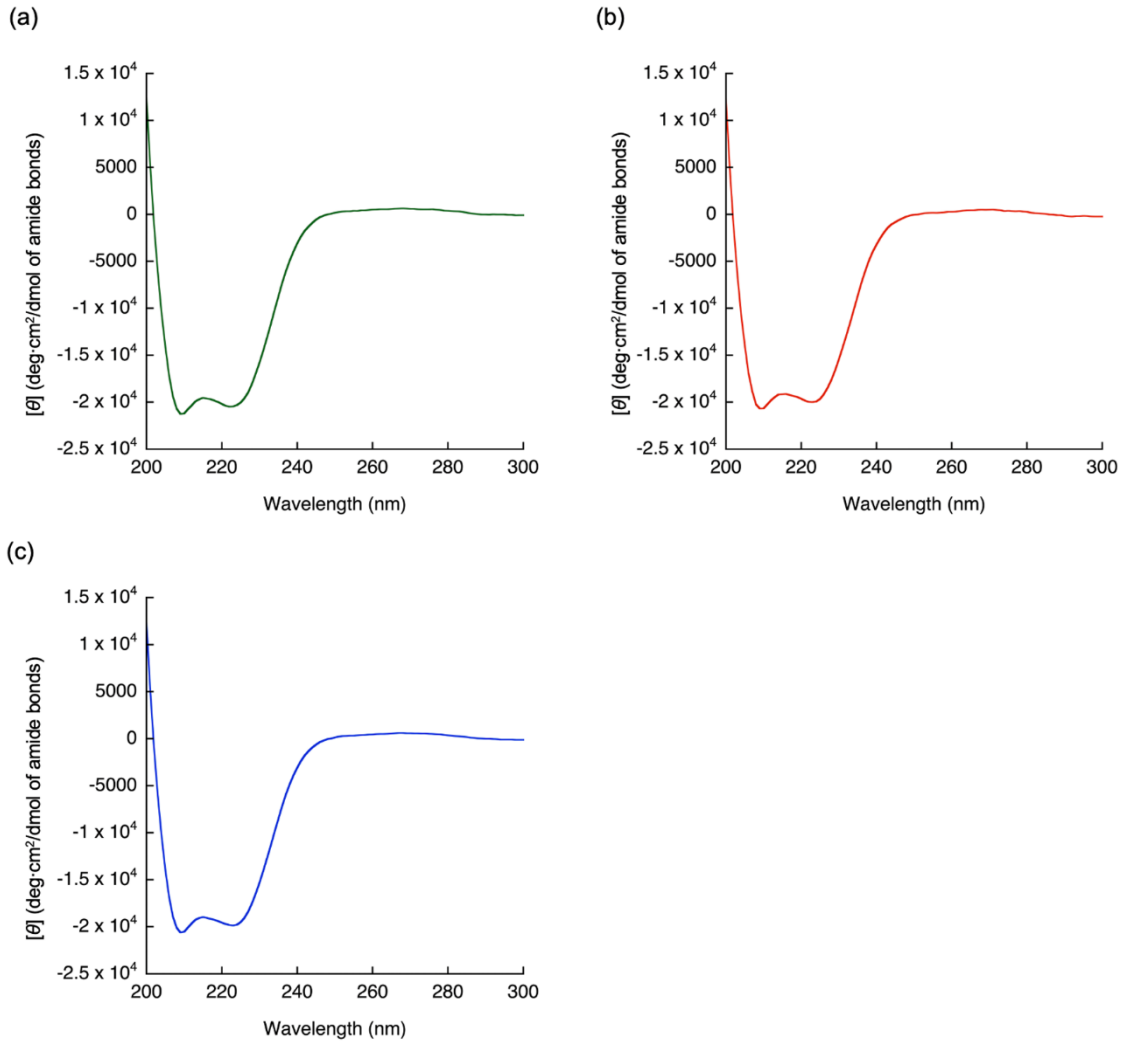

Figure 2-5. Far-UV CD spectra of (a) $HTHP^{WT}$, (b) $HTHP^{R25A}$ and (c) $HTHP^{R38A}$ in 100 mM potassium phosphate buffer at pH 7.0.

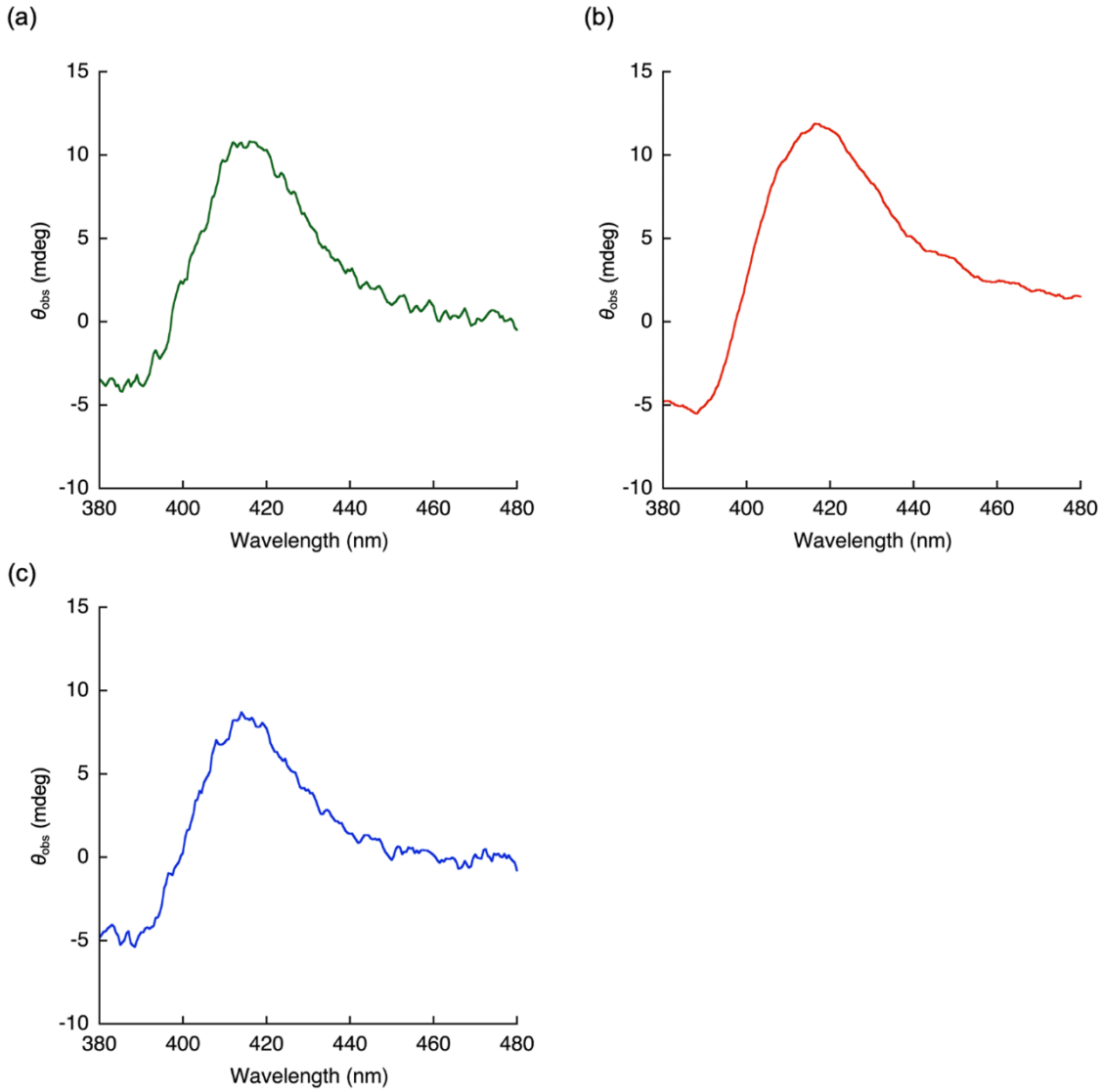

Figure 2-6. Vis CD spectra of (a) $HTHP^{WT}$, (b) $HTHP^{R25A}$ and (c) $HTHP^{R38A}$ in 100 mM potassium phosphate buffer at pH 7.0.

2-2-2. Evaluation of stability of heme–heme pocket interaction in HTHP mutants

The thermodynamic stabilities of the heme-bound forms of the ferric HTHP mutants were evaluated by denaturing titration experiments (Figure 2-7).[23,29–32] The CD intensities in the Soret band region were found to decrease upon addition of guanidium chloride, GdmCl, as a denaturant. The normalized CD spectral changes were analyzed, and the ratio of the bound and unbound states provide the ΔG^{o} value at each of the GdmCl concentrations investigated. Plots of the ΔG^{o} values against GdmCl concentrations were linearly fitted as shown in Figure 2-7 and the y-intercept indicates the ΔG^{o} value for heme binding in the absence of GdmCl. The ΔG^{o} values of HTHP^{R25A} and HTHP^{R38A} as heme-binding energies were determined to be –41 kJ/mol and –40 kJ/mol, respectively. Compared with the ΔG^{o} values of HTHP^{WT} (–57 kJ/mol), the affinity of heme for the protein matrix is decreased by the two mutations.[22] The ΔG^{o} values of the HTHP mutants are similar to those of myoglobin (–45.7 kJ/mol)[30] and cytochrome b_{562} (–46 kJ/mol).[31] In contrast, the ΔG^{o} value of HTHP^{WT} changed to –25 kJ/mol in the presence of sodium dithionite as a reductant, but the binding of heme into the protein matrix was still confirmed by CD signals.[23] However, a CD signal for ferrous HTHP^{R38A} in the Soret region clearly disappeared, indicating that heme-release is triggered by reduction(Figure 2-8). This confirms that point mutations of Arg25 and Arg38 to an alanine residue each decrease the heme-binding affinity of HTHP.

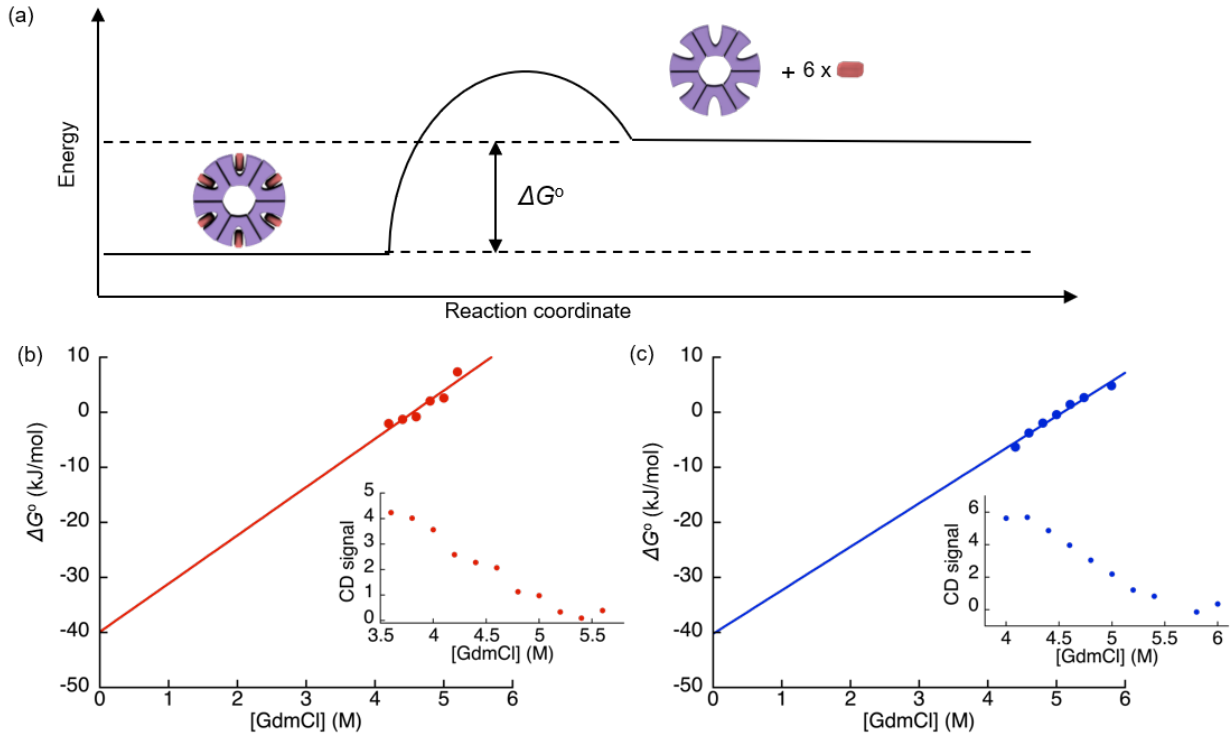

Figure 2-7. (a) Schematic representation of energy diagram of heme binding in HTHP. (b and c) Plots of ΔG^{o} values for ferric HTHP^{R25A} and HTHP^{R38A}, respectively, against the concentration of GdmCl. Insets indicate the CD signal changes upon addition of GdmCl. Conditions: 100 mM potassium phosphate buffer (pH 7.0) at 30 ºC (b) and 60 ºC (c).

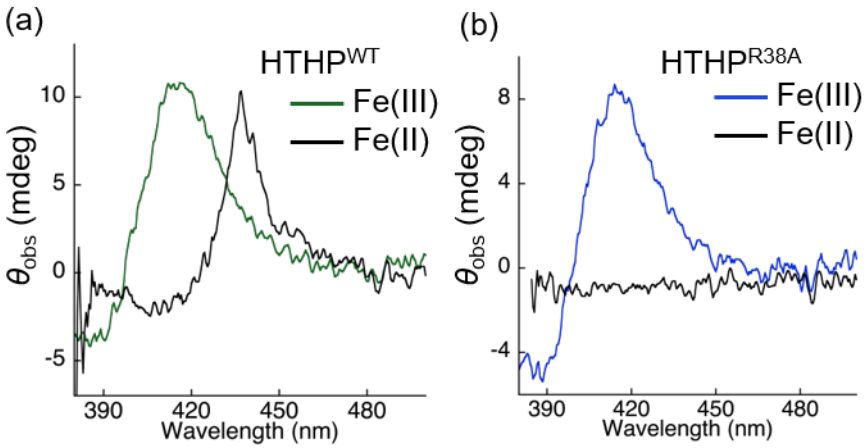

Figure 2-8. CD spectra of Fe(III) and Fe(II) states of $HTHP^{WT}$ (a) and $HTHP^{R38A}$ (b) in visible region.

2-2-3. Preparation of polyacrylamide gels containing reconstituted HTHP mutants as a cross linker

Reconstitution of the HTHP mutants with acryloyl-heme was carried out (Figure 2-1b). First, the apo-forms of the HTHP mutants were prepared by extracting heme with 2-butanone under strongly acidic conditions at pH 1.5. Removal of heme was confirmed by UV-vis spectra, where visible absorption attributed to heme is abolished.[23,33] A large excess of acryloyl-heme was then added into the apo-protein solution, and the reconstituted proteins were purified using an anion-exchange column. Even though the binding affinity decreases as a result of the mutations, UV-vis spectra indicate the formation of the reconstituted ferric protein mutants, rHTHP^{R25A} and rHTHP^{R38A} (Figure 2-9). Next, the rHTHP mutants were utilized as cross-linkers for polyacrylamide gel. First, co-polymerization of 1.0 M acrylamide and 1.0 mM rHTHP mutant was carried out with ammonium persulfate and *N,N,N',N'*-tetramethylethylenediamine. Without any additional cross-linking molecules such as *N,N'*-methylenebis(acrylamide), the gelation occurs in a manner similar to that of HTHP^{WT} reconstituted with acryloyl-heme, rHTHP^{WT}. In the case of control experiments without the rHTHP mutants, gelation does not occur. This finding indicates that the rHTHP mutants have a sufficient amount of heme–heme pocket interactions to serve as a cross-linker for the gel. In addition, it was found that soaking of the polyacrylamide gel containing rHTHP^{R38A} (rHTHP^{R38A}-PAAm gel) into a dithionite solution provides a sol state immediately (Figure 2-10), although the polyacrylamide gel containing rHTHP^{WT} (rHTHP^{WT}-PAAm gel) is maintained with soaking in a dithionite solution. This finding is related to the observation that the ferrous heme cofactor in HTHP^{R38A} is released in a solution under reduction condition. Furthermore, in the Chapter 1, the author observed that the rHTHP^{WT}-PAAm gel is converted to a sol state upon addition of apomyoglobin as a ferrous heme acceptor. The mutation of the Arg38 residue to alanine residue induces a simple redox-responsive gel-sol transition of the polyacrylamide gel containing rHTHP.

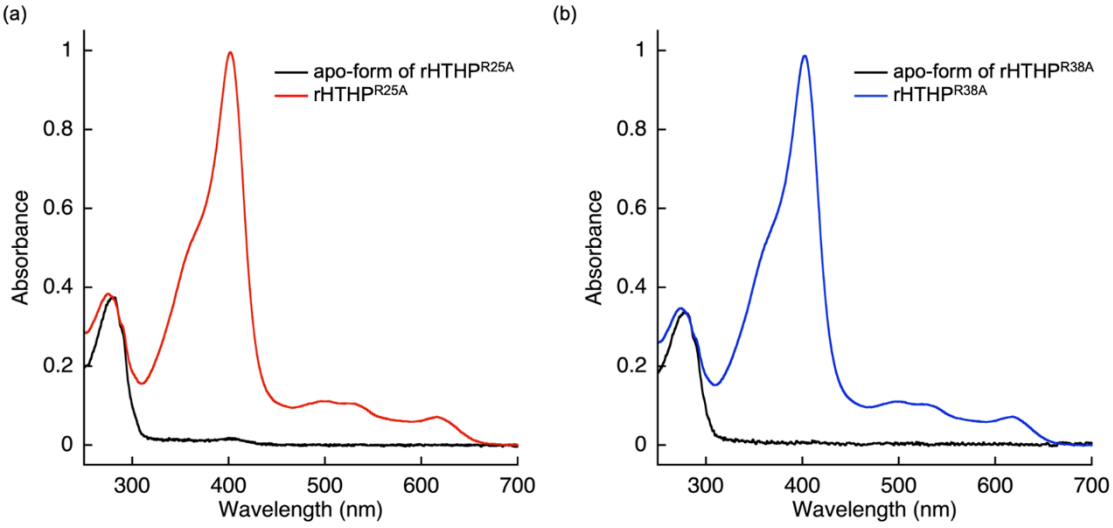

Figure 2-9. UV-vis spectra of apo-forms and reconstituted proteins of (a) HTHP^{R25A} and (b) HTHP^{R38A} in 100 mM potassium phosphate buffer at pH 7.0.

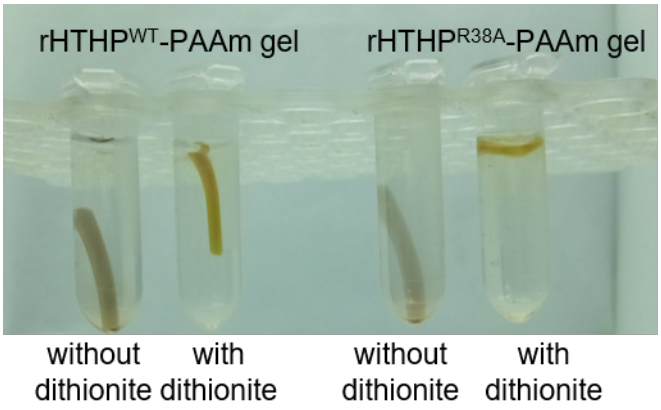

Figure 2-10. Photographs of rHTHP^{WT}- and rHTHP^{R38A}-PAAm gels soaked into buffer solutions with and without dithionite.

2-2-4. Mechanical properties of the hydrogels containing rHTHP and its mutants

To investigate the influence of the mutation on the mechanical properties of the polyacrylamide gel, a tensile test was attempted. However, the polyacrylamide gel containing only rHTHP as a cross-linker was found to be too soft and did not exhibit sufficient toughness for this measurement. Thus, the author prepared a polyacrylamide gel containing both rHTHP mutants and *N,N*'-methylenebis(acrylamide). Co-polymerization of 1.0 M acrylamide, 1.0 mM rHTHP and 2.0 mM *N,N*'-methylenebis(acrylamide) was initiated by ammonium persulfate and *N,N,N',N'*-tetramethylethylenediamine to provide three gels, rHTHP^{WT}-MBA-PAAm gel, rHTHP^{R25A}-MBA-PAAm gel, and rHTHP^{R38A}-MBA-PAAm gel, each having sufficient toughness for tensile testing. FTIR spectrum of rHTHP^{R38A}-MBA-PAAm gel appears to show characteristic peaks derived from the amide bonds of both polyacrylamide and the protein, suggesting that the polymerization occurs in a similar manner to a typical polyacrylamide gel (Figure 2-11). The obtained gels were equilibrated overnight in 100 mM potassium phosphate buffer, and then quickly mounted on a load cell. The tensile testing for rHTHP^{WT}-MBA-PAAm gel, rHTHP^{R25A}-MBA-PAAm gel, and rHTHP^{R38A}-MBA-PAAm gel provides the stress-strain curves as shown in Figure 2-12. Fractures of these three gels occur at 230–250% strain. This indicates that similar polymer network structures are formed in these three hydrogels during the co-polymerization processes. Young's modulus values were determined as slopes of the curves from 0% to 10% strain relative to the strain at fracture. The Young's modulus values for rHTHP^{WT}-MBA-PAAm gel, rHTHP^{R25A}-MBA-PAAm gel, and rHTHP^{R38A}-MBA-PAAm gel are 5.29, 3.81, and 3.49 kPa, respectively, indicating that the mutations reduce the elasticity of the gels to approximately 70%. In the case of hydrogels formed by polymer networks, density and mechanical stability of cross-linking points are known to be critical for elasticity as well as non-covalent interaction between polymer main chains.[34,35] The three hydrogels presented here were constructed using the same main polymer main chain under the same preparation conditions and provided the same

density of cross-linking points. Thus, the decreased Young's modulus values observed for the mutants could be attributed to the lower affinity of heme for the mutants compared to the wild type protein. UV-vis absorption spectra of rHTHP^{R25A} and rHTHP^{R38A} were consistent with that of rHTHP^{wt}, suggesting that the heme molecules in the gels appear to dissociate from the protein matrices by pulling during the tensile test. (Figure 2-13) These results indicate that HTHP works as a cross-linker for hydrogels in which the mechanical elasticity is tunable with mutations.

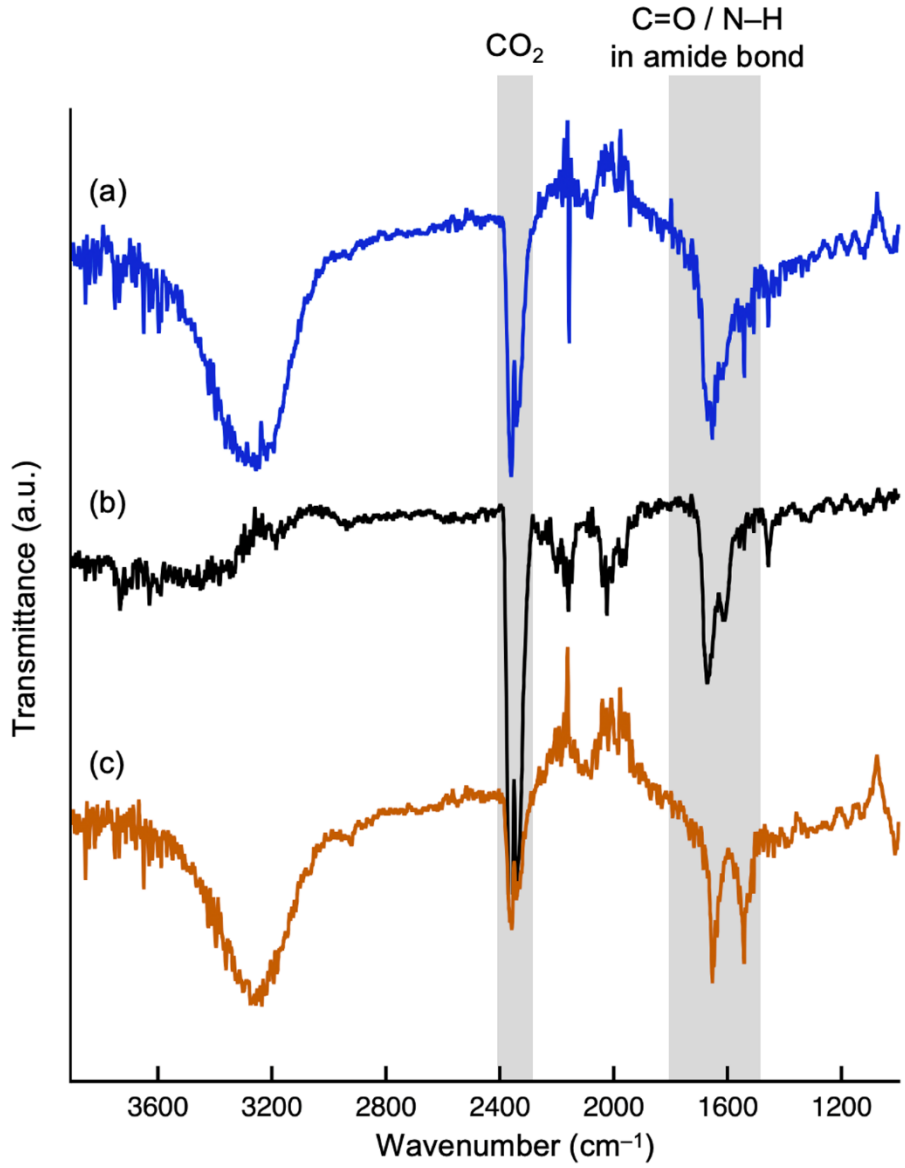

Figure 2-11. FTIR spectra of (a) rHTHP^{R38A}-MBA-PAAm gel, (b) MBA-PAAm gel and (c) rHTHP^{R38A} in a solution state. These samples were measured by attenuated total reflection.

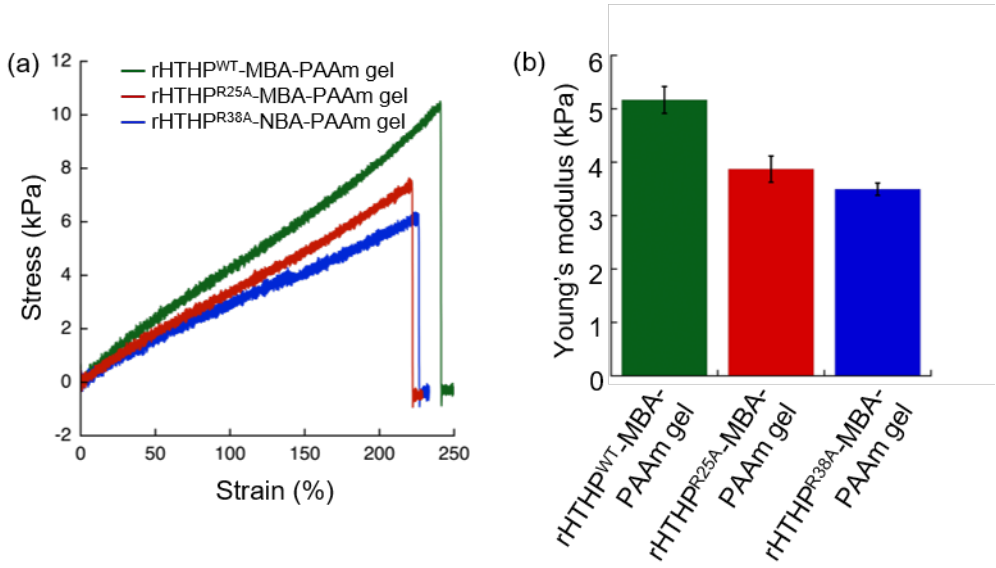

Figure 2-12. (a) Stress-strain curves obtained by tensile tests of rHTHP^{WT}-MBA-PAAm gel (green), rHTHP^{R25A}-MBA-PAAm gel (red) and rHTHP^{R38A}-MBA-PAAm gel (blue). (b) Young's modulus of the gels.

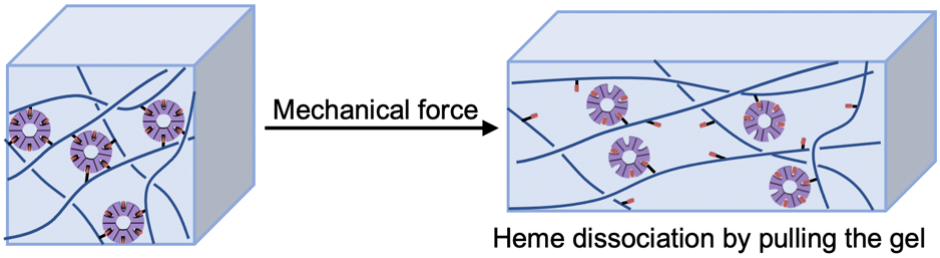

Figure 2-13. Schematic representation for plausibly occurring heme dissociation by mechanical force, supporting the mechanism of Young's modulus reduction by mutation.

2-3. Summary

In summary, the author prepared polyacrylamide gels containing HTHP mutants where the heme–heme pocket interaction is utilized as a supramolecular cross-linkage. The mutations weaken the affinity of heme for the protein matrix, resulting in reduced elastic properties of the gels. To the best of this knowledge, the present results represent the first example of a hemoprotein-based hydrogel possessing tunable elasticity by mutation. Moreover, a reduction-triggered gel-sol transition was simultaneously observed. This finding is expected to lead to development of a new class of biomaterials with fine-tuned elasticity and stimuli-responsiveness. Further studies of the unique mechanical properties of hemoprotein-based hydrogels are currently underway.

2-4. Materials and methods

Instruments

UV-vis spectral measurements of aqueous solution samples were carried out with a Shimadzu UV-2700 or Shimadzu UV-3600 plus spectrophotometer. UV-vis spectra of the gels were recorded using the Shimadzu UV-3600 plus spectrophotometer equipped with an integrating sphere attachment. CD spectra were recorded on a JASCO J-820 spectrometer. Dynamic light scattering was measured using a Malvern Zetasizer μV light scattering analyzer with an 830-nm laser at 25 ˚C. MALDI-TOF MS analyses were performed with a Bruker Autoflex-III mass spectrometer. The pH values were monitored with a Horiba F-52 pH meter. Tensile tests were conducted using a Shimadzu EZ Graph with a 10 N EZ Graph load cell. FTIR spectra were recorded by a JASCO FT/IR 6200 spectrometer equipped with ATR PR0450-S.

Materials

Ultrapure water (Milli-Q) was prepared by a Millipore Integral 3 apparatus. All reagents were of the highest warranted grade commercially available and were used as received unless otherwise indicated. Acryloyl-heme, $HTHP^{WT}$ and $rHTHP^{WT}$ were prepared according to the previous report.[32]

Amino acid sequence of the monomers of $HTHP^{WT}$, $HTHP^{R25A}$ and $HTHP^{R38A}$

$HTHP^{WT}$:
SETWLPTLVTATPQEGFDLAVKLSRIAVKKTQPDAQVRDTLRAVYEKDANALIAVSAVVATHF
QTIAAANDYWKD
$HTHP^{R25A}$:
SETWLPTLVTATPQEGFDLAVKLS**A**IAVKKTQPDAQVRDTLRAVYEKDANALIAVSAVVATHF
QTIAAANDYWKD
$HTHP^{R38A}$:
SETWLPTLVTATPQEGFDLAVKLSRIAVKKTQPDAQV**A**DTLRAVYEKDANALIAVSAVVATHF
QTIAAANDYWKD

Expression and purification of $HTHP^{R25A}$ and $HTHP^{R38A}$

The gene expression system for $HTHP^{WT}$ was reported by Hayashi and coworker[22, 32]. Site-directed mutagenesis was performed using an LA PCR *in vitro* Mutagenesis Kit (Takara Bio) according to the manufacturer's protocol. The HTHP gene cloned into pDEST14 was used as a template to introduce mutations into the HTHP matrix with primers (i) as below. After PCR, the template DNA plasmids were digested with Dpn I (Thermo Fisher Scientific). *E. coli* DH5α competent cells were transformed with the PCR products. After cultivation, the plasmids were purified using a PureLink™ Quick Plasmid Miniprep Kit (Thermo Fisher Scientific). The obtained plasmid was further used as a template for site-directed mutagenesis with primers (ii) as below. The desired plasmid containing the

gene for the mutant of HTHP (R25A or R38A) was obtained using the same method. DNA sequencing was performed to verify each correct mutation in the gene sequence.

The primer sequences used to generate the mutant were:

(i) R25A: (5'- GATCTGGCCGTGAAACTGTCGGCGATTGCGGTCAAGAAAACCC -3') and the complementary primer;

(ii) R38A: (5'- CAGCCAGATGCCCAAGTTGCCGATACTCTCCGTGCTGTG -3') and the complementary primer.

The resulting expression plasmid was used to transform *E. coli* BL21 (DE3). LB medium (4 L) containing ampicillin (400 mg) was inoculated with 50 mL of the culture (OD = 0.5) of the transformed cells. After the cells were grown aerobically with vigorous shaking at 37 ˚C until an OD_{600} value was reached ~0.5, isopropyl-β-D-1-thiogalactopyranoside (IPTG, final concentration: 1 mM) was added to the culture for induction of protein expression. The culture was continued at 37 ˚C overnight. The cells were harvested by centrifugation at 4000xg for 10 min. The harvested cells from 4 L of culture were re-suspended in ca. 50 mL of a 10 mM Tris-HCl buffer at pH 8.0, and lysed by freeze-thaw cycles with subsequent sonication for 30 sec x 10 times at 4 ˚C. The lysate was then centrifuged, and the supernatant was collected. The solution was diluted 10-fold with 100 mM potassium phosphate buffer at pH 7.0 and loaded through a CM Fast Flow (GE Healthcare) cation-exchange column pre-equilibrated with 100 mM potassium phosphate buffer at pH 7.0. The flow-through solution was loaded onto a DEAE Fast Flow (GE Healthcare) anion-exchange column pre-equilibrated with 100 mM potassium phosphate buffer at pH 7.0. The fraction of the target protein was collected with a 100 mM potassium phosphate buffer at pH 7.0 containing 0.3 M NaCl. The obtained solution was concentrated using an Amicon stirred ultrafiltration cell with a 30-kDa molecular weight cut-off membrane (Millipore). The concentrated solution was passed through a Superdex 200 Increase 10/300 GL column with 100 mM potassium phosphate buffer at pH 6.0. The fractions with $R_z > 2$ (R_z is a ratio of absorbance values at 402 nm and 280 nm) were collected and loaded on a Hitrap Q HP 5 mL (GE Healthcare) anion-exchange column pre-equilibrated with 100 mM potassium phosphate buffer at pH 6.0. The fraction of the target protein was then eluted with 100 mM potassium phosphate buffer at pH 6.0 containing 0.35 M NaCl. The obtained HTHP mutant was stored at –80 ˚C.

CD spectra for ΔG^o evaluation[22, 29, 31]

CD spectra were measured in a solution containing HTHP mutant in 100 mM potassium phosphate buffer at pH 7.0. In the case of the Fe(III) state, the temperature was maintained at 30 ($HTHP^{R25A}$) and 60 °C ($HTHP^{R38A}$) by an equipped thermal controller. The optical path length was 1 cm, and the bandwidth was 2 μm.

To analyze CD signal changes of HTHP mutants in the presence of various concentrations of GdmCl, the two-state equilibrium transition is considered as below:

$$\text{heme-bound state} \rightleftharpoons \text{unbound state} \quad (1)$$

The equilibrium constants at each GdmCl concentration were calculated using the following equation:

$$F_B(C) = 1 - F_U(C) = (y_x(C) - y_U(C)) / (y_B(C) - y_U(C)) \quad (2)$$

where $F_B(C)$ and $F_U(C)$ represent fractions of the heme-bound and unbound states, respectively, at a given GdmCl concentration (C). $y_x(C)$ is an observed CD signal intensity at a GdmCl concentration (C). $y_B(C)$ and $y_U(C)$ are the dependencies of the assumed CD signal intensities on denaturant concentrations for the fully heme-bound and unbound states, respectively. Subsequently, the equilibrium constants, $K_{eq}(C)$, were determined as:

$$K_{eq}(C) = F_B(C) / F_U(C) = (y_x(C) - y_U(C)) / (y_B(C) - y_x(C)) \quad (3)$$

The $K_{eq}(C)$ values were converted into $\Delta G°(C)$ values using equation (4), as follows:

$$\Delta G°(C) = -RT \ln K_{eq}(C) \quad (4)$$

The $\Delta G°$ value in the absence of chemical denaturant was determined as a y-intercept of the linear extrapolation model, as shown in Figures 2-7b and c.

Preparation of rHTHP mutants

Twelve equivalents of acryloyl-heme in DMSO (stock solution: 5 mM) were added into a solution of apoHTHP mutant (10 μM in 100 mM potassium phosphate buffer containing 1 M NaCl) at 37 ºC, and the reaction mixture was gently shaken overnight. Dialysis was carried out to remove DMSO against 100 mM potassium phosphate buffer (pH 7.0) at 4 ºC. The excess acryloyl-heme was removed by a HiTrap Desalting column. The obtained rHTHP was characterized by UV-vis spectrum. Purity was confirmed by an R_z value >2.3.

Preparation of polyacrylamide gel containing rHTHP

Reconstituted HTHP mutant was concentrated to 5 mM by ultrafiltration using a 30-kDa cut-off Amicon Ultra tube via centrifugation at 6000 rpm. Polymerization of 1.0 mM rHTHP and 1 M acrylamide in 100 mM potassium phosphate buffer at pH 7.0 containing 1 M NaCl was carried out with 0.25% ammonium sulfate and 0.38% *N*,*N*,*N*',*N*'-tetramethylethylenediamine as a radical initiator. Then, a dual cross-linked hydrogel was prepared in the presence of 2.0 mM *N*,*N*'-methylene bis(acrylamide) and 1.0 mM rHTHP under the same radical polymerization conditions.

Mechanical properties evaluation

Samples were prepared in a cubic shape with ca. 14 mm x ca. 1.0 mm x ca. 1.0 mm in equilibrium swelling states. During tensile tests, samples were attached to a metal sheet using the adhesive reagent Aron Alpha®, within 8 mm. The Young's modulus values were determined by the slope from 0% to 10% strain relative to the strain at fracture.

2-5. References

1 N. P. Balsara, L. J. Fetters, N. Hadjichristidis, D. J. Lohse, C. C. Han, W. W. Graessley, R. Krishnamoorti, *Bull. Chem. Soc. Jpn.* **1999**, *32*, 6137.

2 M. D. Shoulders, R. T. Raines, *Annu. Rev. Biochem.* **2009**, *78*, 929.

3 H. Li, N. Kong, B. Laver, J. Liu, *Small* **2016**, *12*, 973.

4 S. Lv, D. M. Dudek, Y. Cao, M. M. Balamurali, J. Gosline, H. Li, *Nature* **2010**, *465*, 69.

5 J. Fang, A. Mehlich, N. Koga, J. Huang, R. Koga, X. Gao, C. Hu, C. Jin, M. Rief, J. Kast, D. Baker, H. Li, *Nat. Commun.* **2013**, *4*, 2974.

6 H. Li, Y. Cao, *Acc. Chem. Res.* **2010**, *43*, 1331.

7 X. Gao, J. Fang, B. Xue, L. Fu, H. Li, *Biomacromolecules* **2016**, *17*, 2812.

8 H. Lei, L. Dong, Y. Li, J. Zhang, H. Chen, J. Wu, Y. Zhang, Q. Fan, B. Xue, M. Qin, B. Chen, Y. Cao, W. Wang, *Nat. Commun.* **2020**, *11*, 4032.

9 M. Taki, T. Yamashita, K. Yatabe, V. Vogel, *Soft Matter* **2019**, *15*, 9388.

10 A. P. Esser-Kahn, M. B. Francis, *Angew. Chem. Int. Ed.* **2008**, *47*, 3751.

11 A. P. Esser-Kahn, A. T. Iavarone, M. B. Francis, *J. Am. Chem. Soc.* **2008**, *130*, 15820.

12 Y. Cao, H. Li, *Chem. Commun.* **2008**, 4144.

13 W. A. Petka, J. L. Harden, K. P. McGrath, D. Wirtz, D. A. Tirrell, *Science* **1998**, *281*, 389.

14 M. Kojima, S. Abe, T. Ueno, *Biomater. Sci.* **2022**, *10*, 354.

15 T. Miyata, N. Asami, T. Uragami, *Nature* **1999**, *399*, 766.

16 C. Norioka, K. Okita, M. Mukada, A. Kawamura, T. Miyata, *Polym. Chem.* **2017**, *8*, 6378.

17 T. Ono, Y. Hisaoka, A. Onoda, K. Oohora, T. Hayashi, *Chem. Asian J.* **2016**, *11*, 1036.

18 N. Yamaguchi, L. Zhang, B.-S. Chae, C. S. Palla, E. M. Furst, K. L. Kiick, *J. Am. Chem. Soc.* **2007**, *129*, 3040.

19 Y. Kobayashi, Y. Takashima, A. Hashidzume, H. Yamaguchi, A. Harada, *Sci. Rep.* **2015**, *5*, 16254.

20 C. J. Reedy, B. R. Gibney, *Chem. Rev.* **2004**, *104*, 617.

21 K. Oohora, R. Kajihara, M. Jiromaru, H. Kitagishi, T. Hayashi, *Chem. Lett.* **2019**, *48*, 295.

22 K. Kageyama, K. Oohora, T. Hayashi, *RSC Adv.***2023***, 13*, 34610.

23 J.-H. Jeoung, D. A. Pippig, B. M. Martins, N. Wagener, H. Dobbek, *J. Mol. Biol.* **2007**, *368*, 1122.

24 B. A. Springer, S. G. Sligar, J. S. Olson, G. N. Jr. Phillips, *Chem. Rev.* **1994**, *94*, 699

25 D. S. Culbertson, J. S. Olson, *Biochemistry* **2010**, *49*, 6052.

26 S. Ozaki, T. Sato, Y. Sekine, C. T. Migita, T. Uchida, K. Ishimori, *J. Inorg. Biochem.* **2014**, *138*, 31.

27 M. Kanadani, T. Sato, T. Hino, S. Nagano, S. Ozaki, *J. Inorg. Biochem.* **2015**, *151*, 26.

28 M. S. Hargrove, A. J. Wilkinson, J. S. Olson, *Biochemistry* **1996**, *35*, 11300.

29 P. A. Sykes, H.-C. Shiue, J. R. Walker, R. C. Bateman Jr., *J. Chem. Educ.* **1999**, *76*, 1283.

30 C. R. Robinson, Y. Liu, J. A. Thomson, J. M. Sturtevant, S. G. Sligar, *Biochemistry*, **1997**, *36*, 16141.

31 G. I. Makhatadze, *J. Phys. Chem. B* **1999**, *103*, 4781.
32 K. Oohora, T. Mashima, K. Ohkubo, S. Fukuzumi, T. Hayashi, *Chem. Commun.* **2015**, *51*, 11138.
33 J. P. Gong, *Soft Matter* **2010**, *6*, 2583.
34 T. L. Sun, T. Kurokawa, S. Kuroda, A. B. Ihsan, T. Akasaki, K. Sato, M. A. Haque, T. Nakajima, J. P. Gong, *Nat. Mater.* **2013**, *12*, 932.

Chapter 3
Mechanochemical Responses in β-Lactoglobulin-based Hydrogels

3-1. Introduction

Proteins are useful building blocks for biomaterials.[1-4] In particular, collagen and fibronectin are known to be intrinsic extracellular matrices and are also used as the main components of artificial biomaterials.[5-7] Inspired by such protein behavior, oligomerization of monomeric proteins provides unique biomaterials as well as combinations of proteins and synthetic polymers.[8–16] In one notable study, Li and co-workers prepared elastic materials containing an artificial GB-1 protein oligomer which replicates the mechanical properties of titin, a muscle protein.[8,9] The high elasticity was found to be derived from protein folding and unfolding behaviors. In these new materials, mechanical stretching caused protein denaturation and dissipation of energy which resulted in increased toughness.[8] Folding and unfolding were accompanied by large structural changes, providing the materials with high stretchability.[16]

Hydrogels, which are known for their remarkable three-dimensional network structures formed through the cross-linking of polymers, demonstrate significant swelling properties when exposed to water.[17] The unique properties of hydrogels are useful for biocompatible materials.[18,19] An intriguing feature of hydrogels is their ability to undergo transformative changes in shape and properties when exposed to varying physical or chemical stimuli.[20,21] Proteins have been utilized as a cross-linking unit for unique hydrogels with inherent protein functions and properties.[22–27] In one example, metallothionein, a metal-binding protein, is used as a cross-linker in a polymer network for hydrogel formation.[23] This hydrogel functions as a metal-responsive volume-changing material. However, investigations of protein-based hydrogels showing mechanical stimuli-induced functions have been limited.[16,26,27]

β-Lactoglobulin (BLG) is an attractive protein component for development of hydrogels with mechanical stimuli-responsive materials (Figures 3-1a,b). BLG is an abundant and commercially available whey protein with a molecular weight of 18.4 kDa and a unique structure consisting mainly of nine β-strands and a terminal α-helix.[28,29] The generation of artificial metalloenzymes based on BLG has also been explored by introducing alkyl chains with metal complexes within its β-barrel structure.[30,31] Moreover, the presence of specific disulfide bonds and a reactive cysteine residue (Cys121) in its structure provides potential to generate chemical modifications.[29,32-35] The Cys121 residue in the crystal structure is not exposed to solvent and is therefore relatively unreactive. Unfolding of the BLG protein exposes this residue, resulting in its chemical modification. Hong and co-workers have reported a modification of the Cys121 residue of unfolded BLG with a tetraphenylethene derivative tethering a maleimide group (TPE-NMI), which resulted in fluorescence emission.[32-34] In this context, after optimizing the formation of BLG-based hydrogels, the author demonstrates that the macroscopic shape changes of the hydrogels generated by compression will

trigger microscopic unfolding of the protein, thereby causing chemical modifications of the Cys121 residue (Figures 3-1 and 3-2).

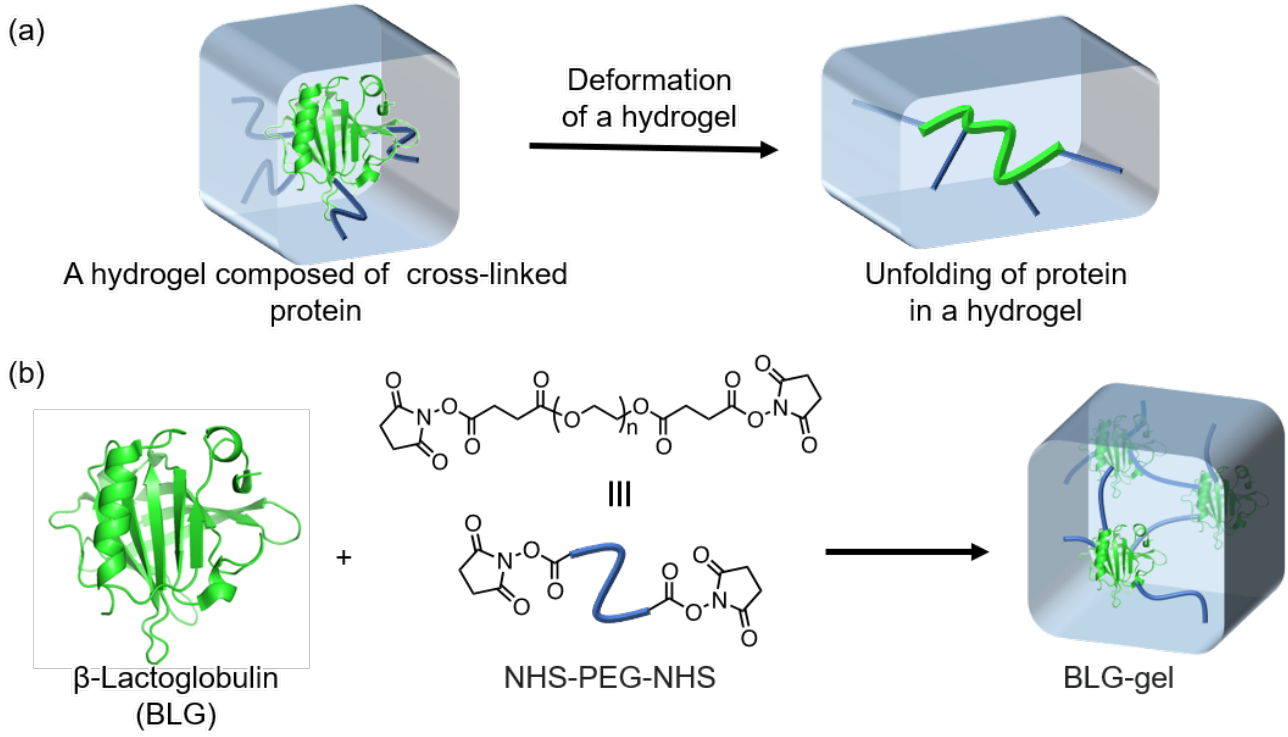

Figure 3-1. (a) A concept of a hydrogel composed of cross-linked protein and its mechanical unfolding by deformation of the hydrogel. (b) Schematic representation for the preparation of BLG-gel.

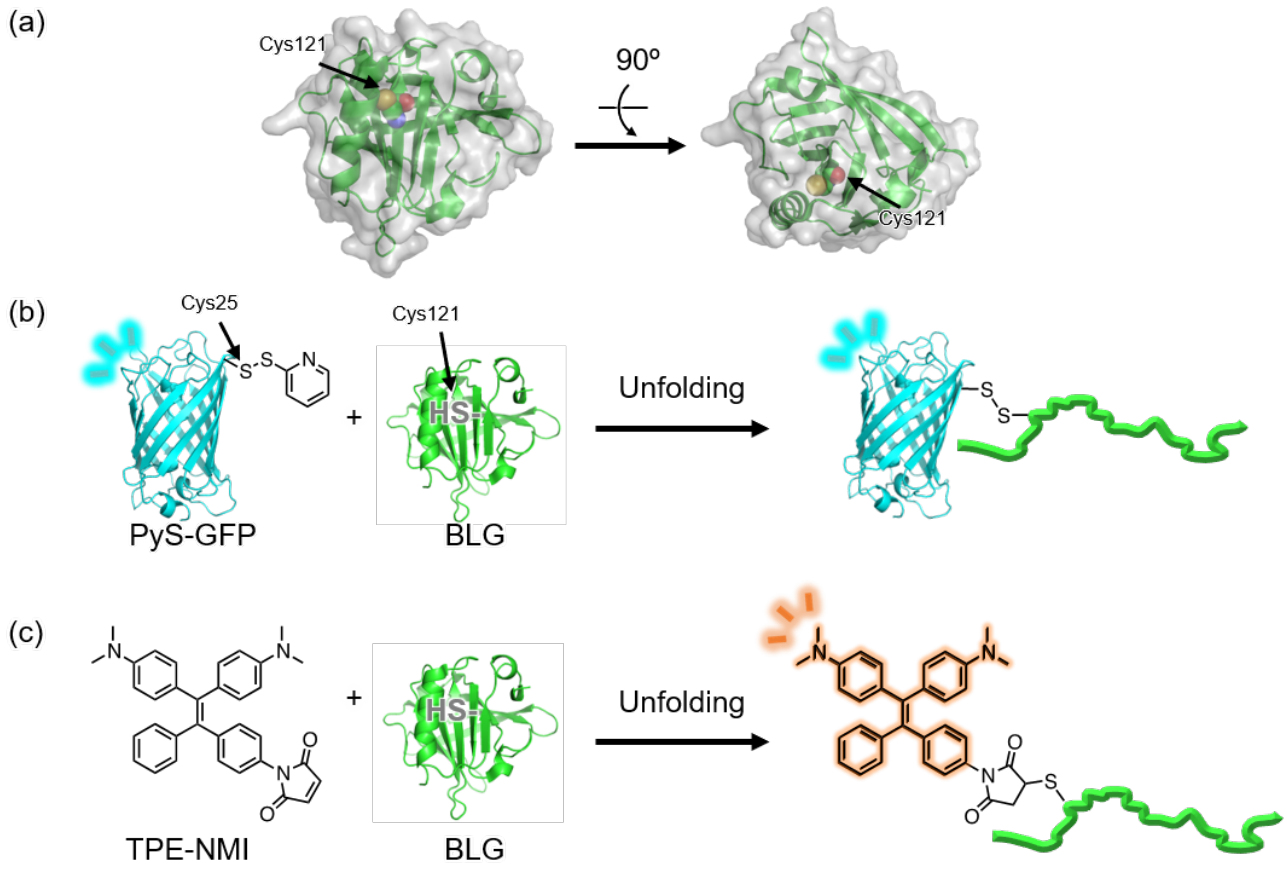

Figure 3-2. (a) Side (left) and top (right) views of BLG crystal structure (PDB: 3NPO) with a solvent-accessible surface. A Cys121 residue is highlighted. (b) Unfolding-induced reaction of the Cys121 residue of BLG with pyridyl disulfide-tethering GFP (PyS-GFP) in a solution and gel. (c) Unfolding-induced reaction of the Cys121 residue of BLG with tetraphenylethene tethering a maleimide group (TPE-NMI) in a solution and gel.

3-2. Results and discussion

3-2-1. Preparation of BLG-based hydrogels

To prepare the BLG-based hydrogels, amide bonds are generated by the reactions of *N*-hydroxysuccinimide (NHS) esters with primary amines of 15 Lys residues and the N-terminus on the protein surface (Figure 3-1b). By reacting these amino groups with the succinimide esters linked at both ends of a polyethylene glycol (PEG) chain, the formation of a three-dimensional network structure containing BLG was expected to occur. Thus, PEG (M_w = 2000) with NHS esters at both ends, NHS-PEG-NHS, was prepared as previously described.[36] A potassium phosphate buffer solution (pH 7.5) of BLG was mixed with a buffer solution of the crosslinker NHS-PEG-NHS (pH 7.5). This mixture was then poured into a mold to form a hydrogel at room temperature for approximately 5 h. The results of the optimization of BLG and crosslinker concentrations are summarized in Table 3-1.

Table 3-1. Gelation of BLG in the reaction with NHS-PEG-NHS under various concentration conditions.

Entry	[BLG] (mg/mL)	NHS-PEG-NHS (eq.)	Gelation
1	80	2.5	–
2	80	5.0	–
3	80	10	–
4	100	2.5	–
5	100	5.0	○
6	100	10	○
7	100	15	○

In entries 1–3 of Table 3-1, no gelation was observed, possibly because of the low-density network structures. Although viscosity is clearly increased in entry 4, the shape was not maintained in the potassium phosphate buffer. Colorless hydrogels were obtained under the conditions of entries 5–7, where the concentration of BLG was 100 mg/mL and more than five equivalents of NHS-PEG-NHS were added to the BLG solution. When non-modified polyethylene glycol was used instead of NHS-PEG-NHS as a control experiment, no gelation was observed even under the conditions of 100 mg/mL BLG and 5 eq. polyethylene glycol. This indicates that formation of covalent bonds is essential to construct the network structure affording the desired hydrogels, BLG-gels, under the optimal conditions of entries 5–7.

3-2-2. Mechanical properties and denaturation-induced swelling behavior of the BLG-gels

Mechanical properties of the BLG-gels were evaluated by tensile tests. Before evaluation, the hydrogels were equilibrated by swelling overnight in a 100 mM potassium phosphate buffer solution (pH 7.0). The results are shown in Figure 3-3 and Table 3-2. Young's modulus was determined by the initial slope of the stress–strain curve up to 10% of the strain to fracture. In entries 1–3, the increase in crosslinker concentration decreases the Young's modulus. In hydrogels, Young's modulus generally increases because the effective crosslinking density increases linearly with the number of polymer chains between crosslinking points.[19] However, in the case of hydrogels containing a protein as a component, the mechanical stability and unfolding pathways of the protein might depend on the direction of applied force,[8,9,16] leading to a decrease in Young's modulus with an increase in the degree of crosslinking. Furthermore, PEG is known to bind to hydrophobic parts of proteins and exhibit mild denaturing effects when used at high concentrations. As a result, destabilization of relatively hydrophobic BLG has been observed.[37] Thus, even in this system, the addition of PEG appears to alter the structure of BLG, resulting in a decrease in the Young's modulus. In addition, too much PEG relative to the reaction site may decrease the cross-linking rate. Entry 4 shows the tensile test results of a BLG-hydrogel soaked in a buffer solution including 7 M urea, which acts as a denaturant. Compared to entry 1, the decrease in Young's modulus suggests that the unfolding of BLG induced by urea reduces the dissipation energy and decreases the mechanical strength of this hydrogel. These results indicate that the folding of BLG in the hydrogel of entry 1 contributes to its elasticity. Considering these results, the sample prepared using 100 mg/mL BLG and 5 equivalents NHS-PEG-NHS was selected as the optimal preparation and this BLG-gel was used in subsequent experiments. The Young's modulus of the BLG-gel shown here is within the range of Young's moduli reported for various protein-based hydrogels (10–30 kPa).[38,39]

Table 3-2. Young's modulus values of BLG-gels determined by a tensile test.

Entry	[BLG] (mg/mL)	NHS-PEG-NHS (eq.)	Young's modulus (kPa)
1	100	5.0	13
2	100	10	11
3	100	15	2.8
4[a]	100	5.0	5.7

[a]BLG-gel soaked in 7 M urea solution before the tensile test.

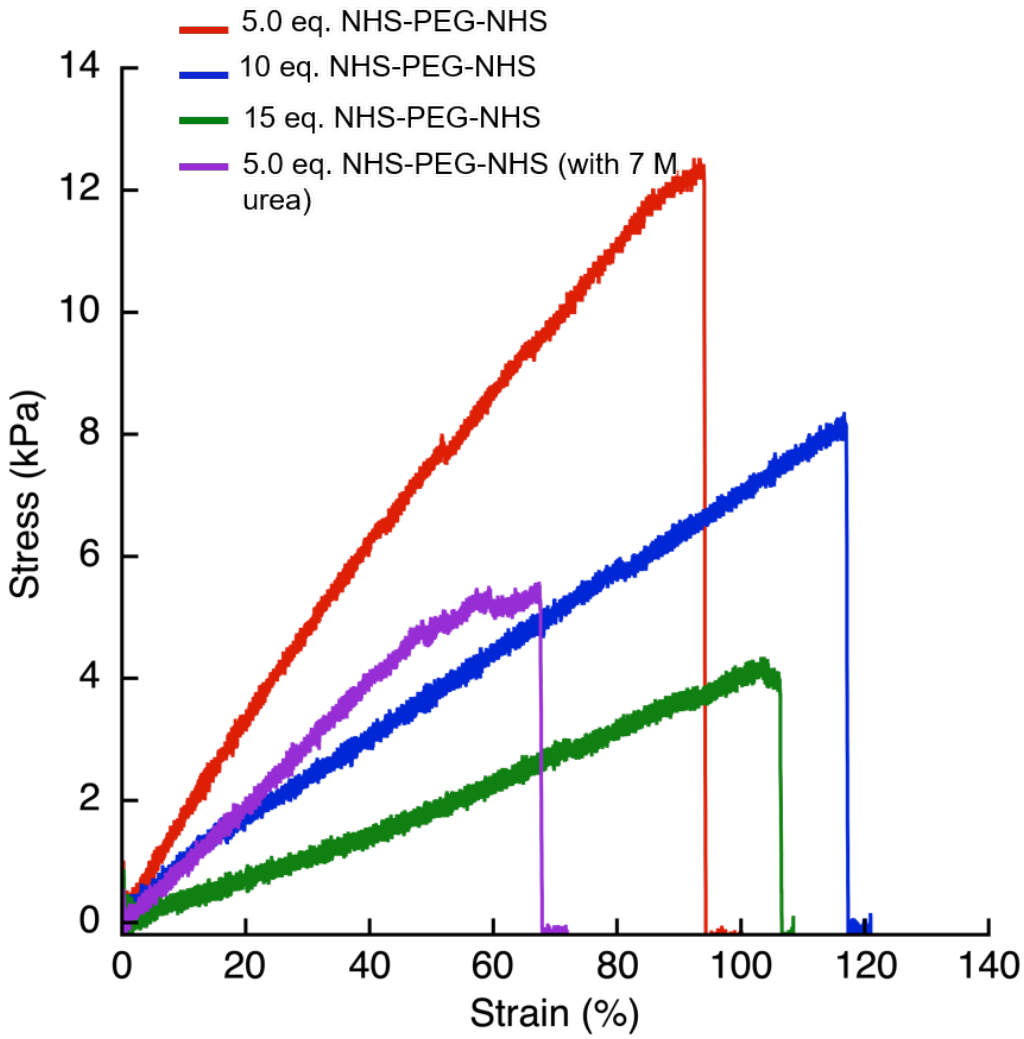

Figure 3-3. Stress-strain curves obtained by tensile tests of BLG-gels which were prepared by the reactions of 100 mg/mL BLG with various equivalents of NHS-PEG-NHS (red: 5.0 eq., blue: 10 eq., and green: 15 eq.). The purple line displays the curve of a BLG-gel soaked in 7 M urea, where the hydrogel was prepared in a reaction of 100 mg/mL BLG with 5.0 equivalents of NHS-PEG-NHS.

It is known that protein folding/unfolding greatly alters the swelling properties of hydrogels comprising protein building blocks.[40] Therefore, these BLG-gels equilibrated by swelling overnight in a buffer solution were soaked in buffer solutions containing various concentrations of urea. The relative volume changes of the hydrogels are shown in Figure 3-4. These changes are mostly consistent with fluorescence titration of a BLG solution by urea. Due to tryptophan fluorescence being sensitive to environmental changes, the unfolding behavior of BLG itself was observed and compared with the swelling behavior of the BLG-gel. Both changes were mainly observed between urea concentrations of 4 M and 6 M. Furthermore, when the urea-treated hydrogel was soaked again in a urea-free potassium phosphate buffer solution (pH 7.0), the volume of the hydrogel returned to its original size before urea treatment. These findings suggest a close relationship between hydrogel swelling and the BLG folding/unfolding.

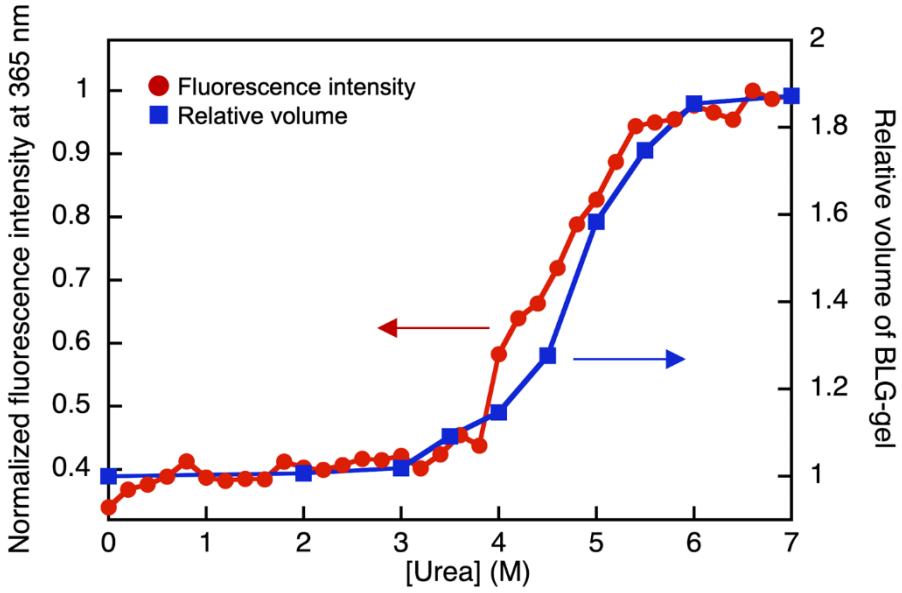

Figure 3-4. Fluorescence titration (red circle) of urea for the BLG-gels in a solution and relative volume changes (blue square) of BLG-gels after soaking in various concentrations of urea.

3-2-3. Chemical modification with GFP mutant via compression-triggered unfolding of protein-units in the BLG gels

Next, the author investigated chemical modifications induced by compression-triggered unfolding of the protein units in the BLG-gels. The Cys121 residue located within the interior of BLG is expected to become exposed and to react with a thiol-selective modifier upon unfolding. As such a modifier, the author employed a pyridyl disulfide-tethered green fluorescent protein (GFP) K25C/C47A mutant, PyS-GFP which was reported previously[41,42]. This mutant was found to react with a reactive Cys residue on a protein to provide a disulfide protein dimer.[41,42] First, the reaction of PyS-GFP with BLG in a solution state was investigated under various urea concentrations (Figure 3-2a). The reactions were carried out at pH 6.5 and 25 ºC for 8 h. SDS-PAGE results indicate that the BLG modification is produced by GFP only in the presence of 4–6 M urea (Figure 3-5a). Second, the reaction was applied to the mechanically deformed hydrogel. In this experiment, a cylindrically shaped BLG-gel with a height of 4 mm and a diameter of 7 mm was used. The hydrogel was soaked in a buffer solution containing 20 μM PyS-GFP for 12 h. The hydrogel was then compressed for 12 h by clipping it with two glass plates using a 1 mm spacer to generate the height constraint (Figure 3-6). This height by the compression is limited by toughness of the gel, because compression with a spacer thinner than 1 mm will fracture the gel. The resulting hydrogel was washed several times with potassium phosphate buffer over 6 days. Photographs of the hydrogels were taken at each step under UV light irradiation (365 nm) (Figures 3-5b,c). The difference in fluorescence intensity between compressed and uncompressed hydrogels was observed in the photographs. To evaluate the relative fluorescence intensity, fluorescence spectra of the hydrogels were measured (Figure 3-7), and a clear difference in fluorescence intensity between the compressed and uncompressed hydrogels was observed with a ratio of approximately 100:57. The modification ratio was dependent on the compression time, which was almost saturated at 12 h for this gel (Figure 3-8). This suggests that more GFP is bound in the compressed hydrogel than in the uncompressed hydrogel due to compression-triggered BLG unfolding. Although non-specific modification of BLG by PyS-GFP also occurs, the disulfide bond formation between GFP and BLG was promoted more efficiently by unfolding of BLG associated with hydrogel compression.

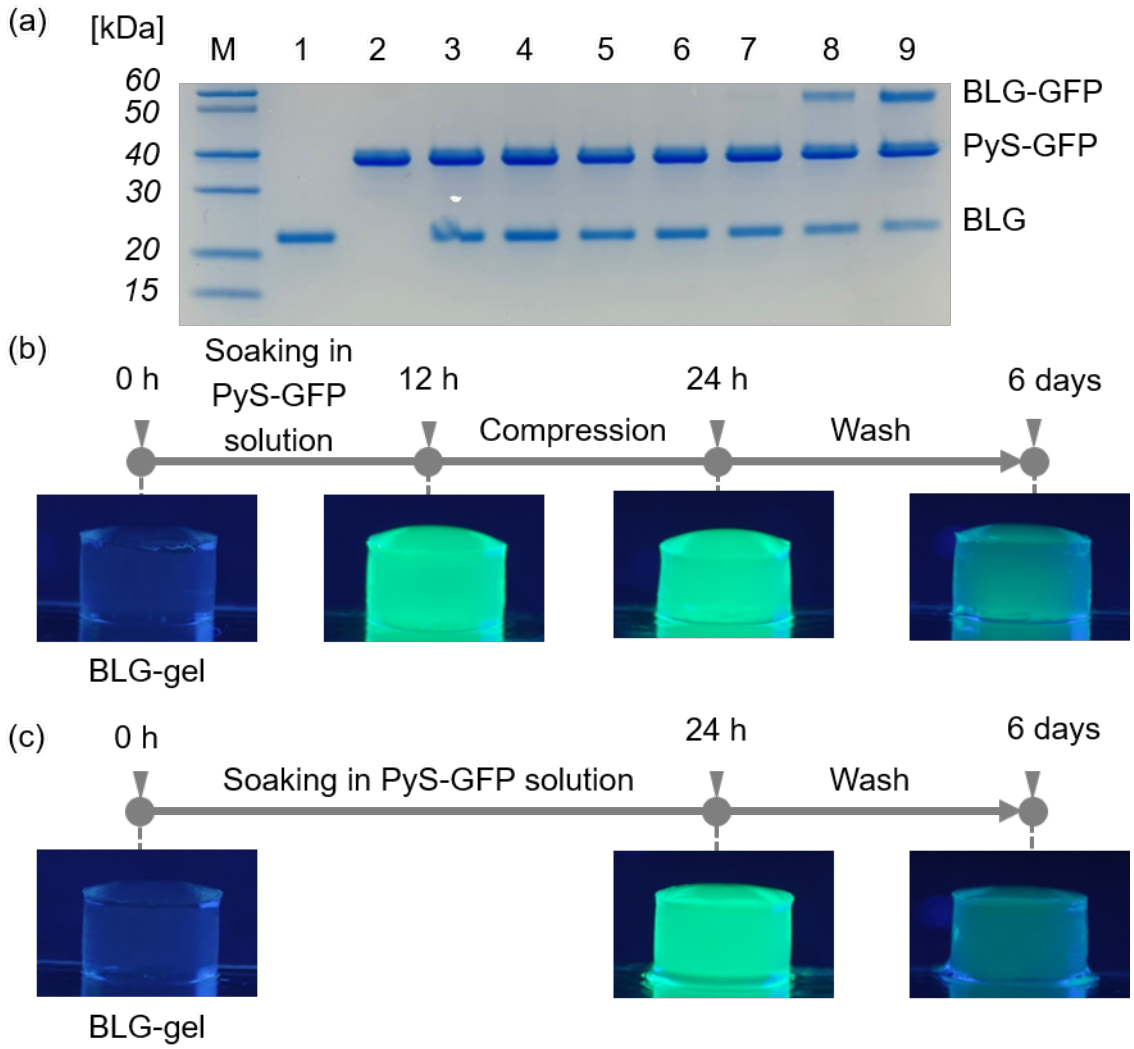

Figure 3-5. (a) SDS-PAGE for the reaction of BLG with PyS-GFP. Lane M: protein marker, lane 1: BLG, lane 2: PyS-GFP, lanes 3–9: reaction mixtures of BLG and PyS-GFP in the presence of various concentrations of urea (lane 3: 0 M, lane 4: 1 M, lane 5: 2 M, lane 6: 3 M, lane 7: 4 M, lane 8: 5 M, lane 9: 6 M). (b,c) Photographs of BLG gels for compression-triggered chemical modification by PyS-GFP (b) with compression and (c) without compression under irradiation of UV-light (365 nm).

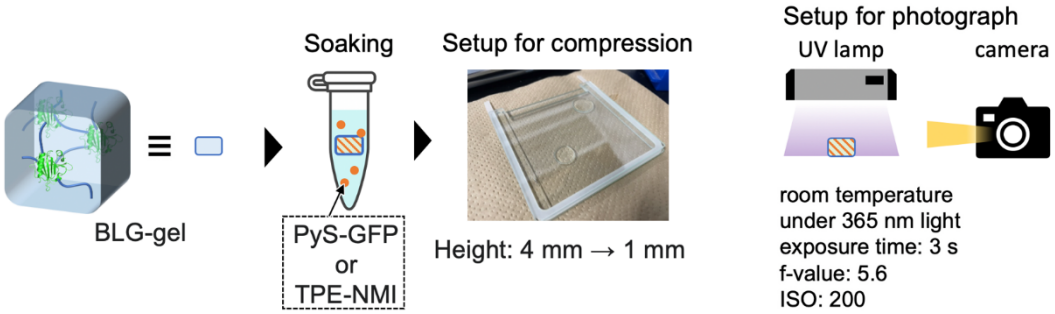

Figure 3-6. Schematic representation of setup for the compression experiments of BLG-gel for chemical modification.

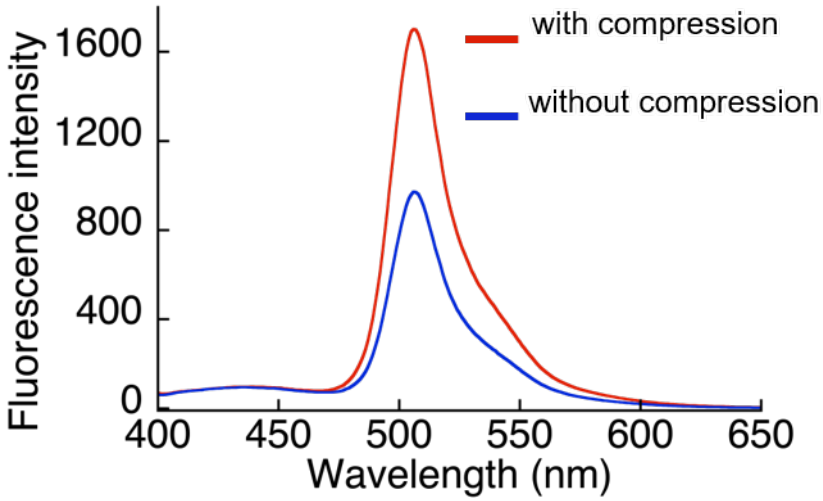

Figure 3-7. Fluorescence spectra of BLG-gels obtained with compression (sample in Figure 3-5b) and without compression (sample in Figure 3-5c).

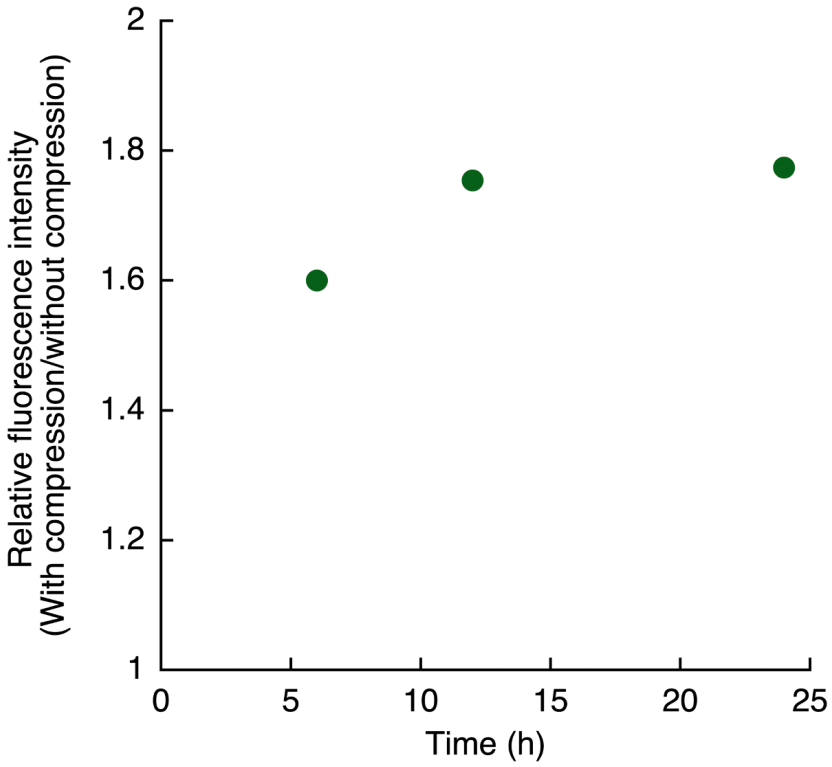

Figure 3-8. Time course plots of relative intensities in fluorescence spectra of BLG-gels modified by PyS-GFP with and without compression.

3-2-4. Chemical modification with tetraphenylethene tethering a maleimide group via compression-triggered unfolding of protein-units in the BLG gels

TPE-NMI has been reported as a useful fluorophore because this molecule shows an increase in fluorescence intensity in the reaction with Cys121 of BLG under the previously described denaturation conditions (Figures 3-2b and 3-9).[32-34] The reason is that the maleimide group in TPE-NMI reacts with the cysteine residue of BLG, disrupting the n-π conjugation and suppressing the rotational motion of the benzene ring. The author further investigated the possibility of complexation between TPE-NMI and the protein moiety within the BLG-gel. This complexation is driven by the structural changes of BLG, which are triggered by compression of the hydrogel. The cylindrically shaped hydrogel was soaked in a 100 mM potassium phosphate buffer (pH 6.5) containing TPE-NMI (50 μM) and 5% dimethyl sulfoxide for 12 h and then compressed for 12 h using two glass plates with a 1 mm spacer. At each step, the hydrogels were photographed under UV light irradiation (365 nm) as shown in Figure 3-10. In the compressed hydrogel, increased fluorescence from TPE-NMI was observed (Figure 3-10a). In contrast, no fluorescence was observed when compression was not applied (Figure 3-10b). Moreover, no fluorescence was seen after compression of hydrogels consisting of unreactive BLG where the Cys121 residue was protected by *N*-phenylmaleimide. (Figure 3-10c). These results suggest that the chemical modification of BLG moieties with TPE-NMI in hydrogel is induced by structural changes in BLG which are generated upon compression.

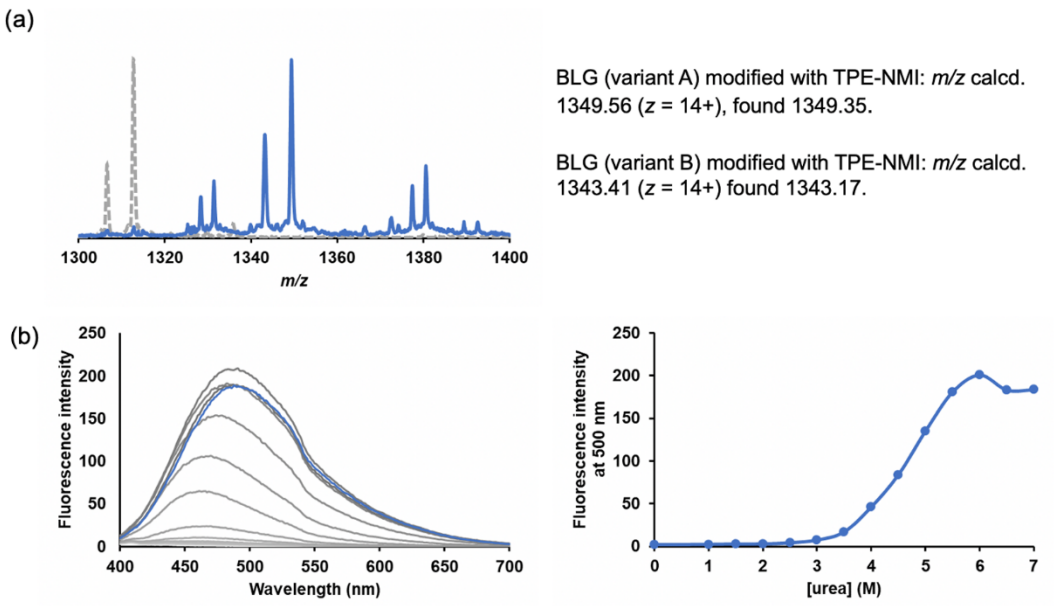

Figure 3-9. Characterization of BLG modified with TPE-NMI in a solution state. (a) ESI mass spectrum of the reaction mixture in the presence of 7 M urea. Dotted line shows the mass spectrum of unmodified BLG. (b) (left) Fluorescence spectra (left) of reaction mixtures under the conditions of various concentrations of urea and (right) plots of fluorescence intensity at 500 nm against urea concentrations.

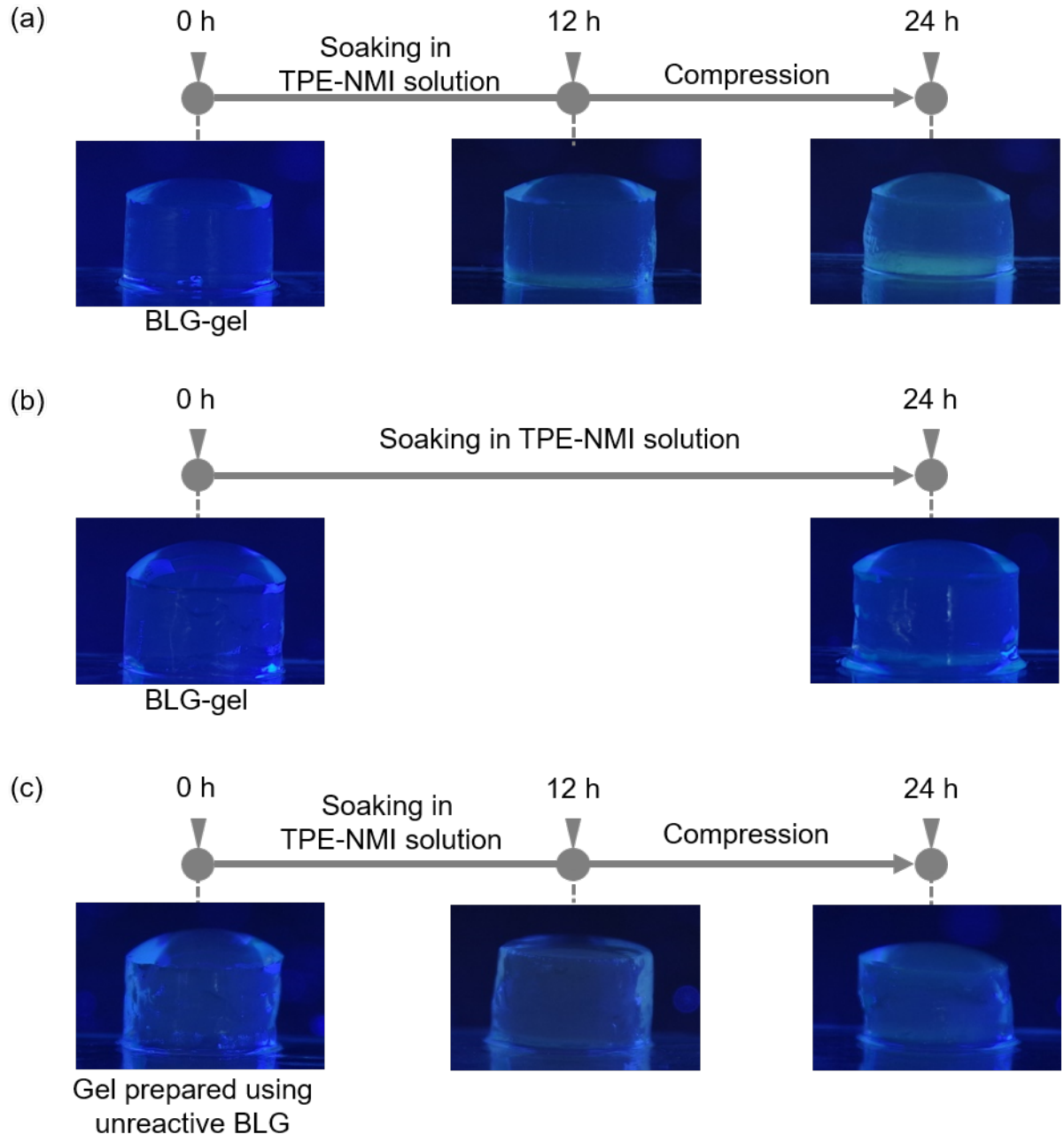

Figure 3-10. Photographs of BLG-gels for compression-triggered chemical modification by TPE-NMI with compression (a,c) and without compression (b) under irradiation of UV-light (365 nm). In (c), a gel obtained by the reaction of NHS-PEG-NHS with unreactive BLG, which was treated with *N*-phenylmaleimide, was used.

3-3. Summary

In summary, hydrogels were prepared in reactions of β-lactoglobulin with PEG modified by N-hydroxysuccinimide esters at both ends. The hydrogels exhibit mechanical properties influenced by the folding energy of the protein as well as volume changes by unfolding of the protein upon the addition of urea. The macroscopic compression of the selected hydrogel triggers microscopic unfolding of the protein units, inducing chemical modification of the exposed cysteine residue. Fluorescence was clearly monitored as a result of chemical modification of the selected hydrogel with engineered GFP or tetraphenylethene derivatives. To the best of this knowledge, this is the first example of protein modification driven by mechanical protein unfolding triggered by hydrogel compression. This finding is expected to contribute to the development of stimuli responsive materials based on mechanical protein unfolding.

3-4. Materials and methods

Instruments

Fluorescence spectral measurements were carried out with a JASCO FP-8600 fluorescence spectrophotometer. ^{1}H NMR spectra were recorded on a Bruker BioSpin AVANCE III HD NMR spectrometer (400 MHz). The chemical shifts were calibrated by residual solvent signals. ESI-TOF MS analyses were performed with a Bruker Daltonics micrOTOF II mass spectrometer. The pH values were monitored with a Horiba F-52 pH meter. Tensile tests were conducted using a Shimadzu EZ Graph with a 10 N EZ Graph load cell.

Materials

Ultrapure water (Milli-Q) was prepared by a Millipore Integral 3 apparatus. All reagents were of the highest commercially available guaranteed grade and were used as received unless otherwise indicated. β-Lactoglobulin, a mixture of variants A and B,[43] was purchased from Sigma-Aldrich and used without any purification. NHS-PEG-NHS and tetraphenylethene tethering a maleimide group (TPE-NMI) was synthesized according to reported procedures.[33,36] Pyridyl disulfide-tethering GFP K25C/C47A mutant, PyS-GFP, was prepared according to Hayashi group's previous reports.[41-42.]

Preparation of BLG-gel

A 100 mM potassium phosphate buffer solution containing 100 mg/mL BLG (pH 7.5, 17.3 μL) was mixed with the same buffer solution containing 5 equivalents of NHS-PEG2000-NHS (pH 7.5, 2.30 μL). This mixture was then poured into a linear mold (width 1 mm, length 11 mm, depth 1 mm) or a ring-shaped mold (diameter 5 mm, height 3 mm). The mixture was allowed to stand at room temperature for approximately 5 hours to gel. Before experiments, the obtained gel was swelled to equilibrium in 100 mM potassium phosphate buffer (pH 6.5 or 7.0).

Tensile tests of BLG-gel

Samples were prepared in cuboid shapes with ca. 14 mm x ca. 1.2 mm x ca. 1.2 mm in equilibrium swelling states in 100 mM potassium phosphate buffer (pH 7.0). During tensile tests, samples were attached to a metal sheet using the adhesive reagent Aron Alpha®, within 8 mm. Young's modulus was determined by the slope in the strain ranging from 0% to 10% of the rupture point.

Modification of BLG with PyS-GFP in a solution state in the presence of urea

A potassium phosphate buffer solution (100 mM, pH 6.5) containing 80 μM BLG and 100 μM GFP-PyS was prepared. A urea-containing potassium phosphate buffer solution (100 mM, pH 6.5) was added to the solution as a denaturant and reactions were carried out at 25 °C for 8 hours under several different conditions with varying urea concentrations. An *N*-phenylmaleimide solution in DMSO (final concentration 200 μM and 10%, respectively) was added, and the mixture was reacted at 25 °C for 1 hour. After quenching the reaction, evaluations were conducted using gel electrophoresis (SDS-PAGE).

Modification of BLG with TPE-NMI in a solution state in the presence of urea

A potassium phosphate buffer solution (100 mM, pH 6.5) containing 30 μM BLG, 30 μM TPE-NMI 5% dimethyl sulfoxide was prepared. Into the solution, a urea-containing potassium phosphate buffer solution (100 mM, pH 6.5) was added as a denaturant and reactions were carried out at 25 °C for 2 hours under several different conditions with varying urea concentrations. Reactions were evaluated by ESI MS and fluorescence spectroscopy.

Compression of BLG-gel

Cylindrically shaped BLG-gels were used: 4 mm in height and 7 mm in diameter in equilibrium swelling states in 100 mM potassium phosphate buffer (pH 7.0). The gel was soaked in a buffer solution containing 20 μM PyS-GFP or 50 μM TPE-NMI for 12 h. In the case of TPE-NMI, a buffer solution containing 5% dimethyl sulfoxide was used. The hydrogel was compressed for 12 h by clipping with two glass plates using a 1 mm spacer to generate the height constraint (Figure 3-6).

3-5. References

1 C. Storm, J. J. Pastore, F. C. MacKintosh, T. C. Lubensky, P. A. Janmey, *Nature* **2005**, *435*, 191.

2 S. van Dun, C. Ottmann, L.-G. Milroy, L. Brunsveld, *J. Am. Chem. Soc.* **2017**, *139*, 13960.

3 T. T. Pham, S. Abe, K. Hirata, K. Katayama, T. Ueno, *Chem. Lett.* **2023**, *52*, 720.

4 R. Adachi, S. Suzuki, T. Mitsuda, Y. Morita, T. Komatsu, *Chem. Commun.* **2020**, *56*, 15585.

5 M. D. Shoulders, R. T. Raines, *Annu. Rev. Biochem.* **2009**, *78*, 929.

6 V. Gribova, C.-Y. Liu, A. Nishiguchi, M. Matsusaki, T. Boudou, C. Picart, M. Akashi, *Biochem. Biophys. Res. Commun.* **2016**, *474*, 515.

7 M. P. Lutolf, J. A. Hubbell, *Nat. Biotechnol.* **2005**, *23*, 47.

8 S. Lv, D. M. Dudek, Y. Cao, M. M. Balamurali, J. Gosline, H. Li, *Nature* **2010**, *465*, 69.

9 J. Fang, A. Mehlich, N. Koga, J. Huang, R. Koga, X. Gao, C. Hu, C. Jin, M. Rief, J. Kast, D. Baker, H. Li, *Nat. Commun.* **2013**, *4*, 2974.

10 Y. Cao, H. Li, *Chem. Commun.* **2008**, 4144.

11 H. Li, N. Kong, B. Laver, J. Liu, *Small* **2016**, *12*, 973.

12 T. Miyata, N. Asami, T. Uragami, *Nature* **1999**, *399*, 766.

13 C. Norioka, K. Okita, M. Mukada, A. Kawamura, T. Miyata, *Polym. Chem.* **2017**, *8*, 6378.

14 T. Ono, Y. Hisaoka, A. Onoda, K. Oohora, T. Hayashi, *Chem. Asian J.* **2016**, *11*, 1036.

15 N. Yamaguchi, L. Zhang, B.-S. Chae, C. S. Palla, E. M. Furst, K. L. Kiick, *J. Am. Chem. Soc.* **2007**, *129*, 3040.

16 H. Lei, L. Dong, Y. Li, J. Zhang, H. Chen, J. Wu, Y. Zhang, Q. Fan, B. Xue, M. Qin, B. Chen, Y. Cao, W. Wang, *Nat. Commun.* **2020**, *11*, 4032.

17 T. Tanaka, *Sci. Am.* **1981**, *244*, 124.

18 J. L. Drury, D. J. Mooney, *Biomaterials* **2003**, *24*, 4337.

19 J. P. Gong, Y. Katsuyama, T. Kurokawa, Y. Osada, *Adv. Mater.* **2003**, *15*, 1155.

20 X. Yan, F. Wang, B. Zheng, F. Huang, *Chem. Soc. Rev.* **2012**, *41*, 6042.

21 M. Nakahata, Y. Takashima, A. Hashidzume, A. Harada, *Angew. Chem. Int. Ed.* **2013**, *52*, 5731.

22 A. P. Esser-Kahn, M. B. Francis, *Angew. Chem. Int. Ed.* **2008**, *47*, 3751.

23 A. P. Esser-Kahn, A. T. Iavarone, M. B. Francis, *J. Am. Chem. Soc.* **2008**, *130*, 15820.

24 K. Oohora, A. Onoda, H. Kitagishi, H. Yamaguchi, A. Harada, T. Hayashi, *Chem. Sci.* **2011**, *2*, 1033.

25 T. Miyata, M. Jige, T. Nakaminami, T. Uragami, *Proc. Natl. Acad. Sci. U.S.A.* **2006**, *103*, 1190.

26 N. Bruns, K. Pustelny, L. M. Bergeron, T. A. Whitehead, D. S. Clark, *Angew. Chem. Int. Ed.* **2009**, *48*, 5666.

27 M. Taki, T. Yamashita, K. Yatabe, V. Vogel, *Soft Matter* **2019**, *15*, 9388.

28 S. Brownlow, J. H. M. Cabral, R. Cooper, D. R. Flower, S. J. Yewdall, I. Polikarpov, A. C. North, L. Sawyer, *Structure* **1997**, *5*, 481.

29 B. Y. Qin, M. C. Bewley, L. K. Creamer, H. M. Baker, E. N. Baker, G. B. Jameson, *Biochemistry* **1998**, *37*, 14014.
30 A. Chevalley, M. V. Cherrier, J. C. Fontecilla-Camps, M. Ghasemi, M. Salmain, *Dalton Trans.* **2014**, *43*, 5482.
31 F. Schwizer, Y. Okamoto, T. Heinisch, Y. Gu, M. M. Pellizzoni, V. Lebrun, R. Reuter, V. Köhler, J. C. Lewis, T. R. Ward, *Chem. Rev.* **2018**, *118*, 142.
32 M. Z. Chen, N. S. Moily, J. L. Bridgford, R. J. Wood, M. Radwan, T. A. Smith, Z. Song, B. Z. Tang, L. Tilley, X. Xu, G. E. Reid, M. A. Pouladi, Y. Hong, D. M. Hatters, *Nat. Commun.* **2017**, *8*, 474.
33 S. Zhang, M. Liu, L. Y. F. Tan, Q. Hong, Z. L. Pow, T. C. Owyong, S. Ding, W. W. H. Wong, Y. Hong, *Chem. Asian J.* **2019**, *14*, 904.
34 S. Zhang, Y. Hong, in *The Unfolded Protein Response*, ed. by Roberto Pérez-Torrado, Springer US, New York, NY, **2022**, Vol. 2378, pp. 3–18.
35 J. Kerr, J. L. Schlosser, D. R. Griffin, D. Y. Wong, A. M. Kasko, *Biomacromolecules* **2013**, *14*, 2822.
36 Y. Zhang, H. Song, Z. Shang, A. Chen, D. Huang, H. Zhao, H. Du, *Biol. Pharm. Bull.* **2014**, *37*, 785.
37 T. Arakawa, S. N. Timasheff, *Biochemistry* **1985**, *24*, 6756.
38 J. Wu, P. Li, C. Dong, H. Jiang, Bin Xue, X. Gao, M. Qin, W. Wang, Bin Chen, Y. Cao, *Nat. Commun.* **2018**, *9*, 620.
39 L. Fu, A. Haage, N. Kong, G. Tanentzapf, H. Li, *Chem. Commun.* **2019**, *55*, 5235.
40 Q. Bian, L. Fu, H. Li, *Nat. Commun.* **2022**, *13*, 137.
41 J. W. Soon, K. Oohora, T. Hayashi, *RSC Adv.* **2022**, *12*, 28519.
42 J. W. Soon, K. Oohora, T. Uchihashi, T. Hayashi, *Chem. Lett.* **2023**, *52*, 105.
43 B. Y. Qin, G. B. Jameson, M. C. Bewley, E. N. Baker, L. K. Creamer, *Protein Sci.* **2008**, *8*, 75.

Conclusion

In this thesis, protein building blocks were utilized toward new types of stimuli-responsive biomaterials. Two types of hydrogels were designed, prepared and evaluated: a polyacrylamide gel containing hexameric hemoprotein (HTHP) as a cross-linker and a gel obtained by cross-linked b-lactoglobulin (BLG) with polyethylene glycol. The former shows unique mechanical properties that are regulated by heme redox states and mutations in the protein matrix. The latter serves as mechanochemical materials, where compression of the gel induces the unfolding of the protein units to promote the chemical modification of a specific cysteine residue.

In chapter 1, the author focused on redox-responsive behaviors of the heme binding in HTHP toward a redox-responsive gel. Thermodynamic stabilities of the interaction between heme and the heme pocket at Fe(II) and Fe(III) states were determined by denaturant titration using CD spectra in visible region. The thermal stability of the heme binding at the Fe(III) state is much higher than that at the Fe(II) state possibly due to the iron-phenolate coordination. To introduce the reaction points for cross-linkage, heme in HTHP was replaced with a synthetic heme derivative tethering an acryloyl group. Copolymerization of acrylamide and the obtained protein produced a polyacrylamide gel containing engineered HTHP as a cross-linker. The gel shows two characteristic behaviors based on intrinsic features of HTHP: Sol-gel transition occurs upon the addition of reductant in the presence of apomyoglobin via a heme-transfer event and compression elasticity of the gel decreases by the reduction of the heme center. Compression analysis indicated the decreased stiffness upon the addition of reductant possibly due to reduced heme binding affinity at the cross-linker point.

In chapter 2, mutation of the protein matrix in the HTHP-based gel was found to tune their elasticity. Two arginine residues, which possibly contribute to cation-p interaction with heme, were mutated to an alanine residue to provide two single mutants, R25A and R38A mutants. Denaturant titration experiments of the mutants revealed lower ΔG^{o} values than that of the wild type protein. Polyacrylamide gels containing engineered HTHP mutants as cross-linkers were prepared according to the same procedure in Chapter 1. Young's modulus values of the mutant-based gels determined by tensile testing show significant decrease relative to the wild type-based gel. Moreover, the reduction-triggered gel-sol transition was observed in the mutant-based gel because the R38A mutant does not bind ferrous heme anymore.

In chapter 3, the BLG-based gel was prepared by the reaction of BLG with PEG tethering activated ester groups at both terminals. The tensile tests revealed that the elasticity and toughness of the gels depend on the concentrations of both BLG and PEG derivative. The optimized preparation condition for the gels is the reaction of 100 mg/mL BLG and 5 equivalents of PEG derivative. The mechanochemical property of the BLG-based gel was evaluated in the presence of an engineered GFP variant or tetraphenylethylene (TPE). Compression of the gels induced the unfolding of the protein units. Unfolding BLG exposed the cystine residue at 121 position which is embedded and unreactive

in the folded BLG. Mechanochemical response of the gel was confirmed by fluorescence enhancement via unfolding of BLG units and subsequent chemical modification of exposed Cys121 residue with GFP variant or TPE.

In conclusion, the newly prepared gels exhibit unique stimuli-responsive properties derived from tunable protein–cofactor interaction and unfolding-triggered reactivity changes of specific amino acid residues. Since structures, physicochemical properties and functions of an enormous number of proteins have been investigated, protein-based gels will provide a variety of unique stimuli responsiveness like two examples shown in this thesis. The material designs and findings in the investigation of HTHP- and BLG-based gels will contribute to the development of practically useful protein-based hydrogels in the future.

List of Publications

1. A polyacrylamide gel containing an engineered hexameric hemoprotein as a cross-linking unit toward redox responsive materials

Kazuki Kageyama, Koji Oohora*, and Takashi Hayashi*

RSC Advances, **2023**, *13*, 34610–34617. DOI: 10.1039/D3RA05897B

2. Tuning Elasticity of a Hexameric Hemoprotein-based Hydrogel through Mutation of its Protein Building Block

Koji Oohora*, **Kazuki Kageyama**, Yuri Hidaka, and Takashi Hayashi

Chemistry Letters, *in press*. DOI: 10.1093/chemle/upad052

3. Mechanochemical Responses in β-Lactoglobulin-based Hydrogels: Protein Unfolding and Chemical Modification through Compression

Koji Oohora*, **Kazuki Kageyama**, Hiroki Innami, and Takashi Hayashi

Chemistry Letters, *in press*. DOI: 10.1093/chemle/upad043

Acknowledgements

The study presented in this thesis has been carried out at Department of Applied Chemistry, Graduate School of Engineering, Osaka University from April 2018 to March 2024. The author would like to express his best gratitude to the supervisor, Professor Takashi Hayashi, for his continuous guidance, constant discussions, and warm encouragement throughout this research. The author would like to deeply thank Associate Professor Koji Oohora for his kind and continuous guidance and valuable discussions. The author would like to deeply thank Assistant Professor Shunsuke Kato for his helpful and insightful suggestion. The author also acknowledges Professors Hiroshi Uyama and Masaya Nogi for reviewing this thesis and their valuable suggestions.

Acknowledgements are also made to Professor Hiroshi Uyama and Assistant Professor Akihide Sugawara at Department of Applied Chemistry, Graduate School of Engineering, Osaka University for their technical support and valuable discussions on tensile test and compression analysis in Chapters 1, 2 and 3.

The author would like to express his gratitude to Professor Akira Onoda for his helpful suggestion and insightful discussion. The author would like to express his gratitude to Ms. Kiyomi Lee for her kind help in laboratory life and all members at Hayashi group.

The author expresses his great gratitude to his family for their heartfelt assistance and encouragements.

Finally, the study was financially supported by Interactive Materials Science Cadet program and establishment of university fellowships towards the creation of science technology innovation supported by JST.

Kazuki Kageyama
January 2024